From Theory to Simulation: Delving into the Dynamics of Burgers Turbulence

by

Kiarash Jalali

THESIS PRESENTED TO ÉCOLE DE TECHNOLOGIE SUPÉRIEURE
IN PARTIAL FULFILLMENT OF A MASTER'S DEGREE
WITH THESIS IN MECHANICAL ENGINEERING
M.A.Sc.

MONTREAL, MARCH 27, 2024

ÉCOLE DE TECHNOLOGIE SUPÉRIEURE
UNIVERSITÉ DU QUÉBEC

BOARD OF EXAMINERS

THIS THESIS HAS BEEN EVALUATED

BY THE FOLLOWING BOARD OF EXAMINERS

Prof. Louis Dufresne, Thesis supervisor
Department of Mechanical Engineering, École de Technologie Supérieure

Prof. François Garnier, Chair, Board of Examiners
Department of Mechanical Engineering, École de Technologie Supérieure

Prof. Giuseppe Di Labbio, External Examiner
Department of Mechanical Engineering, École de Technologie Supérieure

THIS THESIS WAS PRESENTED AND DEFENDED

IN THE PRESENCE OF A BOARD OF EXAMINERS AND THE PUBLIC

ON "MARCH 19, 2024"

AT ÉCOLE DE TECHNOLOGIE SUPÉRIEURE

ACKNOWLEDGEMENTS

I extend my deepest gratitude to Prof. Louis Dufresne for his invaluable guidance and expertise throughout my research. His patience and mentorship have significantly contributed to my academic development.

A heartfelt tribute to my parents; to my father, whose belief in me and guidance continue to be a cornerstone of my journey, even in his absence, and to my mother, for her endless love, and encouragement. Their sacrifices, wisdom, support, and resilience have been a constant source of inspiration and strength, guiding me toward pursuing my ambitions with courage and determination.

Special thanks go to my brother, Kaveh Jalali, for his unwavering support and encouragement. Kaveh has been there for me without any expectations, solely for my progress and well-being. His selflessness and constant presence have been a significant source of strength and motivation throughout my academic journey.

Additionally, my sincere appreciation extends to my two other brothers, Babak and Sina, for their support, understanding, and companionship. Their belief in me and their presence in my life have been invaluable sources of joy and motivation throughout this journey.

Lastly, I express my sincere appreciation to my friend, Hassan Bardareh, for his encouragement and support.

De la Théorie à la Simulation : Plongée dans la Dynamique de la Turbulence de Burgers

Kiarash Jalali

RÉSUMÉ

Cette thèse présente une exploration complète des dynamiques des équations de Burgers linéaires et non linéaires dans le contexte de la turbulence de Burgers unidimensionnelle. La phase initiale de la recherche examine comment la viscosité influence les solutions de ces équations, en mettant l'accent sur l'interaction entre les effets inertiel et visqueux et en explorant la variation de la dissipation à travers différents nombres d'onde et échelles.

L'étude déplace ensuite son focus vers la turbulence de Burgers, en commençant par une caractérisation statistique approfondie de la turbulence de Burgers en décroissance. Cela inclut une analyse des spectres d'énergie, de la densité de probabilité et de divers moments centraux. La recherche s'étend davantage à l'investigation de la turbulence de Burgers forcée sous différentes conditions initiales et termes de forçage. Un aspect clé de cette investigation est l'examen du développement de l'Énergie Cinétique Turbulente dans la turbulence de Burgers forcée et de son invariance aux changements du nombre de Reynolds. Nos résultats confirment que, une fois l'équilibre atteint, les profils de vitesse démontrent une remarquable constance à travers différents nombres de Reynolds, s'alignant sur les observations de la littérature. De plus, comme preuve de l'auto-similarité dans la turbulence de Burgers en décroissance, une auto-similarité jusqu'à la corrélation d'ordre quatre du champ de vitesse a été observée.

De plus, cette thèse met en évidence le comportement unique de l'équation de Burgers par rapport à la turbulence de Navier-Stokes, soulignant sa sensibilité réduite aux conditions initiales et l'absence de dynamiques chaotiques, en plus de sa capacité d'adaptation aux influences externes. L'étude se conclut par un examen approfondi des caractéristiques statistiques de la turbulence de Burgers forcée, incluant le spectre d'énergie, les fonctions de densité de probabilité (PDF), les fonctions de corrélation et divers moments statistiques, fournissant des aperçus significatifs sur les complexités de la turbulence.

Les découvertes de cette étude contribuent au champ plus large de la dynamique des fluides, améliorant notre compréhension des phénomènes de turbulence.

Mots-clés: Dynamique statistique de la turbulence de Burgers, Turbulence de Burgers forcée, Turbulence de Burgers décroissante, Équation d'advection-diffusion, Simulations numériques de la turbulence de Burgers, Simulation Numérique Directe (SND), Méthode spectrale de Fourier Galerkin

From Theory to Simulation: Delving into the Dynamics of Burgers Turbulence

Kiarash Jalali

ABSTRACT

This thesis presents a comprehensive exploration of the dynamics of linear and non-linear Burgers equations in the context of one-dimensional Burgers turbulence. The initial phase of the research examines how viscosity influences the solutions of these equations, emphasizing the interaction between inertial and viscous effects and exploring the variation of dissipation across different wavenumbers and scales.

The study then shifts its focus to Burgers' turbulence, beginning with an in-depth statistical characterization of Decaying Burgers' turbulence. This includes an analysis of energy spectra, inverse cascade of energy, probability density, and various central moments. The research further extends to the investigation of Forced Burgers' turbulence under varying initial conditions and forcing terms. A key aspect of this investigation is examining the development of Turbulent Kinetic Energy in forced Burgers turbulence and its invariance to changes in Reynolds number. Our findings confirm that, upon reaching equilibrium, velocity profiles demonstrate remarkable consistency across different Reynolds numbers, aligning with the literature's observations. Furthermore, the thesis highlights self-similarity in decaying Burgers turbulence, evident up to the fourth-order correlation of the velocity field.

Furthermore, this thesis establishes the unique behavior of the Burgers equation in contrast to Navier-Stokes turbulence, highlighting its diminished sensitivity to initial conditions and the lack of chaotic dynamics, alongside its adaptability to external influences. The study concludes in an extensive examination of the statistical characteristics of forced Burgers turbulence, including energy spectrum, probability density functions (PDFs), correlation functions, and various statistical moments, providing significant insights into the complexities of turbulence.

The findings of this study contribute to the broader field of fluid dynamics, enhancing our comprehension of turbulence phenomena.

Keywords: Statistical dynamics of Burgers turbulence, Forced Burgers turbulence, Decaying Burgers turbulence, Advection-diffusion equation, Numerical simulations of Burgers turbulence, Direct Numerical Simulation methods (DNS), Fourier-Galerkin spectral method

TABLE OF CONTENTS

LIST OF FIGURES

INTRODUCTION

In the diverse and intricate realm of fluid dynamics, turbulence stands as one of the most complex phenomena to understand and model. Its unpredictable nature and intricate structures challenge physicists and engineers alike, manifesting in everything from the gentle flow of rivers and the dynamic patterns of the atmosphere to the formation of large cosmological structures. At the heart of this challenge lies the enigmatic concept of Burgers turbulence, a simplified yet profoundly insightful model for understanding nonlinear dynamics and shock formation in fluids. Originating from the fundamental Burgers equation, this model serves as a cornerstone in the study of turbulence, offering a more manageable framework for exploring the chaotic behavior of fluid flows. Despite its relative simplicity compared to the full Navier-Stokes equations, Burgers turbulence provides a rich platform for examining fundamental aspects of turbulence, including chaos theory and nonlinear dynamics, the existence and smoothness problem, energy dissipation, statistical properties, and pattern formation (Bec & Khanin, 2007).

This thesis delves into the statistical dynamics of Burgers turbulence, a realm where classical physics and sophisticated mathematical modeling converge, offering unique insights into the behavior of turbulent systems. By employing the Fourier-Galerkin numerical method, this research aims to unravel the complexities of both decaying and forced Burgers turbulence, bridging gaps in our current understanding and contributing to the broader field of fluid dynamics. The renowned Burgers equation as a quasi-linear parabolic equation first appeared in an article by Bateman (1915).

The interest to the Burgers model equation of turbulence, which is the investigation of the behaviours of multi-dimensional pressure less Burger's equation with random initial conditions or random forcing increased during the last decades. The motivation for this interest is the simplicity of Burgers turbulence as a nonlinear system out of equilibrium in addition to the applications of the class of Burgers equations including cosmology, statistical physics and the fluid dynamics. The study of adhesion model in cosmology, the random Lagrangian system of

PDEs, the theory of dynamical systems and the multiscale theory of hydrodynamic turbulence are some of the areas which progressed by the developments in Burgers turbulence (Bec & Khanin, 2007).

A key characteristic of this class of equations is that despite having smooth initial data and forces, the solution can still create abrupt changes or shocks (Bakhtin, 2013).

Our research primarily centers on exploring the dynamics of linear and non-linear Burgers equations. To achieve this, we initiate our investigation by examining how viscosity influences the solutions of these equations, paying special attention to the interaction between inertia and viscous effects. We then further explore how viscosity specifically impacts this interaction. In the subsequent subsection, we demonstrate how dissipation varies with different wavenumbers across various scales.

We then redirected our focus to Burgers turbulence, starting with decaying Burgers turbulence. Our attention was concentrated on a more thorough statistical characterization of the flow, which included analyzing the energy spectra, probability density and various central moments. We then discussed the phenomenon of inverse energy cascade following the research work conducted by Girimaji & Zhou (1995). Additionally, revisiting the study carried out by Sefik & Christov, we explored the stochastic self-similarity in multi-point higher-order correlation functions of the velocity field (Sefik & Christov, 1992).

We subsequently extended our research to investigate the characteristics of the forced Burgers turbulence accompanied by various initial conditions and forcing terms. We endeavor to validate the research conducted by Jeng & Meecham (1972), focusing on crucial questions such as whether the development of turbulent kinetic energy (TKE) in forced Burgers turbulence is invariant to changes in Reynolds number. Building upon their findings, our study also demonstrates that, upon reaching equilibrium, velocity profiles exhibit remarkable consistency across different Reynolds numbers (Jeng & Meecham, 1972).

Furthermore, building upon Jeng (1969) research, we confirm that, unlike the Navier-Stokes

turbulence which is highly sensitive to initial conditions, the Burgers equation displays a lack of chaotic dynamics and reduced sensitivity to initial conditions. We also conducted an in-depth exploration of the statistical characteristics of forced Burgers turbulence, which play a vital role in understanding complex turbulence. This included a thorough analysis of the energy spectrum, probability density functions (PDFs), correlation functions, and various statistical moments.

The complexities of Burgers turbulence necessitate a robust and precise methodological approach to explore its intricate details. To achieve this aim, we employed the Fourier-Galerkin numerical method, a powerful tool renowned for its effectiveness in studying nonlinear dynamical systems. This method excels in decomposing complex nonlinear patterns into simpler sinusoidal components, enabling a more detailed and accurate analysis of turbulent flows.

In the context of Burgers turbulence, the Fourier-Galerkin method offers a significant advantage. It provides clear insights into the energy spectrum and the dynamic interactions within the turbulence, essential for understanding both decaying and forced scenarios. This approach is particularly suited to our study as it handles the periodic boundary conditions commonly associated with Burgers turbulence simulations. Moreover, its spectral convergence and capacity for high-resolution modeling make it an ideal choice for examining the intricate details of the statistical dynamics of turbulence (Canuto, 2006).

This thesis aims to advance our understanding of the statistical dynamics of Burgers turbulence, an area crucial to the broader field of fluid dynamics, by employing the Fourier-Galerkin numerical method. Through this investigation, the study seeks to uncover nuanced aspects of both decaying and forced Burgers turbulence, offering insights into their behavior and properties. The research will not only address existing gaps in the theoretical understanding of Burgers turbulence but also demonstrate the efficacy of the Fourier Galerkin method in providing a comprehensive and detailed analysis of such complex fluid systems.

CHAPTER 1

THE STARTING POINT: UNDERSTANDING THE PROBLEM

Burgers equation is a fundamental partial differential equation. It's often used to model shock waves, cosmological events, simulate traffic flow, detonation propagation (reactive Burgers), and examine fluid dynamics among other things. This equation comes in various forms, each serving different physical phenomena.

1.1 A Comprehensive Review of Burgers Turbulence Research

This literature review delves into the study of the dynamics of Burgers turbulence, a key area in fluid dynamics that simplifies the complexities of turbulent flows. It critically examines the evolution of research on both forced and decaying Burgers class of equations, highlighting seminal theories and significant advancements. The review particularly focuses on the dynamics of one-dimensional Burgers turbulence.

1.1.1 Interplay of Inertia and Viscosity in Burgers Turbulence

In the study of Burgers turbulence, the dynamics of fluid motion are encapsulated by two principal terms within the Burgers equation: the advection and diffusion terms. These terms are pivotal in modeling the fundamental physical effects of inertia and viscosity, respectively, offering insights into the behavior of fluids under turbulent conditions.

- Advection Term and Inertial Effects: The advection term, denoted as $u\frac{\partial u}{\partial x}$ where u represents the fluid velocity, characterizes the inertial effects within the fluid dynamics. This term illustrates how fluid parcels transport their momentum as they traverse the flow field. It encapsulates the non-linear interactions within the fluid's velocity field, mirroring the convective dynamics seen in the Navier-Stokes equations. The essence of this term lies in its ability to depict the tendency of fluid elements to retain their momentum, highlighting the influence of inertia on the flow's evolution (Taigbenu, 1999a).

- Diffusion Term and Viscous Effects: On the other hand, the diffusion term, expressed as $\nu \frac{\partial^2 u}{\partial x^2}$ with ν being the kinematic viscosity, reflects the viscous effects within the fluid. Viscosity, the fluid's internal friction, acts to dissipate energy, thereby smoothing velocity gradients and attenuating turbulence at finer scales. This term fundamentally represents how momentum is diffused across the fluid due to viscous forces, emphasizing the role of viscosity in shaping the flow's characteristics, especially in mitigating sharp discontinuities and shock formations (Taigbenu, 1999a).

Together, the advection and diffusion terms in the Burgers equation provide a simplified yet profound framework for examining fluid behavior, particularly under turbulent conditions. The equation's structure allows for a detailed exploration of how inertia and viscosity, two core aspects of fluid dynamics—interact to dictate the flow's behavior. Through the lens of Burgers turbulence, we gain valuable insights into the complex phenomena of turbulence and shock wave formation, underscoring the intrinsic relationship between inertial forces that promote fluid motion and viscous forces that seek to dampen and stabilize it. This duality forms the cornerstone of our understanding of fluid mechanics, offering a gateway to unraveling the complexities inherent in turbulent flows.

1.1.2 Advection-Diffusion equation

The advection-diffusion equation, which is the linearized form of the Burgers Equation, is a combination of two sources of flux which are diffusion and advection (the transport); and defines of any physical quantities such as temperature, concentration, or momentum as they transport into or out of a system. There has been appreciable interest in finding the solution to the advection-diffusion equation analytically and numerically during the last decades (Logan & Zlotnik, 1995). A time dependent advection-diffusion equation contains a linear advection term $a.\nabla u$ and a diffusion term $\nu \nabla^2 u$ and is given by,

$$\frac{\partial u}{\partial t} + a.\nabla u = \nu \nabla^2 u \tag{1.1}$$

where u is the velocity variable, $a > 0$ is the constant advection velocity, ν is the kinematic viscosity, and t is the time. Despite the linear nature of the advection-diffusion equation, a closed-form analytical solution remained elusive in the literature until the 2016 publication by A. Mojtabi and M. Deville. Prior to this, the majority of research efforts were focused on solving the linear advection-diffusion equation with an upstream boundary condition coupled with a Robin or Neumann downstream condition, rather than a periodic boundary condition (Mojtabi & Deville, 2015). The closed-form solution of this equation, subjected to periodic boundary conditions, is detailed in section 2.9.

Numerous studies have been conducted to explore the impact of varying viscosity on the advection-diffusion equation. This includes an analysis of the equation under conditions of diminishing viscosity by Moura, Sherwin & Peiró (2016) and Singh & Das (2019). They conducted research works to investigate how the diffusive solution of the advection-diffusion equation behaves under the influence of non-linear reactions across different conditions using finite difference numerical schemes. We also performed simulations to discuss viscous effects with various kinematic viscosities.

1.1.3 Freely Decaying Burgers Turbulence

During the last century, researchers made great efforts to simplify the Navier-Stokes turbulence model. One effort in the late 1930s by a Dutch scientist, J M Burgers, was the suggestion of a one-dimensional pressure-less model (Burgers, 1939).

$$\frac{\partial u}{\partial t} + u.\nabla u = \nu \nabla^2 u \tag{1.2}$$

This model, now known as the viscous Burgers equation, is the combination of non-linear advection with linear diffusion and is the simplest mathematical formulation to analyze the mixed effects of the advection and diffusion motions.

J. M. Burgers introduced this equation as a model to describe turbulence; however, it was disclosed that this model could not explain turbulent flow adequately. The idea that the Burgers equation can be used instead of the Navier-Stokes equation failed after Hopf (1950), and (Cole,

1951) revealed that the decaying Burgers equation could be solved by explicit integration. So, contrary to Navier-Stokes, the small disturbance in the initial conditions and, consequently, the spontaneous growth of randomness by chaotic dynamics does not affect the solution of the Burgers equation.

It is one of the simplest non-linear unsteady PDEs which possesses general closed-form solutions as discussed by Benton & Platzman (1972) and has very exclusive characteristics. The solutions to the Burgers equation look like that of the kinematic wave equations when the inertia or convective terms are dominant. In this case, the Burgers equation behaves like a hyperbolic PDE. On the other side, its behavior resembles a parabolic equation when the viscous terms are dominant (Taigbenu, 1999b). This model has a lot in common with the Navier-Stokes equation, including the same hydrodynamical (advective) non-linearity, which is regularized by the diffusion term, in addition to the similar invariance and the conservation laws (conservation of energy and momentum in non-viscous fluids) (Bec & Khanin, 2007). The Burgers equation, while simpler than the Navier-Stokes equations, captures the essential nonlinearity that produces shocks or discontinuities in fluid dynamics. Studying its behavior provides insights into the complex behaviors of actual fluid flows, especially in the context of shock formation and propagation. The spectral interactions in Burgers turbulence are more straightforward to study due to the one-dimensional nature of the velocity field (Girimaji & Zhou, 1995), compared with the three-dimensional nature of vorticity fluctuations in Navier-Stokes turbulence (Tennekes & Lumley, 1978).

Another prominent aspect of solutions to the Burgers equation is the emergence of shocks at high Reynolds numbers, which are the primary regions of kinetic energy dissipation. On the other hand, areas of intense velocity gradient in isotropic Navier-Stokes turbulence at similar Reynolds numbers exhibit less singular behaviors, and do not seem to be noticeable locations for energy dissipation (Gotoh & Kraichnan, 1993).

The numerical simulation of Burgers' turbulence, first documented by Jeng et al. in 1966, provided insights into the energy spectrum and the correlation function (Jeng, Foerster, Haaland & Meecham, 1966). These results were subsequently reported by A. Giorgini (Giorgini & Fluid Mechanics and Diffusion Laboratory, 1967) and confirmed by H. Tokunaga

(Tokunaga, 1976).

A different perspective on the dynamics of Burgers turbulence, in contrast to 3D Navier-Stokes turbulence, was provided by Saffman in 1968, including a unique functional form for the inertial subrange spectrum that exhibits a k^{-2} behavior (Saffman, 1968), unlike Kolmogorov $5/3$ law.

In a 1970 article titled "Gravitational Instability," Zel'dovich demonstrated that the Burgers equation could be applied to the study of the formation of large-scale structures in the Universe (Zel'dovich, 1970).

In the 1980 research works, Christov, C.I., and colleagues illustrated how nonlinearity in Burgers turbulence converts an initial Gaussian random velocity field into a series of coherent structures with predictable average shapes (Christov, 1980). Subsequent studies delved deeper into the interactions among these coherent structures. Specifically, Christov in 1990 examined these structures within decaying homogeneous turbulence, employing hierarchy techniques to relate higher-order moments (cumulants) to the lower-order ones (Christov, 1990). These coherent chain structures, which attracted significant interest in the 1970s, highlight a key aspect of turbulence research which is the ability of nonlinear interaction to generate a cascade of random time-invariant structures when subjected to periodic forces (Rabinovich & Sushchik, 1983) that will be discussed in the next section.

In their 1991 study, B. Sefik and C.I. Christov proposed that in the case of Burgers turbulence with decaying initial conditions, a form of statistical self-similarity emerges over time. This leads to the preservation of the shape of correlation functions up to the fourth order. To this aim, they derived correlation functions in various orders. In our research, we have verified their findings with strong agreement.

In 1992, Zhen-Su She and colleagues explored the solution to decaying Burgers turbulence in the limit of vanishing viscosity, focusing on fractal Brownian and Brownian initial velocity fields (She, Aurell & Frisch, 1992). Their work complemented the research conducted by Ya. Sinai in the same year, which delved into the number and locations of shocks and examined the scaling properties of various statistical quantities (Sinai, 1992).

In 1993, Gotoh et al. embarked on a comprehensive study of the statistics of decaying Burgers turbulence. This research included an examination of the power-law tail of the probability density

function (PDF), observation of intermittency in the PDF of density due to infinite compressibility and mass accumulation at shock regions, analysis of the wavenumber spectra, showing a great agreement with the behavior of the energy spectrum in the inertia range compared to the earlier studies, k^{-2} scale, and finally presenting new insights into the high-order moments at low and moderate Reynolds numbers (Gotoh & Kraichnan, 1993).

In 1995, Girimaji & Zhou demonstrated the occurrence of inverse energy transfer in one-dimensional Burgers turbulence, in contrast to three-dimensional Navier-Stokes turbulence where inverse energy transfer is prohibited. However, the question of whether this energy transfer takes the form of a cascade was left unresolved (Girimaji & Zhou, 1995).

Building upon previous studies, J. Bec and U. Frisch, in their 1999 research, demonstrated the existence of a power-law tail in the PDF of the velocity variant in decaying Burgers turbulence defined in the Lagrangian map, particularly in the context of vanishing viscosity (Bec & Frisch, 2000).

This model occurs in various mathematical areas, including fluid dynamics, non-linear acoustic, gas dynamics, and vehicle traffic models (Jaiswal, Chopra & Das, 2019).

As previously noted, the investigation of the Burgers model has been shown to offer qualitative insights into the actual turbulence, as was noted by Jeng (1969). Following this, from the 1980s onwards, researchers, predominantly physicists, have pivoted their attention to the multi-dimensional aspects of the Burgers equation. This shift involves examining the random solutions generated by various initial conditions or random forcing terms, a topic we will delve into in the following subsection.

1.1.4 Forced Burgers turbulence

This model appears in a variety of applications, including statistical physics in condensed matter, adhesion model in cosmology, and as a testing ground for certain types of theories of turbulence in fluid dynamics, especially for the ones applied to compressible hydrodynamics, statistical theory of turbulence and various Lagrangian problems (Bec & Khanin, 2007).

The forced Burgers equation, similar to its decaying counterpart, maintains the same fundamental

structure, including a nonlinear convective term and a linear viscous term, both of which contribute to its nonlinear behavior. This nonlinearity is essential for understanding the dynamics of complex systems. However, in contrast to the unforced Burgers equation, the forced variant does not have a general closed-form solution due to the added complexity of the external forcing term. One prominent feature of this equation is its ability to model a steady-state system where, despite smooth initial data and forcing, the solution can still develop discontinuities or shocks (Bakhtin, 2013).

To derive the forced form of the Burgers equation we first consider the Kardar–Parisi–Zhang (KPZ) equation (1.3) as a model, frequently studied to investigate different interface depositions and growth problems in the presence of a random forcing term. This continuous ballistic decomposition model is responsible for the side growth of the interface (Bec & Khanin, 2007).

$$\frac{\partial h}{\partial t} - \frac{1}{2}|\nabla h|^2 = \nu \nabla^2 h + f \tag{1.3}$$

The shocks that appear in the solution of the inviscid Burgers equation are correlated with the discontinuities in the gradient of the height h. This model is mainly helpful in studying the growth of roughness in various interface problems (Bec & Khanin, 2007). In what follows, we defined the multi-dimensional forced Burgers equation as a gradient of the KPZ model.

$$\frac{\partial u}{\partial t} + u.\nabla u = \nu \nabla^2 u - \nabla f \ , \ u = -\nabla h \tag{1.4}$$

Where the problem is forced by the function $F(x,t)$ that acts as a mechanism through which energy can be injected into the field. The outcome is a mechanism that introduces kinetic energy to the largest scales and transfers it, through the energy cascade, to the smallest scales where dissipation takes place.

Jeng (1969) pioneered the numerical simulation of forced Burgers turbulence, by using a random initial Gaussian velocity field driven by Gaussian random forces. He discovered that the velocity field maintains its Gaussianity, The condition of being Gaussian, progressively transitioning from initial conditions and becoming more influenced by the driving force. This finding demonstrated a lack of sensitivity to initial conditions in Burgers turbulence (Jeng, 1969).

Forced Burgers turbulence with a random forcing term is frequently employed in modeling diverse, complex and dynamic scenarios across various fields. This includes simulating the chaotic and unpredictable nature of atmospheric and oceanic currents in atmospheric sciences, characterizing the instabilities in various reaction-diffusion systems (Yakhot & She, 1988), modeling the formation of large-scale structures in cosmology, and representing chaotic systems in biology (Bec & Khanin, 2007).

In 1972, D. T. Jeng and W. C. Meecham numerically modeled forced Burgers turbulence with a sinusoidal forcing term, a model intended to represent scenarios like the wind's impact on water wave formation, where it acts as a surrogate for wind drag as detailed in their study. They illustrated that the evolution of TKE is unaffected by viscosity. Additionally, their findings reveal that the velocity profile remains nearly identical across various Reynolds numbers, with the exception of regions experiencing shocks (Jeng & Meecham, 1972).

In the 1995 research, Sharath et al. delved into an in-depth analysis of the energy spectrum, the dynamics of energy transfer, the energy form of the Burgers turbulence; and spectral interactions within Burgers turbulence under the influence of a random force at equilibrium. They distinctly outlined how the energy spectra in Burgers turbulence differ from those in Navier-Stokes turbulence, particularly emphasizing the spectral behavior within the dissipation range. They also presented a notable contrast to Navier-Stokes turbulence, demonstrating that, in Burgers turbulence, the small-scale structures are determined by large-scale parameters, including characteristic velocity and characteristic length-scale (Girimaji & Zhou, 1995).

A. Chekhlov and V. Yakhot, in 1995, focused on studying the dynamics of velocity fluctuations in one-dimensional Burgers turbulence, which were driven by a random force characterized as white in time. They detected significant intermittency in the high-order statistical moments of velocity differences with exponents close to unity, along with marked intermittencies within the energy dissipation correlation function with intermittency exponent in the universal range, which were influenced by large-scale shocks (Chekhlov & Yakhot, 1995b). In their subsequent research in the same year, they concentrated on examining how coherent structures impact the shape of the Probability Density Function (PDF) of the velocity fluctuations (Chekhlov & Yakhot,

1995a).

In 1993, A.Polyakov noted a remarkable similarity between the steady flux states in turbulence and irregularities in quantum field theory. He noted that in turbulent flow, the ultra-violet regularization (a concept in quantum field theory to prevent the integrals from going to infinity), which arises due to viscosity, leads to an energy flux traversing through the inertial range and prevents the accumulation of infinite energy at specific scales (Polyakov, 1993). Following that work, in another remarkable paper by A.Polyakov in December 1995, He again studied Burgers turbulent, as a pressureless model, and formulated a new method for analyzing the inertial range correlation functions based on quantum field theory, demonstrate that the intermittencies in the correlation function of the dissipation rate observed by A.Chekhlov and V.Yakhot were due to the breakdown of Galilean invariance, providing a comprehensive explanation for these pronounced intermittencies (Polyakov, 1995).

In their 2003 study, J. Bec and K. Khanin focused on the shock dynamics in the inviscid, randomly forced Burgers equation with a non-periodic forcing term. They investigated the concept of global minimizer curves in the Lagrangian particle trajectories of statistically stationary flows. By identifying areas where minimizers accumulate, they determined shock positions, suggesting that all one-sided minimizers originating at a given time t would converge backward-in-time to the trajectory of the global minimizer, which is indicative of the primary shock. Their research revealed a stationary regime, corresponding to the velocities of one-sided minimizers. They proposed that at any specific time (e.g., t=0) and location x, there is at least one one-sided minimizer. However, due to the fluctuating positions of these minimizers, their findings contradicted previous expectations by showing the absence of global minimizers. This implies that each fluid particle is eventually absorbed by a shock after a certain period. Since all shocks have a finite duration, they concluded that true main shocks do not exist in non-periodic situations (Bec & Khanin, 2003).

In their comprehensive 2007 publication, J. Bec and K. Khanin presented an extensive review and research on diverse facets of decaying, forced, and Kicked Burgers turbulence. Their work delved deeply into both the statistical and numerical aspects of these phenomena, alongside an exploration of the fundamental principles and laws applicable in this field (Bec & Khanin, 2007).

The existence and uniqueness of global minimizers in Burgers turbulence with periodic forcing were established and examined by Y. Bakhtin in 2013. He demonstrated the diffusive behavior of these global minimizers in scenarios involving periodic forcing (Bakhtin, 2013).
In a very recent study, Sadhitro De et al., in 2023, undertook an extensive analysis of dynamic multiscaling in the non-equilibrium yet statistically steady state of forced Burgers turbulence. They introduced the innovative concept of "Interval Collapse Time," defined as the duration for a spatial interval, identified by two Lagrangian tracers, to collapse at a shock. Additionally, they performed calculations of the dynamic scaling exponents across various orders of moments of these interval times. The research uncovered an array of characteristic time scales and established that the probability distribution function of the interval collapse times is distinctly non-Gaussian, characterized by a power-law tail (De, Mitra & Pandit, 2023).

1.2 Research objectives and aims: Investigating Burgers Turbulence

This thesis compiles a series of investigations aimed at elucidating various dynamical aspects of Burgers turbulence. By delving deep into these dynamics, the research aims to study the fundamental principles that govern the evolution and statistical characteristics of Burgers turbulence, thereby contributing to the broader field of fluid dynamics with novel insights and methodologies.

- Our inquiry begins with an exploration of the dynamics governed by linear and non-linear Burgers equations. We delve into understanding the impact of viscosity on the solution of these equations, assessing the intricate interplay between inertial and viscous effects. A significant portion of our study is dedicated to dissecting how viscosity and scale differences influence this dynamical interaction.
- In the research objectives section of my thesis, we aim to conduct a comprehensive analysis of dissipative Burgers turbulence. Our initial focus will be on investigating the presence of an inverse energy cascade, attributed to local spectral interactions, to enhance our understanding of its dynamics, drawing upon the foundational work by Girimaji & Zhou (1995). Subsequently, we will re-examine the seminal studies by Sefik & Christov (1992), with

the goal of confirming the existence of self-similarity within the velocity field's correlation functions. This discovery suggests that at significantly long durations, acquiring results for varied times becomes unnecessary, thereby enhancing efficiency and saving computational effort in subsequent simulations.

- Building upon this foundation, we replicate the pivotal research conducted by Jeng & Meecham (1972), marking our initial foray into modeling forced Burgers turbulence within an Eulerian framework with a sinusoidal forcing term. Our primary aim is to validate their findings, particularly regarding the TKE development independence from variations in the Reynolds number. Our research extends these findings by demonstrating consistent velocity profiles at equilibrium across different Reynolds numbers, with notable distinctions primarily in the dissipation region. Furthermore, we aim to elucidate the degree of dependence of the system on the forcing terms by comparing the correlation functions of the velocity field and the forcing term.
- Advancing to a more complex scenario, we aim to rigorously examine the dynamic characteristics associated with turbulent behavior. To corroborate the findings of Jeng (1969), we investigate whether a system initiated with a random Gaussian velocity field and subjected to a random Gaussian forcing term retains its Gaussianity over time. This section will highlight the Burgers equation's distinct lack of chaotic dynamics and diminished sensitivity to initial conditions compared to Navier-Stokes turbulence, shedding light on the nuances of complex turbulence phenomena.

Our research casts a wide net by considering two distinct forcing terms, drawing inspiration from Jeng & Meecham (1972) on sinusoidal forcing and from Jeng (1969) employed a random Wiener process as a forcing mechanism.

Research Gaps Addressed

Despite the extensive body of research on Burgers turbulence, several gaps remain unbridged, which this thesis aims to address:

- Complex Interplay of Inertia and Viscous Effects: Despite extensive studies on this topic, we offer a clearer and more comprehensive perspective to thoroughly elucidate the intricate

interplay between inertia and viscous effects within Burgers turbulence. Our discussion specifically focuses on how varying viscosity conditions and differing scale characteristics influence this dynamic relationship.

- An in-depth analysis of local interactions and energy transfer between various scales and sub-ranges in Burgers turbulence aims to enhance our understanding of the inverse cascade of energy.
- Impact of forcing terms: There is a lack of comprehensive understanding regarding the system's sensitivity to different types of forcing terms, especially in comparing sinusoidal and random Gaussian forces in shaping the turbulence characteristics and analyzing its true dynamics.
- Turbulence behavior under varied conditions: The behavior of Burgers turbulence, particularly in terms of its Gaussian nature and sensitivity to initial conditions when subjected to complex forcing scenarios, remains inadequately explored.
- Intermittency caused by disruption of Galilean invariance: The interplay between viscous Ultra Violet regularization in small-scale structures and Infrared divergence in the large-scale and quantitative connection between these theoretical frameworks and empirical evidence of intermittency remained inadequately explored.

CHAPTER 2

MATHEMATICAL DEFINITION OF THE PROBLEM: THE EQUATIONS AND PRELIMINARY TOOLS

Transport phenomena, including turbulent flow, can be approximated by differential equations. The one-dimensional Burgers equation is the simplest nonlinear mathematical model frequently used to simulate such fluid regimes. In this chapter, we outline the foundational elements of the numerical simulation that yield solutions to our research problem. Initially, we explore the basic principles of chaotic systems, focusing on the fundamentals of randomness. Subsequently, we direct our attention towards the specifics of our research problem.

2.1 Deterministic versus stochastic models

The irregular and chaotic motions of the turbulent flows are characterized by the Stochastic processes. Stochastic processes are defined by equations that incorporate elements of randomness or uncertainty in their behavior. These equations reflect that, despite having knowledge of the initial conditions and governing laws, the future state of the system cannot be predicted with certainty. Instead, outcomes are understood probabilistically.

Conversely, deterministic or non-random systems are processes whose equations do not incorporate any terms that represent randomness or uncertainty. Such systems, governed by deterministic equations, allow for predictions about future states with complete certainty, provided that the initial conditions are known (Lord, Powell & Shardlow, 2014). In this section, our aim is to introduce the general form of stochastic differential equations, which encompass both deterministic and stochastic terms. A scalar, autonomous stochastic differential equation (SDE) in differential form is outlined below,

$$dX(t) = f(X(t))\,dt + g(X(t))\,dW(t), \quad 0 \le t \le T \tag{2.1}$$

The first term on the right-hand side of the equation is the deterministic term and the second term is considered as the stochastic process where f and g are both scalar functions and X is a

random variable. $W(t)$ is a scalar standard Brownian motion or standard Wiener process, and $dW(t)$ is the increment of the random process (Higham., 2001).

2.2 Randomness and correlation

Turbulence is a stochastic random phenomenon. After an initial transient phase, a turbulent flow can become statistically stationary, meaning that its statistical characteristics become time-independent. Typically, the auto-covariance function is the simplest tool that is employed to define the behavior of the variables compared to each other in a statistically stationary random process (Pope, 2000). In a more general manner in some literature, it is also referred to simply as the covariance function.

The general formula to calculate various orders of covariance functions for two points is as follows (Sefik & Christov, 1992):

$$Q_{ij}(s) = \langle u(k)^i u(k+s)^j \rangle = \lim_{L\to\infty} \frac{1}{2L} \int_{-L}^{L} u\,(k+s)^i + u\,(k)^j\, ds \tag{2.2}$$

Where i and j are covariance orders of each point, and $Q_{ij}(s)$ is a two-point, multi-order covariance function in terms of the wavenumber spectrum, and is only dependent on the wave number difference s. If we define the covariance function between two spatial points then s is called spatial separation, and if they are defined at different points in time then s is called time lag (Pope, 2000).

The normalized form of the above formula at one time over the spatial domain is

$$R_{ij}(r,t) = Q_{ij}(r,t)\ \{max_x \mid Q_{ij}(r,t)\}^2 \tag{2.3}$$

Where $R_{ij}(r,t)$ is called a two-point, one-time, multi-order correlation function.

As is evident in Figure 2.1, the normalized form of the correlation function of the initial random data used in the decaying Burgers simulation is zero over all the bandwidth which indicates that the values of the process are completely uncorrelated except for a value of unity at mode zero. It expresses one important characteristic of the white noise, which is Dirac's delta correlation

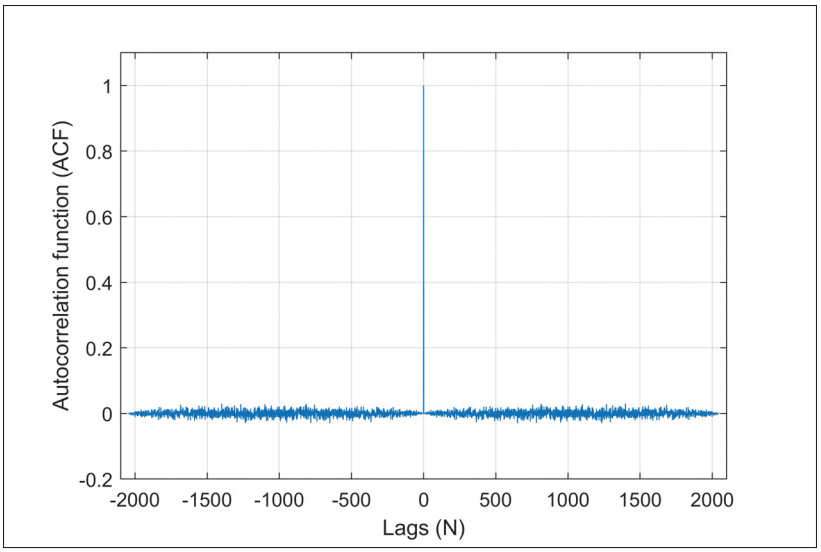

Figure 2.1 two-point, one-time, second-order correlation function of the initial data shows zero-correlation between the values of the initial random data

function, due to the inherent characteristic of the auto-correlation function (Sefik & Christov, 1992).

2.3 The Wiener process

The Wiener process, also known as Brownian motion, stands as a fundamental Markov stochastic diffusion process, serving as the basis for deriving all other random samples. This process is used to model aspects of turbulence, particularly in the stochastic modeling of turbulent diffusion (Pope, 2000).

It is defined as a random continuous process dependent on $t \subset [0, T]$ and satisfies the following conditions (Higham., 2001),

- The process starts at zero value with a probability of one: $W(0) = 0$.

- The process has Gaussian increments: for any $0 \leq t_1 \leq t_2$, the random variable $(W(t_2) - W(t_1))$ is normally distributed with mean 0 and variance $t_2 - t_1$, correspondingly, $dW(t) \sim \sqrt{dt}\mathcal{N}(0, 1)$ where $\mathcal{N}(0, 1)$ defines normal distribution with zero mean and unit variance.

- The process has continuous paths: for every t, the function $W(s)$ is continuous at $s = t$.

- The process has independent increments: for any $0 \leq t_1 \leq t_2 \leq t_3 \leq t_4$, the random variables $(W(t_2) - W(t_1))$ and $(W(t_4) - W(t_3))$ are independent.

Here we tried to mention the main features of this process briefly. We direct any readers seeking further information to Lawler (2006), Pope (2000), and Capasso & Bakstein (2005).

2.4 Problem definition

This study numerically simulates various forms of the one-dimensional Burgers equation for Newtonian fluids. The generalized form of the one-dimensional Burgers equation is as below,

$$\frac{\partial u}{\partial t} + a u^n \frac{\partial u}{\partial x} = \nu \frac{\partial^2 u}{\partial x^2} + f \tag{2.4}$$

Where u is the velocity vector, ν kinematic viscosity and f forcing term. We considered that the properties of the fluid including ν are constant.

For the linear advection-diffusion scenario, we set a equal to constant and $n = 0$ with no forcing term ($f = 0$).

For decaying turbulence, $a = 1$ and $n = 1$ are assigned, and in the inviscid case, we take viscosity $\nu = 0$.

In forced Burgers turbulence, a forcing term f is incorporated into the equation.

2.5 Initial conditions

We posed various initial conditions based on our aims in different simulations.

Considering the one-dimensional unsteady linear advection-diffusion equation and non-linear Burgers equations (2.4), we employed a sinusoidal initial velocity field $u\,(x, 0) = -U_0 \sin kx$ in which $U_0 = 1$, the initial wave number $k = n\frac{2\pi}{L_x}$ and n is the mode of the wave number. This approach was chosen to simplify the examination of the fundamental phenomena and to facilitate the validation of the solver, prior to investigating the turbulent phenomena.

For the decaying Burgers turbulence, we chose uniform white noise as our initial velocity field to guarantee an equal distribution of values, ensuring that no single value is predisposed towards

any specific mode. Uniform white noise defines a generalized stationary, constant mean and variance, stochastic process, which is uniformly distributed about the middle of the interval, with a constant energy level in all modes, and a finite variance (Kuo, 1996).

Conversely, for forced Burgers turbulence subjected to sinusoidal forcing, we employed a zero velocity field.

Meanwhile, for forced Burgers turbulence driven by a random forcing term, we adopted a random Wiener initial data, that is spatially homogeneous, with Gaussian distributed increments in line with the approach described by Jeng (1969), which is defined by the following formula;

$$u(x,0) = \int U(x-x')a(x')dx' \tag{2.5}$$

Where the kernel function U is an exponential weighting function, and is a crucial component that shapes the interaction between different points in space,

$$U(x) = 2(2/3)^{1/2}(1/2\pi)^{1/4}(1-2x^2)exp(-x^2) \tag{2.6}$$

where x is the point at which we are evaluating the velocity field u. When we compute $u(x,0)$, we are determining the velocity at the point x at the initial time ($t = 0$). x' is the variable of integration in our integral expression. It represents all possible points in the spatial domain that could contribute to the velocity at point x. So, when we integrate over x', we're effectively summing up (or integrating) the influences from all points x' on the velocity at point x.

2.6 Probability density function of the initial data

One of the key tools in our analytics toolkit is the probability density function (PDF). This statistical method plays a pivotal role in understanding the behavior and characteristics of turbulent dynamics. The PDF is a statistical function that describes the likelihood of a variable within a specific range in our dataset. It enables us to understand how velocity is distributed across its range to trace the formation of inherent structures. In this research, we generated initial data featuring various distributions.

For decaying Burgers turbulence, we employed a velocity field where the velocity is uniformly distributed within the interval $a \leq U < b$. This results in the following PDF function

$$f(U) = \begin{cases} \dfrac{1}{b-a}\,, & a \leq U < b. \\ 0\,, & U < a \text{ and } U \geq b. \end{cases} \tag{2.7}$$

In the case of forced Burgers turbulence with a random Wiener process initial velocity field, in section 2.3, we used Gaussian distributed data for the increments of the Wiener process with the following PDF function:

$$f(U) = \mathcal{N}(U; \mu, \sigma^2) \equiv \frac{1}{\sigma\sqrt{2\pi}} exp[-\tfrac{1}{2}(U-\mu)^2/\sigma^2] \tag{2.8}$$

where σ is the standard deviation and μ is the mean value of the data set (Pope, 2000).

2.7 Introducing forcing terms

In this thesis, we considered two distinct forcing terms, building upon the research works previously mentioned. One is the sinusoidal force term, and the other is a random force generated by the Wiener process, which is homogeneous in the x-direction and stationary over time.
Now consider Burgers turbulence subject to a driving force over a reasonably extended period of time. Equation 1.4 can be presented as follows in one dimension

$$\frac{\partial u}{\partial t} + u\frac{\partial u}{\partial x} = \nu\frac{\partial^2 u}{\partial x^2} + f \tag{2.9}$$

In the first scenario, the driving force F can be a smooth function that acts as a mechanism through which energy can be injected into the field. The outcome is a mechanism that introduces kinetic energy to the largest scales and transfers it, through the energy cascade due to nonlinear interactions, to the smallest scales where dissipation takes place. We confine the forcing term to

a sinusoidal function and we suppose

$$f = -Asin\,(\xi)\,, \quad A > 0 \tag{2.10}$$

with

$$\xi = kx - \omega t \tag{2.11}$$

Our primary focus is on analyzing the steady state, which signifies a state of equilibrium (Jeng & Meecham, 1972).

We now turn our attention to the second scenario: a force generated by a random Wiener process. A Gaussian forcing term $f(x,t)$ which is statistically homogenous in x and stationary in t (Jeng, 1969), as follows

$$f(x,t) = \int \int F(x-x',t-t')a(t')a(x')dx'dt' \tag{2.12}$$

where $a(x')$, $a(t')$ are Gaussian random data which were generated by a Wiener random process with Gaussian increments for both space and time. $F(x-x',t-t')$ is the specified non-random kernel function which is defined to inject most of the energy to the larger turbulence structures (small wavenumbers),

$$F(x,t) = (8/\pi)exp\{-2(x^2+t^2)\} \tag{2.13}$$

with the following characteristics (Meecham & Siegel, 1964),

- The kernel has a Gaussian, or bell-shaped, profile both in space and time. This means the influence of a point in space and time (denoted by x' and t') on another point (x and t) diminishes exponentially as the distance between them increases.
- The function is symmetric in both space and time which implies that the interaction is the same in all directions in space and uniformly changes over time.
- Due to its exponential nature, the Gaussian kernel has a localized effect. This means that points

close to each other in space and time have a stronger influence on each other than points that are far apart. The influence drops off rapidly with distance, which is characteristic of Gaussian functions.

- The kernel function itself is homogeneous in space and stationary in time; as its form does not depend on the absolute values of x or t, but only on the differences $x - x'$ and $t - t'$ and can support the homogeneity and stationary characteristics of the final forcing function.

2.8 Boundary conditions

In all cases, a periodic boundary condition was imposed, defined as $u(-l, t) = u(l, t)$ where the domain length is $L_x = 2l$.

Initially, we employed a domain length ($L_x = 2$), $-1 \leq x \leq 1$, to model the equations as a preliminary step. However, in order to model forced Burgers turbulence with a sinusoidal forcing function, we adhered to the domain length proposed by Jeng & Meecham (1972). They recommended a domain length of $L_x = 1$, with ($0 \leq x \leq 1$), and for modeling forced Burgers turbulence with random forcing we switched to $-\pi \leq x \leq \pi$, denoting $L_x = 2\pi$, to accommodate integer wave numbers. Each simulation was accompanied by its own specific boundary conditions.

2.9 Analytical solutions

In this section we briefly discuss the analytical solutions of the different forms of the Burgers equation.

As we assume the Advection-Diffusion equation is dependent on spatial periodic conditions, after making the change of variables, imposing the method of separation of variables, and using the orthogonality property of Fourier expansions, then the analytical solution will be obtained as follows (Mojtabi & Deville, 2015),

$$u(x, t) = -sin(n\pi(x - at))e^{-\nu\pi^2 t} \tag{2.14}$$

Figure 2.2 demonstrates the analytical solution of the advection-diffusion equation,

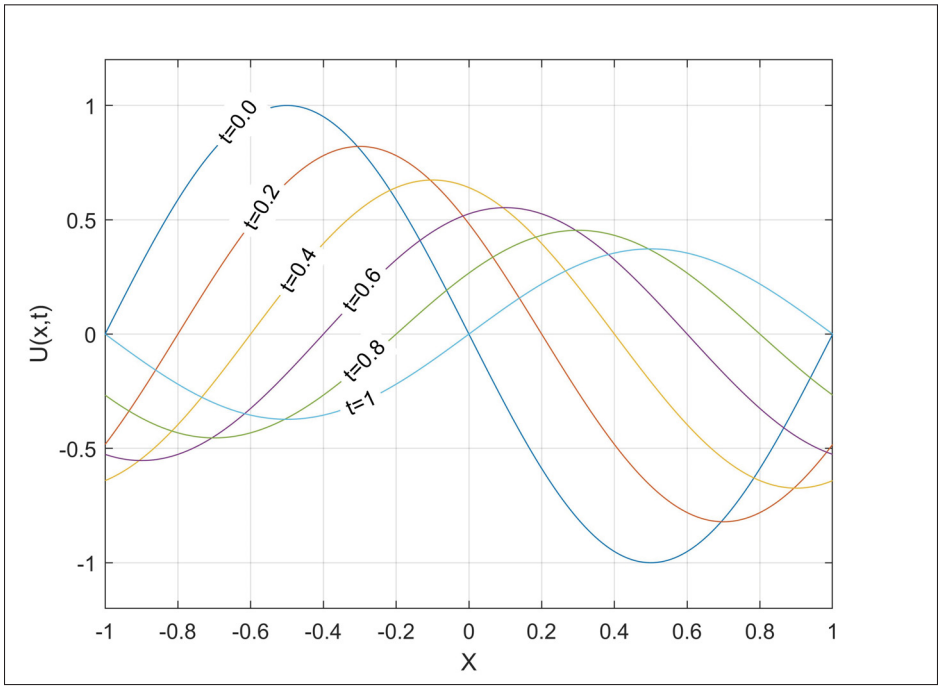

Figure 2.2 Analytical solution of the advection-diffusion equation with kinematic viscosity $\nu = 0.1$, at different times

Now we are considering the analytical solution of the unforced one-dimensional decaying Burgers equation. A spatially periodic analytical solution of this equation in which Fourier coefficients can be stated explicitly as a function of t was obtained by Cole (1951) and compiled by Benton & Platzman (1972). However, as their solution was not tractable in a small time ($0 \leq t \leq 2\pi$) a better solution was proposed by Basdevant *et al.* (1986).

For this problem, the periodic domain is taken to be $L_x = 2\pi$ with the initial function $u\,(x, 0) = -U_0 \sin k_x x$ in which $k_x = \pi$ and $U_0 = 1$.

$$u\,(x,t) = \left[\frac{-\int_{-\infty}^{\infty} sin\ \pi(x-\eta)\ f(x-\eta)\ exp(-\eta^2/4\nu t) d\eta}{\int_{-\infty}^{\infty} f(x-\eta) exp(-\eta^2/4\nu t) d\eta} \right] \tag{2.15}$$

In which $f(y) = exp(-cos\ \pi y/2\pi\nu)$ and the integral is evaluated using Hermite integration (Basdevant *et al.*, 1986). Figure 2.3 depicts the analytical solution of the Burgers' equation at various times.

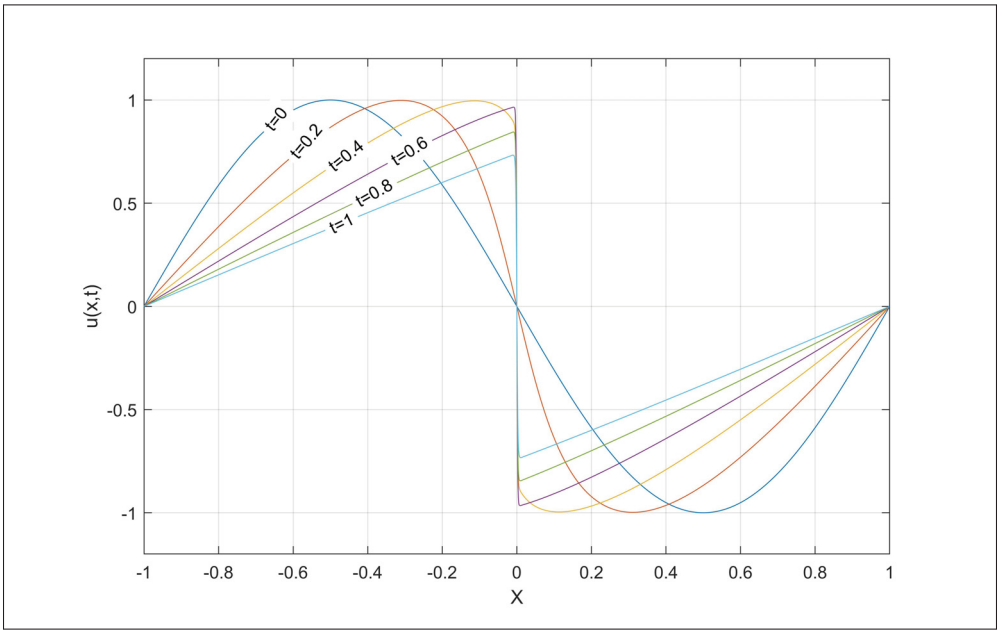

Figure 2.3 Analytical solution of the one-dimensional Decaying Burgers equation where $\nu = 0.001$, with the number of terms in each series equal to 250

Let's examine Burgers turbulence when it is influenced by a driving force over a significant time duration. The equation, referred to as 1.4, can be expressed in one dimension as:

$$\frac{\partial u}{\partial t} + u\frac{\partial u}{\partial x} = \nu\frac{\partial^2 u}{\partial x^2} + f \tag{2.16}$$

For the purpose of simplicity of the analytical solution, we can consider the inviscid ($\nu = 0$) forced Burgers equation

$$\frac{\partial u}{\partial t} + \frac{1}{2}\frac{\partial u^2}{\partial x} = f \tag{2.17}$$

By substituting Equation 5.1 as the forcing term in Equation 2.17 and solving, we have the following solution which is depicted in figure 2.4

$$u = c \ \pm \ c(2a)^{1/2} cos\frac{\xi}{2} \tag{2.18}$$

Which is confirmed for the values of the force with $a = \frac{2A}{kc^2}$ where $k = 2\pi/L_x$ is the wavenumber

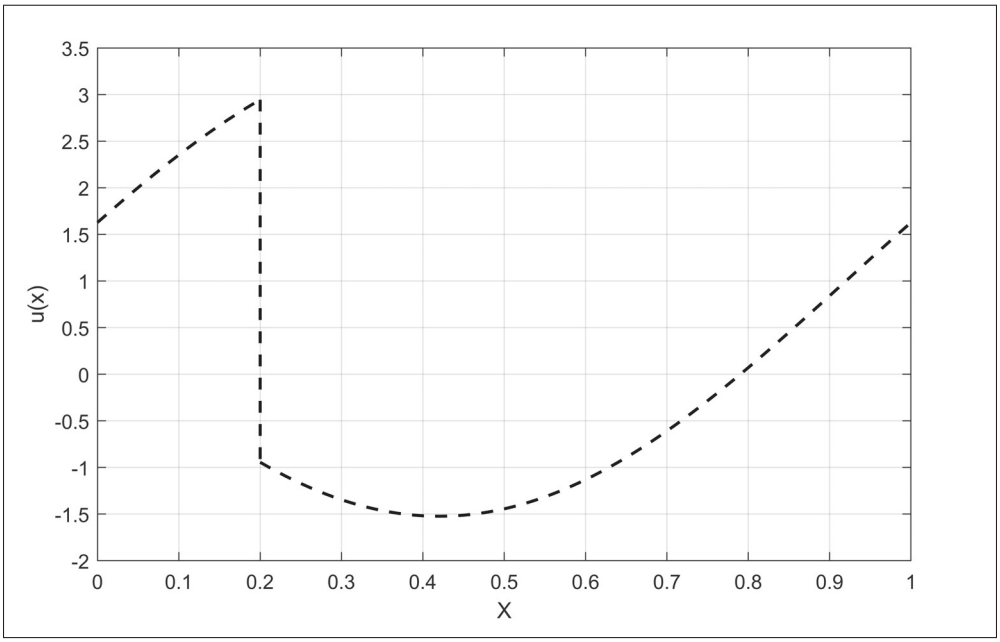

Figure 2.4 Analytical inviscid solution of the one-dimensional Burgers equation with sinusoidal forcing term. The two sides of the inviscid solution are bridged by a vertical line representing a discontinuity, which is identified as the shock position

of the forcing term and $c = \frac{\omega}{k}$ is the speed of the moving force, and the sign change happens by a discontinuity at the shock position ξ_0 (Jeng & Meecham, 1972).

$$\xi_0 = 2sin^{-1}(\pi^2/8a)^{\frac{1}{2}} \tag{2.19}$$

The magnitude of the forcing term is manipulated by varying the amplitude A of the sinusoidal function. Increasing amplitude will increase energy input and likely the magnitude of the velocity fluctuations. Thus, to ensure accuracy in our numerical results, we construct an inviscid

solution due to its close resemblance to the solution for small, non-zero viscosities, Figure 2.4. This approach aids in validating the integrity and reliability of our findings.
The final simulation we are going to discuss in this research, namely forced Burgers turbulence with a random force, lacks an analytical solution, and therefore, we are unable to present any exact solution for it in this section.

2.10 Introduction to the spectral approximation and the Fourier method

When it comes to the periodic domains, same as our problem, the expansion of the Fourier series is the elected candidate due to the presence of sines and cosines terms, as the renowned trial (basis) functions for all the periodic problems (Boyd, 2001). The existence of the trial and test functions in the fundamental formulation of the spectral methods made them a valuable class of spatial discretization to solve ordinary and partial differential equations. It is crucial to keep in mind that the trial functions and the test functions are essentially the same in the Fourier-Galerkin method and should satisfy the orthogonality condition (Sahnkar,Dale Anderson, 2020).
Consider $u(x)$ as a function that we want to present using the Fourier series. Suppose one spatial dimension with a periodic continuous domain bounded on $0 \leq x \leq 2\pi$. The Fourier expansion of the function $u(x)$ is as follows,

$$u\left(x\right) = \sum_{k=-\infty}^{\infty} \hat{u}\left(k\right) \times e^{ikx} \tag{2.20}$$

As the infinite number of terms in the formal expansion of $u(x)$ is not easy to achieve, we consider the approximated function $u^N(x)$ that corresponds to N degree of freedom which is presented here as the truncated Fourier series of $u(x)$ (Canuto, 2006),

$$u^N\left(x\right) = \sum_{k=-N/2}^{N/2-1} \hat{u}\left(k\right) \times e^{ikx} \tag{2.21}$$

In which $|u(x) - u^N(x)|$ uniformly converges to zero as N tends to infinity (Canuto, 2006). In the above formula, the fundamental unknown is the Fourier coefficient $\hat{u}\left(k\right)$ which obtains as a

function of wavenumber. It defines as the FFT function,

$$\hat{u}\,(k) = \frac{1}{2\pi}\int_{-\pi}^{\pi} u^N\,(x)\,e^{-ikx}dx \tag{2.22}$$

2.11 Spectral convergence and accuracy

The Fourier series has the property of exponential or spectral convergence, which means the decay rate of Fourier coefficients is faster than the algebraic convergence in high wave numbers.

$$\hat{u}\,(k) \ll \frac{1}{k^n}\,, \qquad k \gg 1 \tag{2.23}$$

In which n is the algebraic index of convergence and the Lebesgue integral of $|u(x)|$ is finite. This behavior can easily be concluded using the Riemann-Lebesgue lemma as a result of the Fourier analysis (Gottlieb & Orszag, 1977).

As the exponential convergence rate of Fourier coefficients causes the truncated Fourier series to converge toward the exact solution faster than any finite power of $\frac{1}{k}$, likewise, the maximum error will decay faster than algebraic as the grid spaces get finer and the spectral resolution increases. This is the reason for the spectral methods' significant accuracy and their remarkable advantage which we will benefit from in our simulations (Beardsell, 2016).

CHAPTER 3

METHODOLOGICAL FRAMEWORK: NUMERICAL TECHNIQUES AND DISCRETIZATIONS

In this chapter, our goal is to introduce the various tools we utilized to implement the different stages of simulations for modeling Burgers' turbulence. This research work is carried out using solvers developed within the MATLAB software environment.

3.1 Initial Implementations: Tools and Techniques

The initial implementation as a pre-processing stage is the foundational phase in numerical simulations where we set the groundwork for our analysis. This stage focuses on introducing the tools and techniques necessary for establishing the simulation environment and preparing the initial data required to conduct our simulations.

3.1.1 Generating initial velocity field

As mentioned earlier in section 2.5, we selected different initial data tailored to specific objectives. Now consider the scenario of decaying Burgers turbulence. To generate uniformly distributed random white noise as the initial data, we used Mersenne Twister algorithm to generate pseudo-random uniform data and Ziggurat random normal distributed data generator algorithm for Gaussian distributed data in various sample sizes and rooted the data, setting a fixed seed for a random number generator to ensure that the same sequence of "random" numbers is produced every time the code is run or the random data will not change in different simulations. This algorithm is the most popular choice for generating random numbers due to its long period $2^{19937} - 1$ which is relatively large in addition to being relatively fast (Matsumoto & Nishimura, 1998). Moreover, every two values of this random velocity field are uncorrelated, with zero auto-correlation. As a random variable is fully characterized by its one-time Probability density function (PDF), so we can define a uniformly distributed velocity field in the interval of

$-0.5 \leq U \leq 0.5$ in the form of the probability density function $f(U)$ as follows (Pope, 2000),

$$f(U) = \begin{cases} 1 & -0.5 \leq U \leq 0.5. \\ 0 & U < -0.5 \text{ and } U > 0.5. \end{cases} \tag{3.1}$$

We used Kernel Density estimation, Kernel smoothing, to evaluate the PDF of the uniformly distributed random initial velocity field U in Figure 3.1

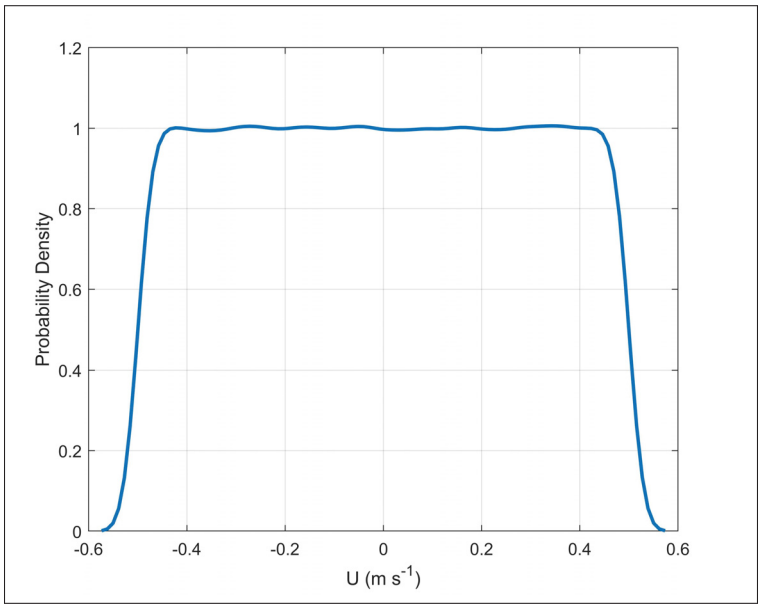

Figure 3.1 Probability density function of the uniformly distributed white noise in the interval of $-0.5 \leq U \leq 0.5$ with sample size equal to $N = 2^{11}$

Now, consider the forced Burgers turbulence driven by a random Wiener process forcing term following Jeng (1969). To generate the initial Gaussian velocity field using Wiener process, equation 2.5, we initially created random white noise base data following a Gaussian distribution, which represented the increments, of the Wiener process 3.2.

Then, we used these increments to generate a new dataset through the application of the Wiener process as depicted in fig 3.3

To support spatial homogeneity condition in the initial velocity field we inject a Gaussian kernel function 2.6 to the random data set to make their statistical properties dependent on position

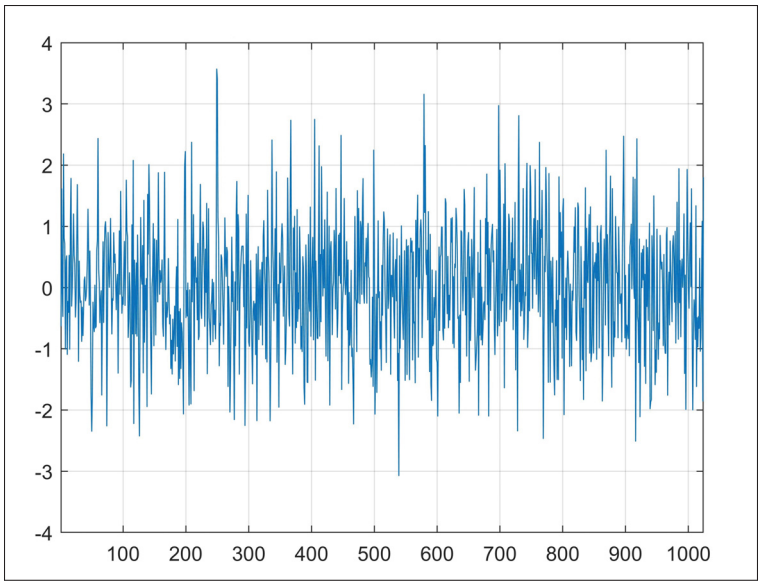

Figure 3.2 random white noise data with Gaussian distribution as the increments of the Wiener process

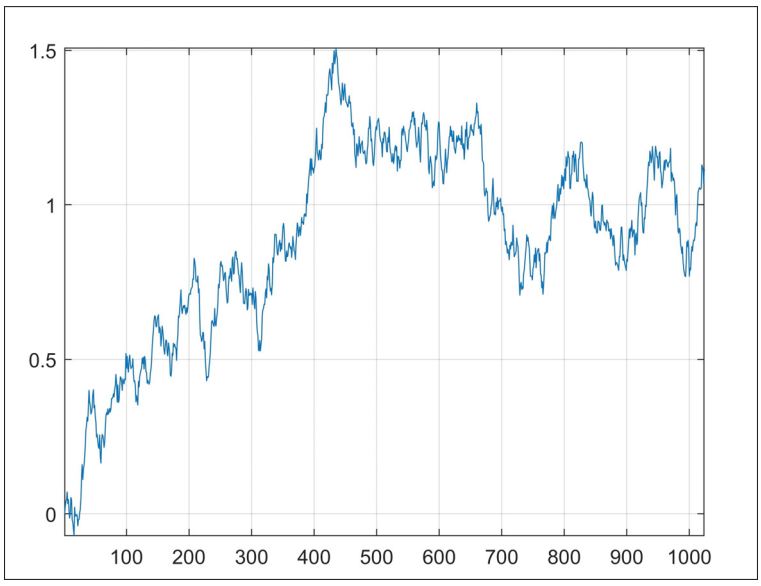

Figure 3.3 wiener process random data with gaussian increments

differences, not the absolute positions; and finally we integrate it over the entire domain to obtain the expected initial velocity field as clarified in section 2.5.

In our research, we will employ another set of initial data for the simulations discussed in Section 5.5.2. This selection is designed to explore the interactions across various energy spectrum ranges by selectively eliminating the energy at certain wavenumbers. To achieve this, we start by initializing the system with uniform re-normalized random data, ensuring that no initial values are biased towards specific wavenumbers. Our simulation started with initial data whose wavenumber range was confined within the inertial range, ensuring that wavenumbers outside this range were initially unenergetic. By identifying the inertial range through the k^2 power law, section 4.6, we then characterized the remaining wavenumbers outside this range as follows (Girimaji & Zhou, 1995):

$$\hat{u}\,(k,0) = \begin{cases} \hat{u}\,(k,0) & k_i \;\leq k \leq k_f, \\ 0 & \text{for other } k, \end{cases} \tag{3.2}$$

In the following section, we delve into further details on the process of renormalizing data.

3.1.2 Re-normalizing Initial data

In turbulent flows, energy is typically distributed across a range of scales or frequencies, each corresponding to a distinct Fourier mode in our simulation. For a state of fully developed turbulence, where energy is generally perceived as being distributed more or less evenly across these scales, it is necessary to maintain a uniform energy level across all modes, ensuring that no particular value is biased towards any specific mode. The process of re-normalizing the initial data helps us achieve this uniform energy distribution. This involves adjusting the amplitudes of the Fourier modes so that the sum of the squares of these amplitudes - which represents the total energy - remains constant across all modes. To accomplish this, we re-normalize each mode by dividing them by the modulus of the mode, thereby achieving an equal modal energy level across all modes as depicted in Figure 3.4,

After re-normalization, we observed an interesting behavior. The initial random data transformed from a uniform distribution to the Gaussian Figure 3.5. When we re-normalizing data, we

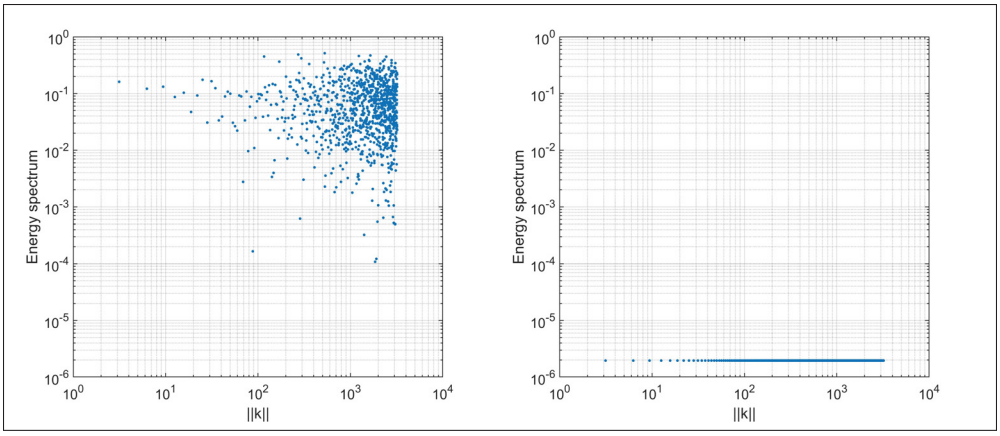

Figure 3.4 Energy spectrum of the initial data before re-normalization (on the left) and after re-normalization (on the right). The re-normalization process creates a constant modal energy level (Sample size equal to $N = 2^{11}$)

are effectively creating a new set of random variables. The renormalization process we are performing can be seen as a form of averaging, where we're dividing each Fourier mode by its modulus. This process is similar to summing a large number of independent random variables and then dividing them by their number, which is the kind of operation that applies to the theory called the Central Limit Theorem (CLT). The CLT states that the sum of a large number of independent and identically distributed random variables, each with a finite mean and variance, will approximate a Gaussian (or normal) distribution, regardless of the shape of the original distribution (Montgomery & Runger, 2011). Considering the preceding discourse, the data, having been re-normalized, is suitably prepared to initiate the subsequent computational simulations.

For the Gaussian Wiener process random velocity field, no re-normalization was performed. However, for the kinetic energy, we utilized a re-normalization technique by dividing the initial kinetic energy by its magnitude and setting it to 1.

For the forced Burgers with random force term, we determine the Reynolds numbers as $Re = \frac{VL}{\nu}$, then we select the velocity scale V as the square root of the initial kinetic energy $u^2(x, 0)$ equal to unity. The length scale L is chosen as $2k_{max}^{-1}$ in which k_{max} represents the wave number at where the initial energy spectrum peaks. With these scales, the initial kinetic energy is renormalized and set to 1, and the initial energy spectrum reaches its maximum when $k = 2$, ensuring that the

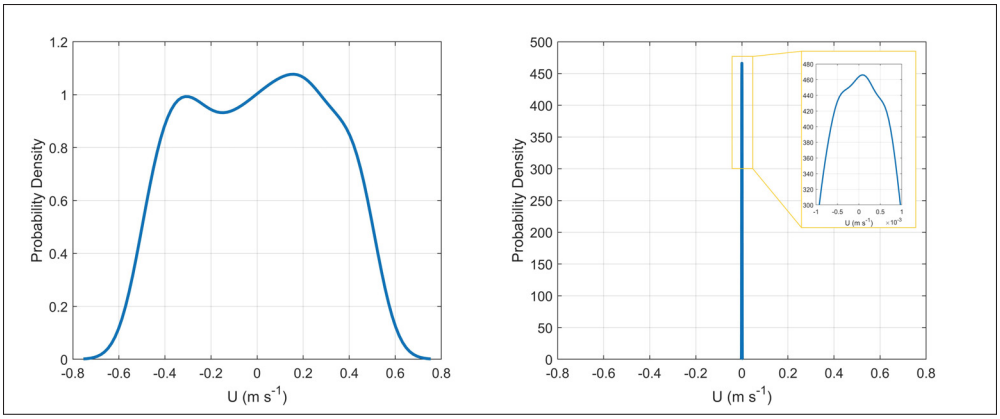

Figure 3.5 The probability density function of the initial random data before re-normalization (on the left) and after re-normalization (on the right). The re-normalization process transforms data toward Gaussian distribution, regardless of the shape of the original distribution (Sample size equal to $N = 2^{11}$)

integral of the initial energy spectrum across the entire wavenumber domain equals 0.5(Jeng, 1969). Thus we have $Re = \frac{1}{\nu}$.

3.1.3 Generating the Forcing Term

We have already covered the generation of sinusoidal forcing in detail. In this section we just mention extra details to produce the random forcing term following the research work conducted by Jeng (1969). The forcing term follows the equation 2.12.

Here, we apply similar steps to the Gaussian random force as we did with the Wiener initial velocity field, albeit with added complexities. To apply double integration over the domain of the equation 2.12, we executed nested summations across discrete grid points, covering both spatial and temporal dimensions. To add spatial homogeneity and temporal stationarity to the forcing term $f(x,t)$ we employed a kernel function, 2.12, possessing these characteristics and multiplied it by the aforementioned random functions. The kernel function F is illustrated in figure 3.6.

What we obtain is the random Gaussian forcing term, derived from the Wiener process, which exhibits homogeneity in space and stationarity in time.

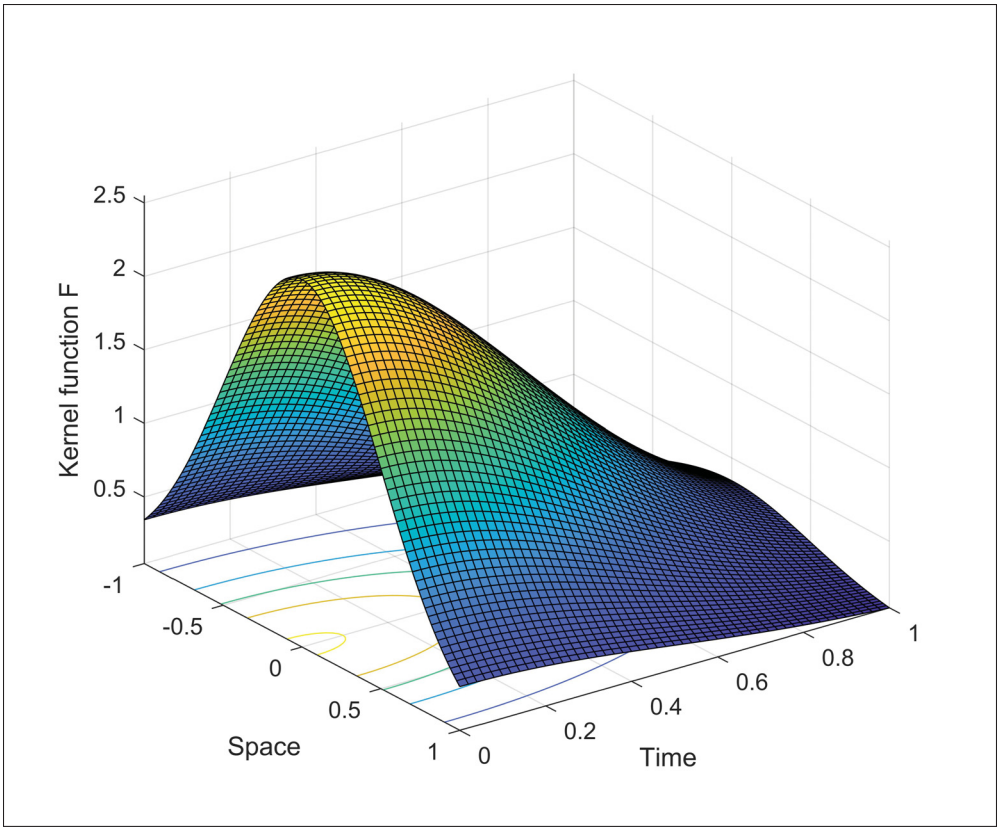

Figure 3.6 The Gaussian kernel function F which supports the homogeneous and stationary characteristics of the final forcing function

We ultimately advance the unforced equation using the appropriate time integration method and subsequently incorporate the forcing term, f, into the velocity field after each time step δt.

3.2 Processing stage: Spectral solver, discretizations and errors

In this section, we delve into the processing stage of the numerical simulations, a vital phase where our initial setups and theories are actively implemented. We'll explore key aspects of this stage, focusing on solving equations using spectral solvers, spatial discretization, and time integration, as well as addressing significant errors in our solvers. This subsection aims to demonstrate how these components collaboratively transform our initial ideas and models into practical and insightful findings.

3.2.1 Fourier-Galerkin spectral solver

In each time step, we implemented the Fourier transform through the whole spatial domain to transform the governing equations into the Fourier space.

$$\hat{u}_k\left(k,t\right)=\frac{1}{2\pi}\int_{-\pi}^{\pi}u^N\left(x,t\right)e^{-ikx}dx \tag{3.3}$$

Then, we transformed back the solution of the obtained coefficient system into the physical space by the following Fourier expansion.

$$u\left(x,t\right)\approx P_N u(x,t)=u^N\left(x,t\right)=\sum_{k=-N/2}^{N/2-1}\hat{u}\left(k,t\right)\times e^{ikx} \tag{3.4}$$

where $k=m\frac{2\pi}{L_x}$ is the wavenumber, L_x is the domain length equal to 2π and $\frac{-N}{2}<m<\frac{N}{2}+1$.

3.2.2 Spatial discretization in the Fourier space

The spatial Fourier transform of Eq.(1.4) specified as,

$$\left(\frac{d}{dt}+k^2\nu\right)\hat{u}=-\widehat{u.\nabla u}+\hat{f}(k) \tag{3.5}$$

In which the spatial Fourier transform of the forcing term is given by $\hat{f}(k)$. Imagine eliminating the forced term; what will remain is the discretized version of the nonlinear decaying Burgers in the Fourier space, the Fourier transform of Eq.(1.2) yields

$$\left(\frac{d}{dt}+k^2\nu\right)\hat{u}=-\widehat{u.\nabla u} \tag{3.6}$$

By substituting constant advection velocity a as a coefficient of diffusion, instead of instantaneous velocity u, we get the linearized form of the above equation. Thus, the linear Convection-Diffusion

equation in Fourier space is as follows,

$$\left(\frac{d}{dt} + k^2\nu\right)\hat{u} = -ika \tag{3.7}$$

Which is identified as the governing ODE in the Fourier space (Canuto, 2006).

3.2.3 Integrating factor technique

Consider the strong form of the decaying Burgers equation 2.4. After Integrating the functions of the PDE in Sobolev space of the test function; we will obtain the weak form of the semi-discrete Fourier Galerkin formulation of the Burgers equation, which is shown below in one dimension

$$\frac{d\hat{u}_k}{dt} + \hat{\mathcal{G}}_k(\hat{u}) + k^2\nu\hat{u}_k = 0 \tag{3.8}$$

In which the discrete nonlinear $\hat{\mathcal{G}}_k(\hat{u})$ operator is defined as an advection term. After multiplying both sides of the above equation by the integrating factor $e^{\nu k^2 t}$, we have

$$\frac{d}{dt}\left[e^{\nu k^2 t}\hat{u}_k\right] = -e^{\nu k^2 t}\hat{\mathcal{G}}_k(\hat{u}_k) \tag{3.9}$$

By using a change of variable and imposing 1st order Explicit Euler approximation as a testing ground, one obtains

$$\hat{u}_k^{n+1} = e^{-\nu k^2 \Delta t}\left[\hat{u}_k^n - \Delta t\hat{\mathcal{G}}_k(\hat{u}_k^n)\right] \tag{3.10}$$

Thus, only the nonlinear term is responsible for the accuracy and instability of the temporal scheme as the linear viscous term is exactly integrated and is unconditionally stable. A more detailed discussion is available in (Canuto, 2006).

3.2.4 Time integration

We evaluated three distinct numerical methods as time discretization techniques to deal with the diterministic terms. To approximate stochastic differential terms, such as the random force, we employed Itô calculus. The forcing term is integrated into the velocity field and introduced to the model at the end of each time step δt (De *et al.*, 2023). Time steps were selected based on the CFL condition and the trial-and-error approach, to keep the simulations stable in various viscosities.

3.2.4.1 Diterministic terms

In this work, we used Finite difference time discretization methods in conjunction with the spatial spectral techniques. To this aim, the transient term of equation 2.4 plugged into three different Finite Difference methods, including first-order Explicit Euler, second-order Adam-Bashforth, and third-order compact Runge-Kutta scheme to integrate temporal derivative explicitly. Subsequently, we assessed these three schemes to identify the most suitable one among them. Ultimately, considering both the order of accuracy and stability, the compact Runge-Kutta 3rd-order scheme was selected as the most appropriate method. Detailed information about these numerical schemes can be found in Appendix I.

3.2.4.2 Stochastic terms

One approach to deal with the stochastic differential terms, such as the random forcing term in our model, involves employing Itô calculus. One simple numerical scheme for approximating solutions to stochastic differential equations (SDEs) based on the Itô calculus is the Euler-Maruyama method. This scheme is an extension of the Euler method for ordinary differential equations to stochastic calculus. the Euler-Maruyama numerical method for a stochastic differential equation (**?**), Consider $\tau_j = j\Delta t$

$$X_j = X_{j-1} + f(X_{j-1})\Delta t + g(X_{j-1})(W(\tau_j) - W(\tau_{j-1})) \tag{3.11}$$

If g function is equal to one then we have a constant diffusion process coefficient. In this case, the noise impacts the system in a state-independent way, which means the SDE is directly proportional to the Wiener process increment. This would be the case for a simple Wiener or Brownian motion process.

3.2.5 Aliasing error and de-aliasing techniques

Returning to solve the discretized governing equations in the Fourier space in section 3.2.3 and specifically equation 3.6, the general quadratic non-linear advection term $u.\nabla u$, which is the product of two functions, defines under the Fourier Galerkin treatment in a one-dimensional case as follows,

$$u\partial_x u = \left(\sum_{|m| \leq \frac{N}{2}} \hat{u}_m e^{imx} \right) \left(\sum_{|n| \leq \frac{N}{2}} in\hat{u}_n e^{inx} \right) = \sum_{|k| \leq N} \widetilde{s}_k e^{ikx} \tag{3.12}$$

The above formulation that is obtained by the expansion of truncated Fourier series generates higher wavenumber k that is equal to $m + n$, wavenumbers out of the physical domain $S_N \in [-\frac{N}{2}, \frac{N}{2}]$, that are aliased into the original wavenumbers m and n inside the range of S_N. The $\hat{s}_k$ is the Fourier coefficient of the non-linear advection term which is subjected to a convolution sum in the spectral domain. There are two approaches to calculating this $\hat{s}_k$. One is to calculate it inside the Fourier space as a direct convolution of the two functions $\hat{s}_k = \sum_{m+n=k} \hat{u}_m \hat{u}_n$ which takes $O(N^2)$ operations in one dimension and $O(N^4)$ operations in three dimensions as discussed in (Canuto, 2006). Thus, it is too expensive to calculate compared with many other schemes like finite differences as it takes $O(N)$ operations in one dimension ($O(N^3)$ in three dimensions). However, (Orszag, 1971) developed a technique that requires $O(N \log_2 N)$ operations ($O(N^3 \log_2 N)$ operations in three-dimension) called pseudo spectral method, which evaluate the convolution sum inside the physical space instead, to make the spectral Galerkin methods affordable (Canuto, 2006).

Here, we consider a new Fourier coefficient $\widetilde{s}_k$; that amounted to the coefficients in the physical domain and the coefficients with the wavenumbers aliased into the same range; the latter is

marked as the aliasing error.

$$\widetilde{s}_k = \widehat{u.\nabla u} = \sum_{\substack{m+n=k \\ |k|\leq \frac{N}{2}}} in\hat{u}_m\hat{u}_n + \sum_{\substack{m+n=k \\ \frac{N}{2}<|k|\leq N}} in\hat{u}_m\hat{u}_n = \hat{s}_k + \sum_{\substack{m+n=k \\ \frac{N}{2}<|k|\leq N}} in\hat{u}_m\hat{u}_n \tag{3.13}$$

As explained earlier, the second term on the right-hand side is the aliasing error (Canuto, 2006) which can cause artificial energy accumulation at small scales, uncontrolled growth of energy, and eventually numerical instability. This instability generates an amplified cascade of energy spreading over the whole wavenumber spectra of the turbulent flow (Boyd, 2001).

The researchers suggested multiple techniques to deal with aliasing errors in the decades. As a result, some researchers evade de-aliased pseudospectral methods (of even strongly damped flows). They believe aliasing errors are presented chiefly on smaller scales with high wave numbers and vanishing viscosities. So, larger energy-containing scales are less affected by Aliasing (Bowman & Roberts, 2011).

One technique to remove aliasing is filtering out high wave number components, termed the Zero padding technique or two-third rule (alternatively 3/2 Rule), which was suggested by Orszag firstly in 1971 in an article less than a page, removes aliasing wavenumbers utilizing discrete transform with $|k| < (\frac{2}{3})K$ rather than K wavenumber where $K = \frac{1}{2}L_x\pi$. He showed that if we filter out all waves with $|k| > (\frac{2}{3})K$ then the non-linear quadratic interaction of each two wave numbers equation3.13 will be aliased only to the purged wavenumbers (Boyd, 2001). We need to keep (2/3) N grid points to have an alias-free approximation. But cutting off high wavenumbers leads to the Gibbs phenomenon and loss of L2 energy. So, the trick is to calculate non-linear terms on (3/2) N physical grid points but add N/2 zeros to the Fourier coefficients in the Fourier space (Boyd, 2001). Thus, surviving wavenumbers are alias-free.

There are also some other alternative remedies to remove aliasing from non-linear quadratic terms. The most promising one is the phase shift technique (Patterson & Orszag, 1971) which acts by disrupting the alignment of the modes through random phase shifts without altering their amplitudes, however, it is always more expensive than the two-third rule (Canuto, 2006).

After numerous attempts, we ultimately selected the pseudospectral method with the 2/3 de-aliasing technique in all of our solvers.

3.3 Post-Processing Strategies: Tools and Techniques for Analyzing Simulation Results

The 'Post-Processing' stage is a critical phase in simulations, where the raw data generated during processing is transformed into meaningful insights. In this subsection, we delve into the methods and tools used to analyze and interpret the results of our simulations.

3.3.1 Energy Spectrum

We present the energy spectrum of the velocity field $E(k)$ to show the validity of our numerical simulations. The energy spectrum is a measure of the distribution of energy across the wavenumber spectrum in a turbulent flow. It is a powerful tool for understanding the characteristics of turbulent flow, such as the scale of the turbulent eddies and the amount of energy present at each scale. It is considered as the Fourier transform of the auto-covariance function $R(s)$ (Pope, 2000), section 2.2.

$$E\left(k\right) = \frac{1}{2\pi} \int_{-\infty}^{\infty} R\left(s\right) e^{-iks} ds \tag{3.14}$$

In which, $R_{ij}(s)$ has the Fourier series.

$$R_{ij}\left(s\right) = \sum_{k} \hat{R}_{ij}\left(k\right) e^{iks} \tag{3.15}$$

And the Fourier coefficients of the two-point velocity correlation are as follows,

$$\hat{R}_{ij}\left(k\right) = \mathcal{F}_k\left(R_{ij}\left(s\right)\right) = \langle \hat{u}_i^*(k)\hat{u}_i(k)\rangle \tag{3.16}$$

From complex conjugate symmetry $\hat{u}_i\left(k\right) = \hat{u}_i^*\left(k\right)$, it is more convenient to consider half energy spectrum for any non-negative wavenumber,

$$E\left(k\right) = \frac{2}{\pi} \int_{0}^{\infty} R\left(s\right) \cos\left(k * s\right) ds \qquad k > 0 \tag{3.17}$$

The half energy spectrum is a common technique used in turbulence analysis, particularly for flows that exhibit mirror symmetry. Since the energy spectrum is symmetric about the origin in Fourier space, the energy for negative wavenumbers is equal to the energy for positive wavenumbers, so we can obtain the full energy spectrum by doubling the energy values for positive wavenumbers.

In addition, the energy at the $k = 0$ mode is frequently called the "zeroth mode" and signifies the energy associated with the greatest length scale (Pope, 2000). To calculate the overall energy density, you must evaluate the energy associated with the zeroth mode and combine it with the half-energy spectrum.

3.3.2 Turbulent Kinetic Energy, TKE

Turbulent kinetic energy (TKE) is a measure of the energy associated with turbulent fluid motion. TKE plays a crucial role in turbulence as it governs the transfer of energy between different scales in a turbulent flow. It is defined as the sum of the kinetic energy of the turbulent fluctuations around the mean flow velocity. In mathematical terms, TKE in physical space can be expressed as (Tennekes & Lumley, 1978).

$$TKE = \frac{1}{2} \int_{-\infty}^{\infty} K\left(x\right) dx \tag{3.18}$$

Where $K(x) = \frac{1}{2}u(x)^2$ is the Kinetic energy at each collocation point at a single time stage and $u(x)$ is the fluctuating velocity deviating from the mean flow velocity. To calculate the kinetic energy content of flow in the Fourier space we use the following formula.

$$TKE = \frac{1}{2} \int_{0}^{k} E\left(k\right) dk \tag{3.19}$$

In which $E(k)$ is the energy spectrum of Fourier coefficients discussed earlier.

3.3.3 Energy dissipation rate

Up to this point, we have talked about the change in the kinetic energy content of the system within both the physical and spectral domains. Now we are trying to discuss the dissipation of this energy caused by the viscous interactions on small-scale structures. The rate at which energy dissipates is characterized by the energy spectrum of the flow in the Fourier domain, so if we assume that the flow is statistically homogenous and isotropic and the energy spectrum follows the power law in the Inertial subrange (Pope, 2000), then we can define the energy dissipation as

$$\varepsilon = \sum_{k} 2\nu k^2 E\left(k\right) \tag{3.20}$$

In which ε is called the energy dissipation rate. To obtain the energy dissipation rate in Physical space we first define the viscous dissipation rate of the isotropic turbulence in the physical space as follows (Tennekes & Lumley, 1978),

$$\varepsilon = 2\nu\overline{s_{ij}s_{ij}} \tag{3.21}$$

The above equation is the rate at which viscous stresses carry out work on the fluctuating strain rate through deformation which always leads to the drain of energy. $\overline{s_{ij}s_{ij}}$ is the mean value of the quadratic form of the strain rate and in 1D Burgers Turbulence is related to the velocity gradient.

$$\varepsilon = 2\nu \int \left(\frac{\partial u}{\partial x}\right)^2 dx \tag{3.22}$$

This expression represents the rate at which kinetic energy is converted into internal energy due to the viscous forces in the physical space. As a result, the viscous stresses in the 1D Burger's equation play a critical role in damping the kinetic energy of the flow and promoting its dissipation.

3.3.4 Analyzing PDF at Various Time Stages

In this research, we evaluated the Probability Density Function (PDF) to understand the dynamics of the flow and observe its evolution over time. For this purpose, we employed the Kernel Density Estimation (KDE) method, as outlined by (Węglarczyk, 2018). The KDE is mathematically represented as follows:

$$f(U) = \frac{1}{nh} \sum_{i=1}^{n} K\left(\frac{U - U_i}{h}\right) \tag{3.23}$$

Here, n represents the number of data points, U_i denotes the individual data points, h is the bandwidth, and K is the kernel smoothing function. We utilized the Normal smoothing kernel function for Gaussian datasets and the Epanechnikov smoothing kernel for Non-Gaussian datasets.

3.3.5 Higher order central moments of distribution

In turbulence research, studying higher-order central moments, particularly skewness and kurtosis (flatness factor), provides valuable insights into the behavior and structure of turbulent flows. They serve as measures to quantify the asymmetry and intermittency of the turbulence, which helps in understanding the underlying dynamics and structure formation of turbulent flows (Davidson, 2015).

Skewness is a measure of the asymmetry of a probability distribution. For a real-valued random variable, skewness is defined as the standardized third central moment. It is calculated as:

$$S = \int_{-\infty}^{\infty} x^3 f(x) dx / \sigma^3 = \langle X^3 \rangle / \langle X^2 \rangle^{3/2} \tag{3.24}$$

In which σ is the standard deviation of the distribution with zero means $\langle X \rangle = 0$. The skewness can provide information on the asymmetry of the velocity distribution, which may arise due to the non-linear advection term leading to the formation of the shock-like structures.

Kurtosis is a measure of the "tailedness" of the probability distribution, which essentially

quantifies the occurrence of extreme events in the flow. It is defined as the standardized fourth central moment as follows,

$$K = \int_{-\infty}^{\infty} x^4 f(x) dx / \sigma^4 = \langle X^4 \rangle / \langle X^2 \rangle^2 \tag{3.25}$$

In turbulence, kurtosis can be used to study intermittency, i.e., the occurrence of intense, sporadic events. These events are of interest because they transport a significant amount of energy and momentum, and influence the overall characteristics of turbulence. So, the kurtosis can indicate the presence of extreme velocity gradients, which correspond to the sharp transitions at the shocks. Thus, the evolution of higher-order statistics like skewness and kurtosis can offer important insights into the non-linear dynamics and structure formation in this system.
The outcomes of this discussion will be presented in the following chapter.

CHAPTER 4

ENSURING RELIABILITY: THE VALIDATION PROCESS

In this chapter, we aim to determine the accuracy of our model's output in representing a theoretical system. This will be achieved through various validation exercises derived from the available literature.

4.1 Verification of the spectral solver

Verification of a spectral solver against an analytical solution is a crucial part of computational simulation. This is an important step to confirm the correctness of the implemented solver. To validate our advection-diffusion solver we used the analytical solution proposed by Basdevant *et al.* as discussed in the first chapter. We used 250 terms of the series and kinematic viscosity $\nu = 0.001$ to implement this solution. As is illustrated in Figure 4.1, the analytical and numerical

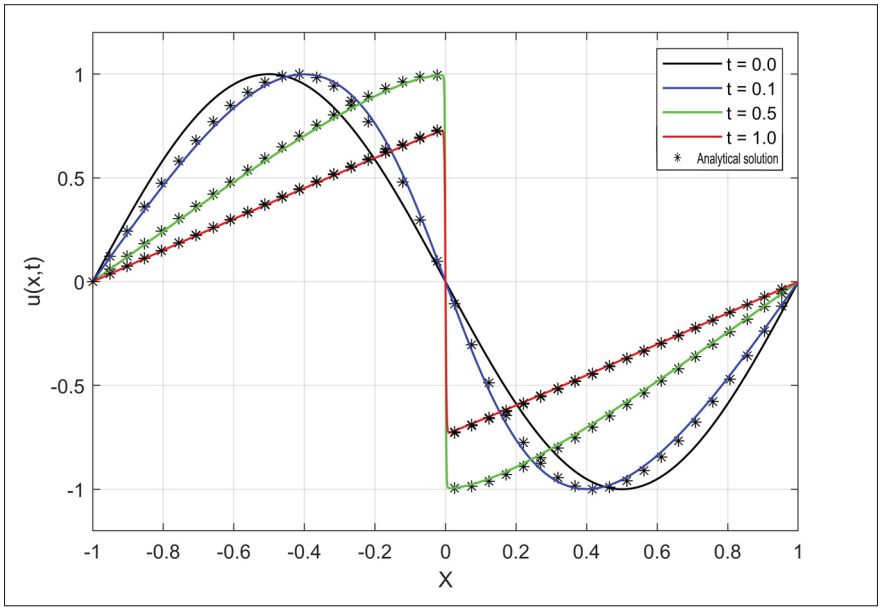

Figure 4.1 Significant agreement between analytical solution (dotted lines) and Fourier-Galerkin numerical solutions using 3rd-order Runge-Kutta temporal discretization (solid lines) of 1D Decaying Burgers equation in different final times ($\nu = 0.001$)

solutions are compared in intermediate time stages until the final time $t_f = 1$. The above plot,

Figure 4.1, demonstrates that there is significant agreement between numerical and analytical methods. For the forced Burgers equation with a sinusoidal forcing term, replicating the work of Jeng & Meecham, we referenced the studies by Jeng & Meecham and Okamura & Kawahara to derive the analytical solution. Our simulations align with the analytical solutions, with the exception of a slight shift in the position of discontinuity, Figure 4.2.

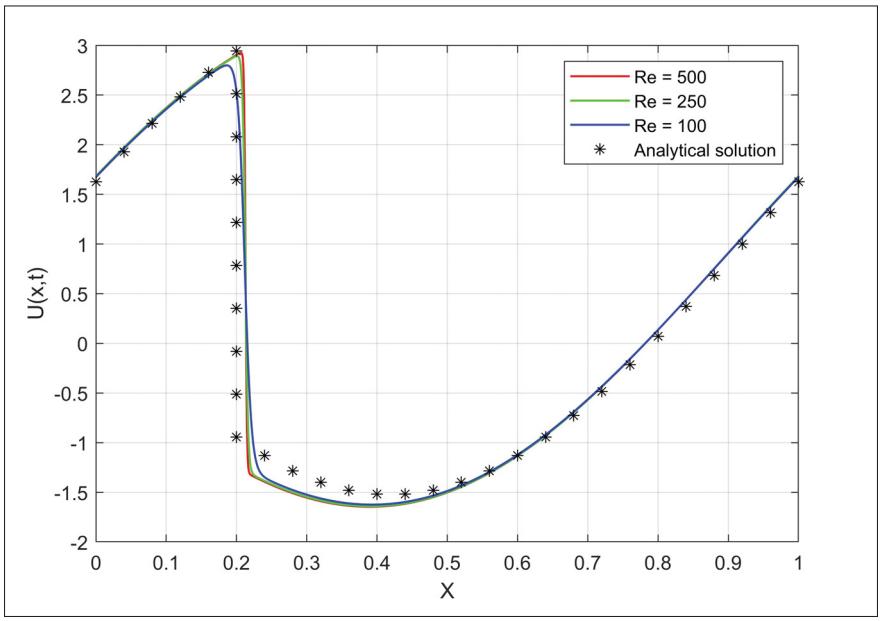

Figure 4.2 Significant agreement between analytical solution and numerical simulations of one-dimensional forced Burgers equation with sinusoidal driving force across various Reynolds numbers at equilibrium

For a more detailed discussion regarding the accuracy of the solver, we direct interested readers to appendix I.

4.2 Error Analysis

To quantify the discrepancy between the numerical and analytical solutions, we employ the following error metrics:

4.2.1 L2 Norm error

The results of these simulations are compared against the analytical solution of the Burgers equation, serving as the benchmark for accuracy. To quantify the discrepancy between the numerical and analytical solutions, we employ the L2 norm error. It provides a measure of the overall difference and is defined as

$$L2 \text{ Norm} = \sqrt{\frac{1}{N}\sum_{i=1}^{N}(u_i' - u_i)^2} \tag{4.1}$$

Here, N represents the number of data points, u_i' is the value from the analytical solution at the i-th point, and u_i is the corresponding value from the numerical simulation. This formula calculates the square root of the average squared differences between the numerical and analytical solutions, providing a measure of the overall error across the domain.

At time $t = 1$, the calculated L2 norm error for the simulation of the numerical decaying Burgers equation was found to be 0.0031. An L2 norm error of this magnitude highlights the simulation's high accuracy, suggesting that the numerical solution closely approximates the analytical benchmark with minimal deviation. This level of precision underscores the effectiveness of our numerical approach in accurately capturing the dynamics of the decaying Burgers equation within the computational domain.

For the forced Burgers equation with sinusoidal forcing at time $t = 1$ we observed a higher error of 0.018 in the simulation suggests a moderate discrepancy between the numerical solution and the analytical benchmark. However, this outcome was anticipated since we compared the analytical inviscid solution with numerical approximations at small Reynolds numbers, far from the regime of vanishing viscosity. This discrepancy arises due to the lack of an appropriate analytical solution for the forced Burgers equation under these conditions.

4.2.2 Relative error

In addition to the aforementioned metrics, we also compute the relative error for each point to evaluate the accuracy of the numerical solution in relation to the analytical solution. The relative

error is defined as:

$$\text{Relative Error} = \frac{|u_i' - u_i|}{|u_i|} \tag{4.2}$$

Computing the relative error across the domain allows for a nuanced analysis of where and how the numerical simulations diverge from expected outcomes, offering a more detailed perspective on the solver's performance.

The relative error obtained in our numerical simulations of the decaying Burgers equation at time $t = 1$ was measured at 0.0072. This value represents the proportional discrepancy between the numerical solutions and the analytical benchmark, normalized by the magnitude of the analytical solutions themselves. A relative error of 0.0072 across the domain indicates that, on average, the numerical solution deviates from the true value by less than 1%, underscoring the precision of our simulation approach. This level of error further affirms the fidelity of the numerical decaying Burgers model in capturing the essential dynamics of the Burgers equation, reinforcing the solver's capability to generate highly accurate predictions within the computational framework employed.

4.3 Parseval's theorem

Based on Rayleigh Energy Theorem (Parseval's Identity of Fourier Transform), the energy content of the square-integrable function in L^2 space will be equal to the summation of the squared amplitude of its Fourier coefficients in the wavenumber space divided by the domain length or divided by the number of collocations in discrete form. This theorem in discrete form is defined as follows (Canuto, 2006)

$$\sum_{n=-\frac{N}{2}}^{\frac{N}{2}-1} |u_n|^2 = \frac{1}{N} \sum_{k=\frac{N}{2}}^{\frac{N}{2}-1} |\hat{u}_k|^2 \tag{4.3}$$

As is evident, the left side of the above formula is proportional to the kinetic energy in physical space, while the right side corresponds to its Fourier transform. In other words, Parseval's

theorem demonstrates the conservation of energy between the velocity field and its Fourier transform. However, it does not directly discuss TKE; rather, it refers to the energy density at each point in physical space or wavenumber space.

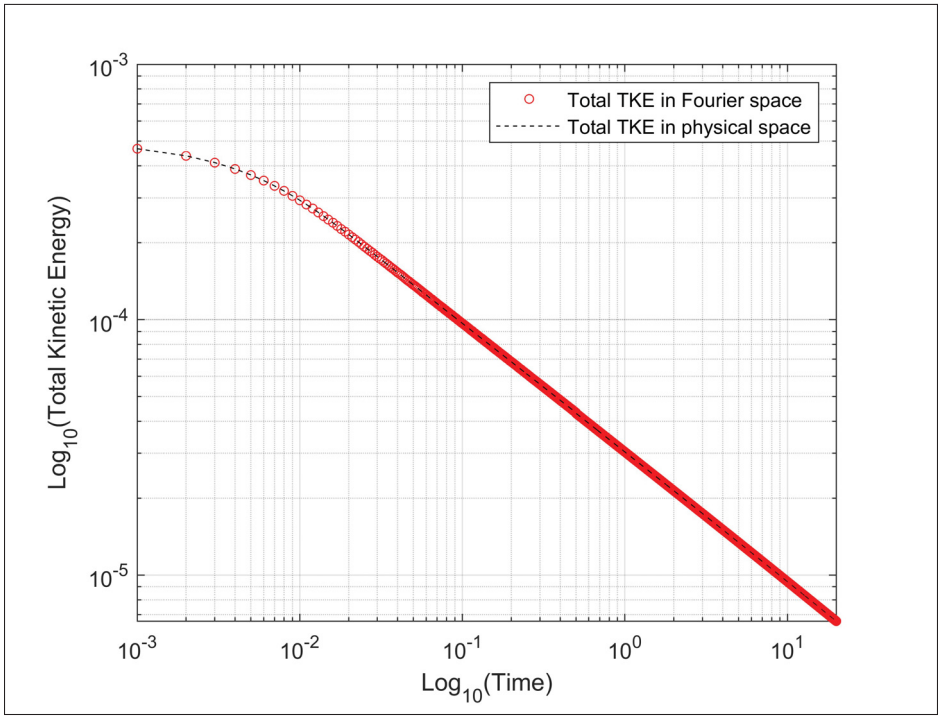

Figure 4.3 Comparing the total energy containing of the system in the physical versus Fourier spaces in logarithmic scale in the limit of vanishing viscosity $\nu = 0.0001$

To obtain the TKE in a discrete domain, we can multiply both sides of equation 4.3 by 1/2. As is depicted above, figure 4.3 portrays the dual nature of the kinetic energy by comparing TKE in both physical and spectral spaces, so we can determine the degree of agreement between our simulation and Parseval's theorem, which serves as a proof of whether our model captures all of the energy or not.

4.4 Energy form of the Burgers equation

We can easily obtain the energy form of the Burgers equation by multiplying both sides of equation 2.4 with the velocity u, then integrating over the spatial domain and finally applying

the product rule and integration by parts. The energy form of the unforced Burgers equation 2.4 ($F(x,t) = 0$) in unsteady state can be expressed in the following manner (Anguelov, Djoko & Lubuma, 2007),

$$\frac{1}{2}\frac{d}{dt}\int u(x,t)^2 dx = -2\nu \int (\frac{\partial u(x,t)}{\partial x})^2 dx \tag{4.4}$$

Which can be rewritten in the form of the evolution of the kinetic energy, decaying Burgers turbulent kinetic energy budget, as follows

$$\frac{d}{dt}TKE(t) = -\nu \, ||\frac{\partial u(x,t)}{\partial x}||^2 \tag{4.5}$$

Where $\frac{d}{dt}TKE(t)$ is the rate of change of turbulent kinetic energy over time, and $||\frac{\partial u}{\partial x}||^2$ is the square of the $L2$ norm of the spatial derivative of the velocity field which can easily be evaluated using a fast Fourier transform and considered as the rate at which kinetic energy dissipated. To measure this dissipation rate over time, we can calculate ε at each time step and plot it as a function of time. The absence of an energy production term in this equation due to the lack of pressure and rotational components, in contrary to more complex Navier-Stokes turbulence, indicates that the mechanisms of energy interaction in 1D decaying Burgers turbulence are fundamentally different from those in Navier-Stokes turbulence.

Both sides of the equation 4.5 have been graphically represented evolving over time in figure 4.4. To ensure a positive orientation of the vertical axis, the negative values of the rates have been taken into account. Upon analyzing the slope of the logarithmic curve presented in Figure 4.4, we have found that the curve exhibits a diminishing trend with an asymptotic algebraic rate approximating 1.5. This illustration serves to substantiate the principle of energy equality in decaying Burgers' turbulence, demonstrating our model's alignment with theoretical concepts.

Now, by considering equation 2.4 with the forcing term and following the steps mentioned earlier to obtain the energy form of the forced Burgers equation in steady (equilibrium) state, we have

$$\frac{d}{dt}TKE(t) = -\nu \, ||\frac{\partial u(x,t)}{\partial x}||^2 + ||f(x,t)u(x,t)|| \tag{4.6}$$

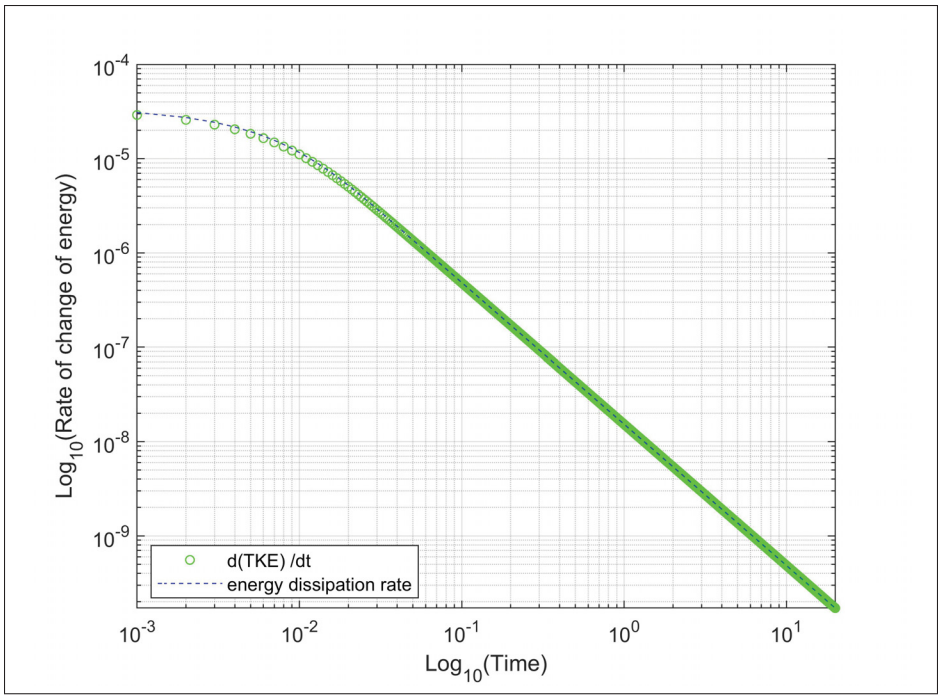

Figure 4.4 Energy equality in the energy form of the decaying Burgers equation in the limit of vanishing viscosity $\nu = 0.0001$. The black dotted curve represents the energy dissipation rate (right side of equation 4.5) evolving over time, and each of the green circle symbols represents the time derivative of turbulent kinetic energy evolving over time(left side of equation 4.5) , which its slope is the second time derivative of TKE, both in Logarithmic form. The curve decays over time by an algebraic rate close to 1.5

The second term on the right-hand side of this equation 4.6, which stems from the driving force, defines as the rate of work done by the forcing term and can indicates energy input per wave number period. This factor amplifies the energy exchange between various wave numbers or scales in contrast to the decaying version of the phenomenon.

4.5 Equilibrium state

Unlike decaying Burgers turbulence, forced Burgers turbulence has the ability to reach an equilibrium state by adjusting the driving force. in this case, when the system reaches a state where the energy injected by the forcing equals the energy dissipated by viscosity, it is said to be

in equilibrium. Note that this doesn't necessarily mean the flow fields themselves are steady; they might still change, but the system's total energy remains constant. In the case of the Burgers equation, we primarily look at the total energy in the system that should eventually be stabilized in an equilibrium state. To this aim, we can also monitor the rate of change of the kinetic energy and the viscous dissipation rate (Girimaji & Zhou, 1995).

4.5.1 Injected energy by the forcing term

To calculate the energy injected into the system due to the forcing term, we will need to consider the work done by this forcing on the fluid. For the 1D Burgers equation, as both the forcing term and velocity field are scalar functions of time and position, work is typically represented by the integration of the multiplication of the force (in this case, the forcing term) and the velocity of the fluid $u(x,t)$ (Jeng & Meecham, 1972). With the forcing term $F(x,t)$, the power (rate of energy input) per unit volume due to the forcing at any given time t and position x is:

$$P(x,t) = F(x,t) \times u(x,t) \tag{4.7}$$

where $P(x,t)$ is the injected energy to the wavenumber k of the fluid by the forcing term.

4.5.2 Dissipated energy by the viscous term

As detailed in chapter 3, viscous dissipation represents the conversion of kinetic energy into internal energy due to the viscous effects in the fluid. For a more comprehensive discussion, consult section 3.3.3. Figure 4.5 depicts the energy equilibrium state. It clearly shows that in our simulation of forced Burgers' turbulence with a sinusoidal forcing term, the kinetic energy stabilizes at a constant value once a steady state is reached $t \geq 0.8$. Similarly, the amounts of injected and dissipated energies also stabilize.

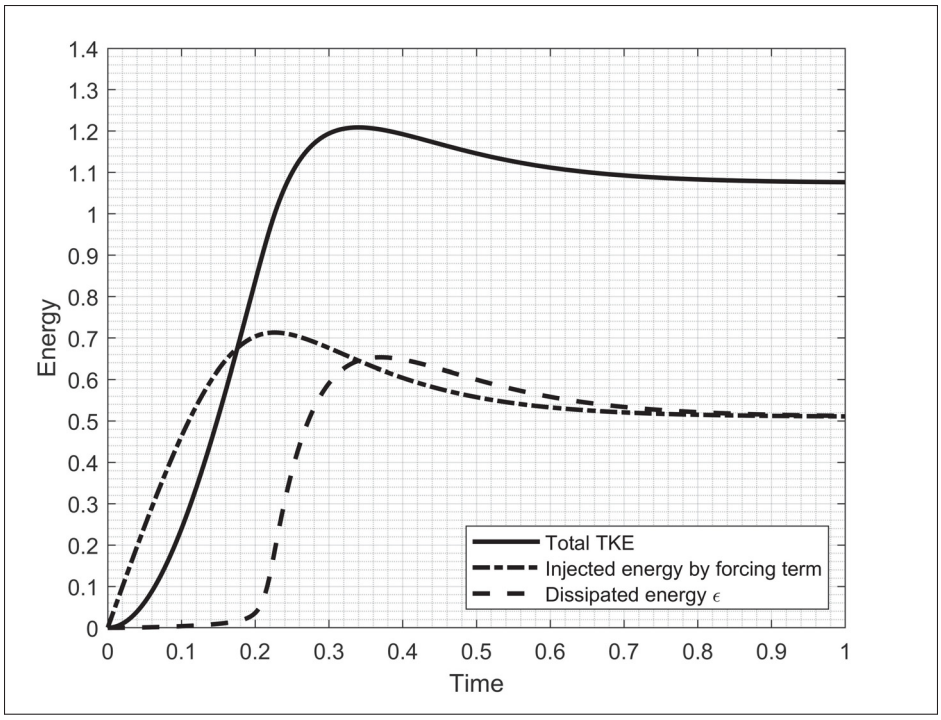

Figure 4.5 Formation of Equilibrium state between injected and dissipated energy levels in the forced Burgers' turbulence. Total kinetic energy tends towards a constant value when the system reaches equilibrium $t \geq 0.8$. Energy introduced into the first largest scale k=2π

4.6 Theoretical energy spectrum

In this section, we compare the energy spectrum of the decaying and forced Burgers turbulence with theoretical spectra. While previous studies have thoroughly established the behavior of the Burgers spectrum in the inertial range, we include the spectra from our calculations in this paper to verify that our simulated model conforms to the statistical characteristics predicted by the literature. It is an indirect verification that all scales are resolved almost properly.

By directly applying the Kolmogorov hypothesis to the spectra, we can derive the Kolmogorov spectrum, which is known as the Kolmogorov $5/3$ law. The Kolmogorov energy spectrum is a theoretical prediction to validate the shape of the energy spectrum of a fully developed three-dimensional isotropic, and homogeneous turbulence governed by the Navier-Stokes equations in the inertial subrange; however, due to the lack of some complexities in the Burgers

one-dimensional turbulence including vortex stretching mechanism, Kolmogorov 5/3 law can only be applied on a superficial level just in the presence of the hyper-viscosity scenarios (Chekhlov & Yakhot, 1995b). By considering the second Kolmogorov similarity hypothesis, the Kolmogorov energy spectrum function of turbulent flow in the inertial subrange is (Pope, 2000),

$$E\left(k\right) = C\varepsilon^{\frac{2}{3}}k^{-\frac{5}{3}} \tag{4.8}$$

$E(k)$ is a power-law spectrum with a spectral index equal to $-\frac{5}{3}$ in which C is the Universal Kolmogorov constant, we set $C = 1.5$ (Sreenivasan, 1995). The energy dissipation rate ε can be calculated in the physical space or Fourier space, which is discussed earlier and is a constant value in the inertial range of a fully developed turbulence, as per the Kolmogorov second hypothesis.

Extensive research have proposed an alternative behavior in Burgers turbulence dynamics, characterized by a k^{-2} power law, first suggested by Saffman (1968), differing from Kolmogorov's predictions.

To verify that our simulated decaying Burgers turbulent flow adheres to the statistical characteristics predicted by Kolmogorov or Saffman theories to a certain degree, we compared the energy spectrum in Fourier space against the mentioned spectra, figure 4.6.

To visualize whether the actual energy spectrum follows the expected scaling behavior, compensated energy spectrum which involves dividing the energy spectrum $E(k)$ by a theoretical power-law scaling $k^{-5/3}$ is calculated in the same plot, figure 4.6. If the system indeed follows the expected power-law scaling, the compensated energy spectrum plot will show a relatively flat or constant line in the inertial subrange (Chekhlov & Yakhot, 1995a). As observable in the aforementioned graph, the energy density spectrum demonstrates an alignment with the Kolmogorov 5/3 law within the range of wavenumber $60 < k < 94$ with a tolerance of 0.1, in the spatial domain $[0, 2\pi]$.

On our second attempt, we contrasted the energy spectrum with the k^{-2} scale, as proposed by Saffman (1968) in figure 4.6. In the second case, the numerical solution covered a broader wavenumber range of $52 < k < 124$ as the inertial subrange, and shows greater agreement

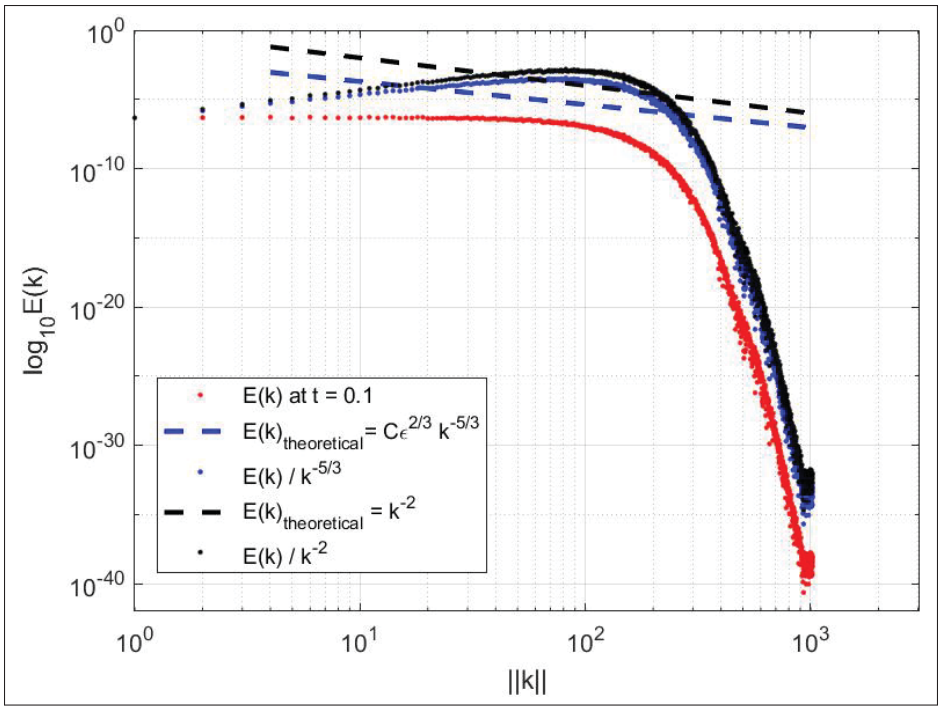

Figure 4.6 The degree of agreement among the energy spectrum of the decaying Burgers' turbulent with the Kolmogorov $-5/3$ law, and the k^{-2} power law scaling. The initial data were distributed uniformly through the use of a random white noise generator. The red dotted curve is the energy spectrum of our numerical result at t=0.1. The dashed lines show the theoretical energy spectra based on the Kolmogorov 5/3 law and the k^{-2} law for the inertial subranges. The black and blue dotted curves represent the energy-compensated versions of the Kolmogorov $5/3$ law and the k^{-2} law, respectively, for the inertial subranges at a near-zero viscosity limit ($\nu = 0.0001$). These curves demonstrate strong adherence to the aforementioned laws, as indicated by their flatness across the wavenumber range

with the theoretical power-law literatures (Saffman, 1968), (Girimaji & Zhou, 1995). The wave numbers smaller than the mentioned ranges are more probable to behave like an energy-containing subrange which is dominated by the largest structures, where the energy is injected into the system, while the wavenumbers larger than the mentioned range can be considered as dissipative subrange which dominated by the small scale behaviors, where the energy is dissipated as heat due to the formation of the shockwaves and the action of the viscosity (Girimaji & Zhou, 1995). Considering Burgers' turbulence which is primarily driven by an external Wiener random force

that mainly supplies energy to the large-scale structures, the energy spectrum that emerges aligns with the k^{-2} scale as discussed by Sinai (1992). This agreement is illustrated in figure 4.7 by depicting both the k^{-2} scale line and the compensated energy spectrum.

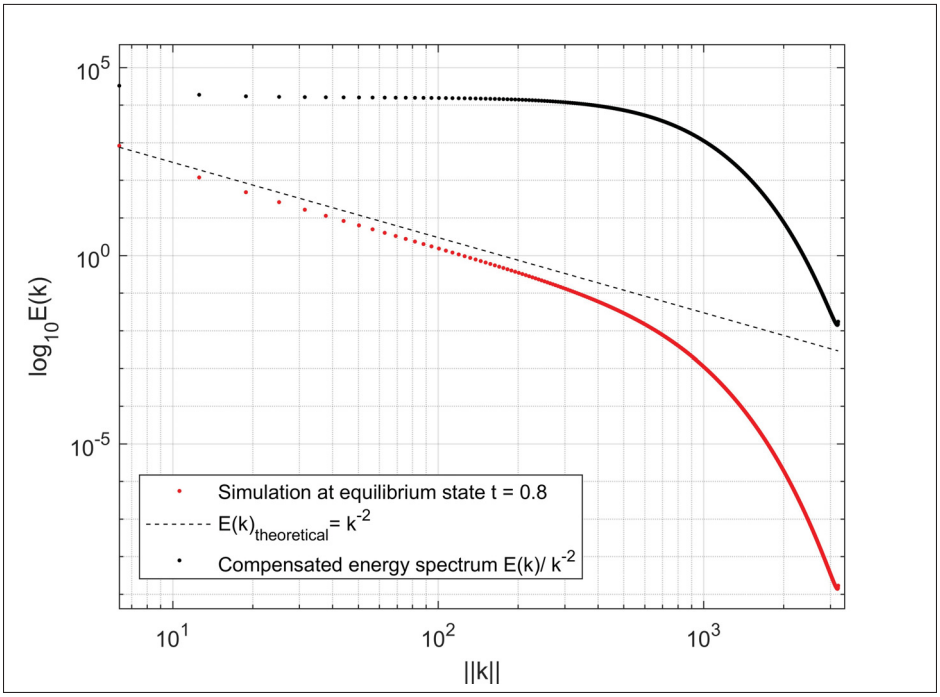

Figure 4.7 The degree of agreement among the energy spectrum of the Forced Burgers' turbulent with the k^{-2} power law scaling when driven by the large scale random forcing term. The red dotted curve is the energy spectrum at equilibrium state; the straight line has the exact slope of k^{-2} and the black dotted curve is the compensated energy spectrum

CHAPTER 5

UNVEILING THE RESULTS: IN-DEPTH DISCUSSIONS AND ANALYSIS

In this chapter, we will discuss the results of our research work conducted using the Fourier Galerkin solvers. Our work commenced with modeling equations from the Burgers class, which we then expanded to encompass various scenarios, particularly decaying and forced Burgers' turbulence, across diverse initial velocity fields and forcing terms.

This chapter begins with an examination of the advection-diffusion equation. We then transition to the discussion of Burgers equation. Following that, we will investigate the decaying Burgers turbulence, and finally, our focus will shift towards exploring the complexities of the characteristics of forced Burgers turbulence.

As outlined in the previous chapter, we employ the Fourier-Galerkin spectral solver accompanied by a 3rd-order Runge-Kutta scheme for time integration.

5.1 Evaluation of viscous term

In this chapter, we initially explore the effects of viscosity on the behavior of the Burgers class of equations to assess their key characteristic: the interplay between inertial and viscous effects. First, we start with the advection-diffusion equation, denoted as equation 1.1. The initial function is similar to the one discussed in section 1.1.2, and the ratios of advection velocity $a = 1$ over kinematic viscosity $\frac{a}{\nu} = [1, 10, 100, 1000]$ are considered as a scale representing the balance between the intensity of advection versus the diffusion state. Figure 5.1 illustrates this interaction, along with the analytical solutions of the equation.

In the case of the advection-diffusion equation, reducing the kinematic viscosity diminishes the effect of the diffusion term, causing the equation to behave more like a linear advection equation, predominantly following the advection velocity. As a result, the majority of the energy is conveyed by the advection phenomenon, the inertial effects, leading to numerical simulations that are susceptible to displaying dispersion error when compared to the exact solutions. Conversely, higher viscosity results in more pronounced diffusion behavior, making the diffusion term increasingly dominant. Over time, our approximation will more closely

resemble the heat equation, which accounts for viscous effects, and consequently, it exhibits higher dissipation errors relative to the exact solutions. Figure 5.1 is the proof of this behavior.

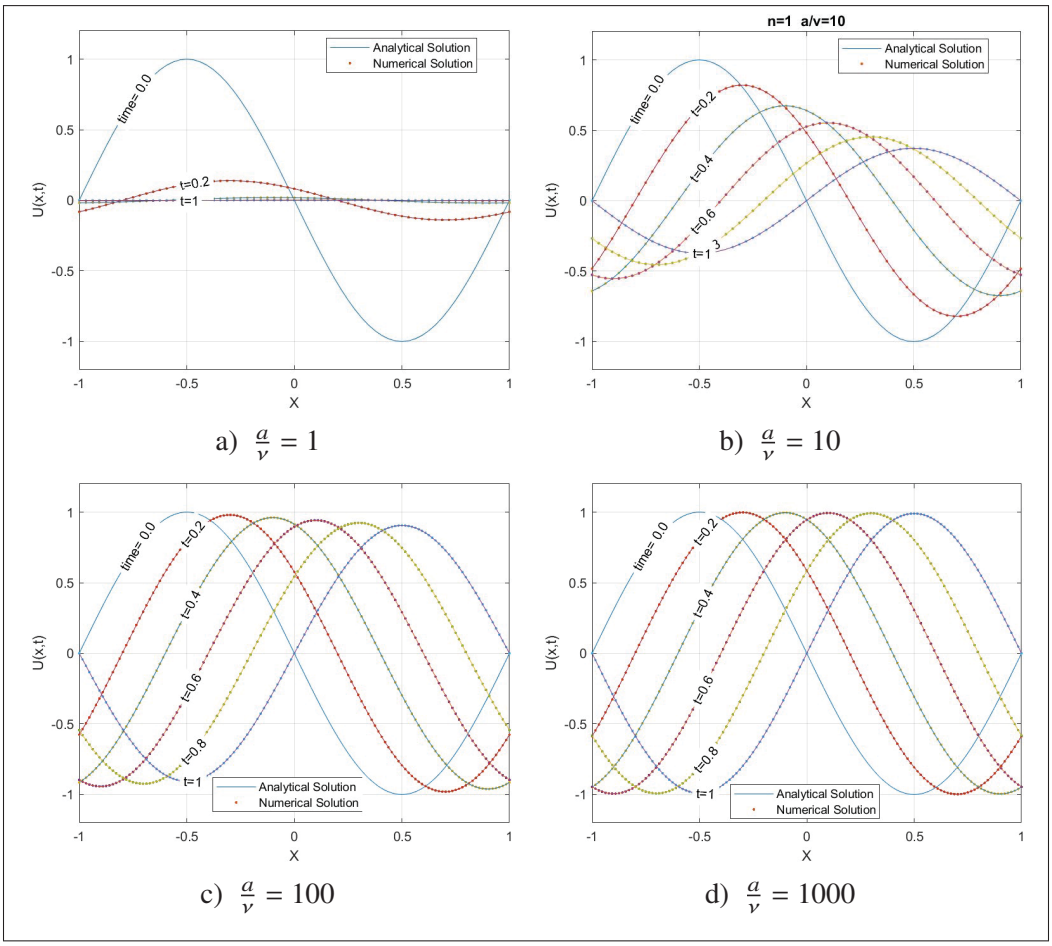

Figure 5.1 The Advection-Diffusion equation in different ratios of advection velocities over diffusion viscosities $\frac{a}{\nu} = 1, 10, 100, 1000$ reveals the interaction between advection and diffusion terms through varying viscous effects
($N = 64, \Delta t = 10^{-5}$)

5.2 The existence and smoothness problem

While solutions to the Burgers equation always exist, they may not always be smooth, especially in the inviscid limit as viscosity approaches zero. To enhance our understanding, we conducted multiple simulations of the decaying Burgers equation across different kinematic viscosities

ν, as illustrated in figure 5.2. In the vanishing viscosity limit, the Burgers equation can lead

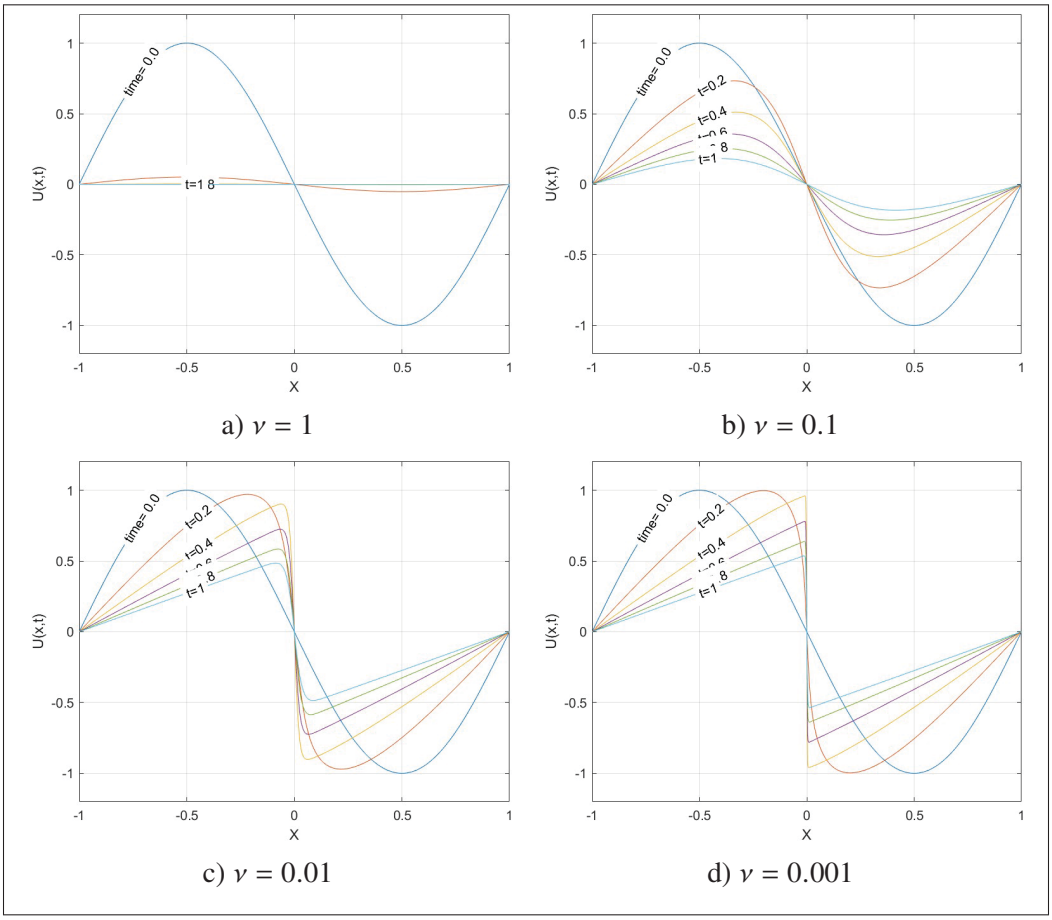

Figure 5.2 Discontinuities or singularities are not exist in high viscosities. Decaying Burgers equation for $\nu = 1, 0.1, 0.01, 0.001$. For extremely high viscosity, the waveform takes on a smooth shape; however, as the viscosity ν lowers, the waveform grows increasingly sharp and ultimately evolves into a form featuring a pronounced shock structure
($N = 512, \Delta t = 10^{-5}$)

to the formation of discontinuities or "shocks" over time, even from smooth initial conditions. The formation of shocks in the Burgers equation can be understood as a result of the non-linear convective term in the equation, which tends to steepen the velocity profile, leading to the formation of discontinuities and shocks. The viscous term, on the other hand, tends to smooth out the velocity profile and prevent the formation of shocks. This phenomenon of discontinuity development is well-documented in fluid dynamics and contrasts with the incompressible Navier-

Stokes equations, where the emergence of discontinuities or singularities remains a significant unresolved issue. This is one of the key reasons the Burgers equation is frequently employed as a simplified model for studying aspects of turbulence and shock formation, highlighting its utility in probing various physical phenomena.

5.3 The behavior of higher wavenumbers

With the aim of our research, we implemented the simulations one more time, but this time, in a fixed viscosity and different modes of the wavenumber $n = [1, 2, 5, 10]$ in various final times $t_f = 0.2, 0.4, 0.6, 0.8$ and 1.

As shown in figure 5.3, increasing the mode of wavenumbers leads the energy to decay faster in Advection-Diffusion equation. This behavior is caused by the fact that the values of the higher wave numbers are more sensitive on diffusion terms compared to the advection terms, due to the fundamental mathematical characteristic of these phenomena as it is proportional to k^2 in Fourier space leading to greater dissipation of energy at smaller scales. Additionally, Figure 5.3 explicitly shows that higher wavenumbers exhibit elevated dissipation errors relative to analytical solutions. This is due to the diffusion effects, which are primarily responsible for dissipation error, becoming more pronounced.

In Figure 5.4 the behavior of higher wavenumbers is illustrated but this time using the viscous Burgers equation. It can be concluded that in this case as well, by increasing the mode of initial wave number n, the diffusion effects would become more potent; in other words, the diffusion term has more interest in damping higher wavenumbers than the lower ones, so in turbulent flow with multiple scales it damps out smaller scale structures faster which are located in the dissipation range that is responsible for dissipation of energy due to viscous effects.

In the 1D decaying Burgers equation, the non-linear term $(u\frac{du}{dx})$ represents the advection of momentum, which tends to create sharp gradients (small scale structures), while the linear term $(\nu\frac{d^2u}{dx^2})$ corresponds to the viscous diffusion of momentum, which tends to smooth out these gradients. When we increase the kinematic viscosity, the influence of the diffusion term becomes more dominant. This increased diffusion "smooths" out small-scale structures faster

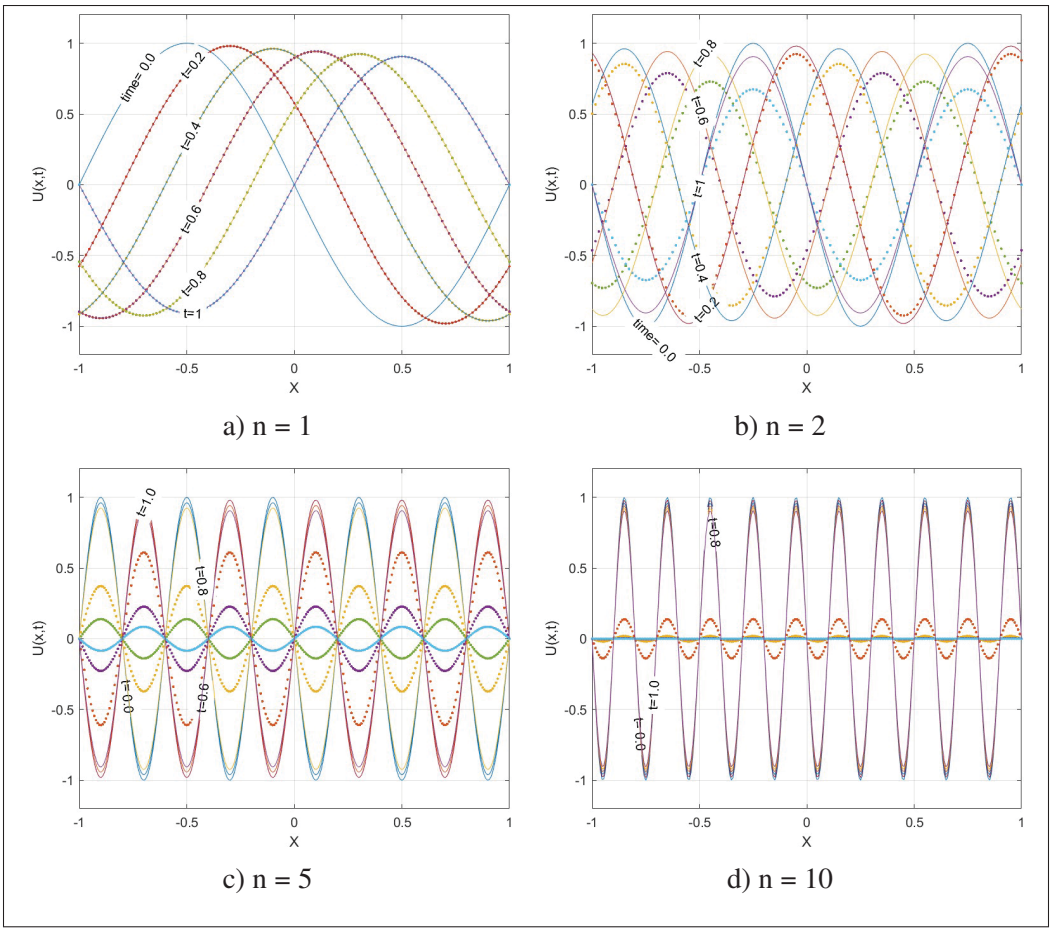

Figure 5.3 The behavior of Advection-Diffusion equation in different modes $n = 1, 2, 5, 10$ shows the higher wavenumbers, smaller scales, are damper more effectively. The diffusion effects in higher wavenumber, smaller scales. Diffusion term tends to smooth out ($\nu = 0.01, N = 128, \Delta t = 10^{-4}$)

and thus, more energy is contained in larger scales (smaller wave numbers). This is because the viscous term acts as a damper to high-frequency (small-scale) fluctuations, causing the energy to concentrate at larger scales.

This phenomenon is related to the intrinsic nature of the Burgers' equation and the effect of the kinematic viscosity on the system. So, we can say that in Burgers' turbulence, the kinematic viscosity determines the scale at which the non-linear advection and the linear diffusion (viscous damping) balance each other. This balance is crucial in shaping the energy spectrum of turbulence.

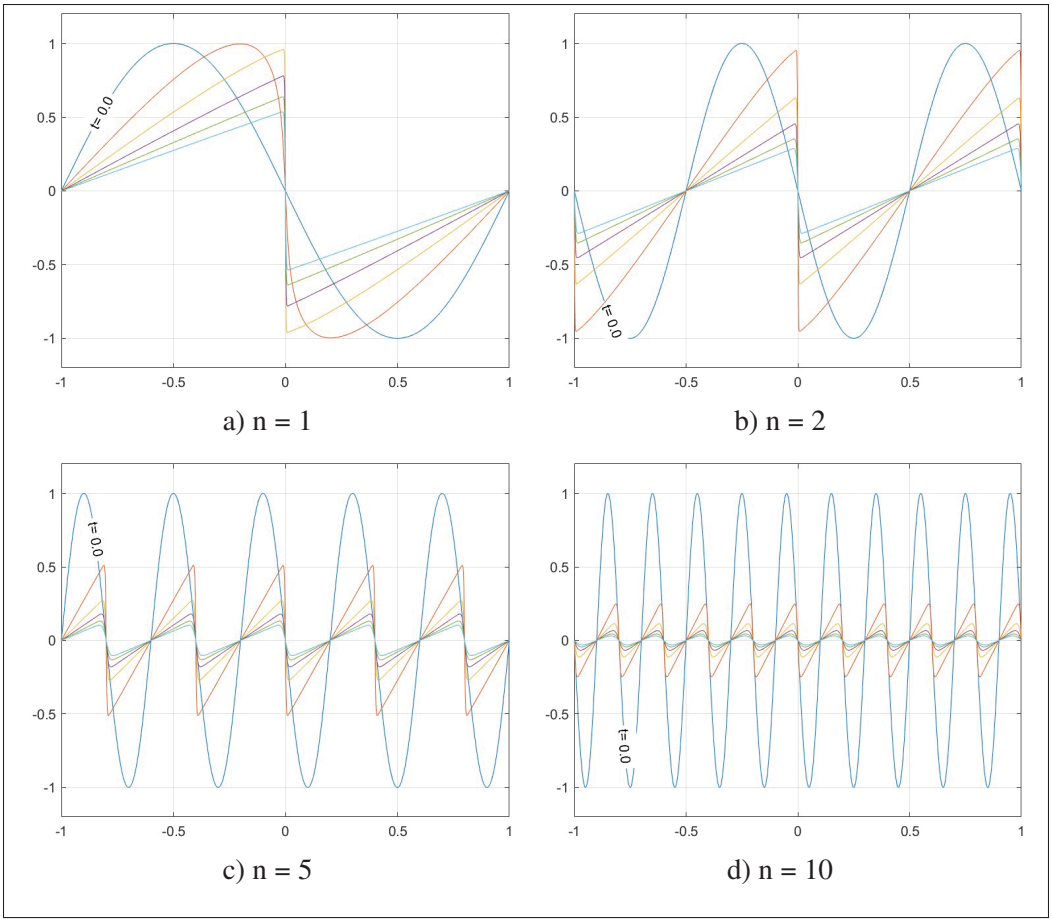

Figure 5.4 Numerical approximations of the Burgers equation for various modes $n = 1, 2, 5, 10$ illustrate that the diffusion term increasingly dominates at higher wavenumbers ($\nu = 0.001, N = 1024, \Delta t = 10^{-4}$)

5.4 Effects of varying viscosities on the energy spectrum

In this section, we explore how varying viscosities influence the energy spectrum. In figure 5.5 the Energy spectrum of the velocity field of the decaying Burgers equation in various viscosities is depicted. By increasing the kinematic viscosity, we are enhancing the role of viscous diffusion, which tends to abolish small-scale structures and shifts energy concentration towards larger scales or smaller wavenumbers. Consequently, energy dissipates more rapidly and approaches zero at smaller scales (higher wavenumbers), leading to the emergence of the dissipative range

at larger scales while diminishing the inertial subrange. Thus, as previously discussed in section 5.3, it is evident that the diffusion term in the equation acts to attenuate higher wavenumbers.

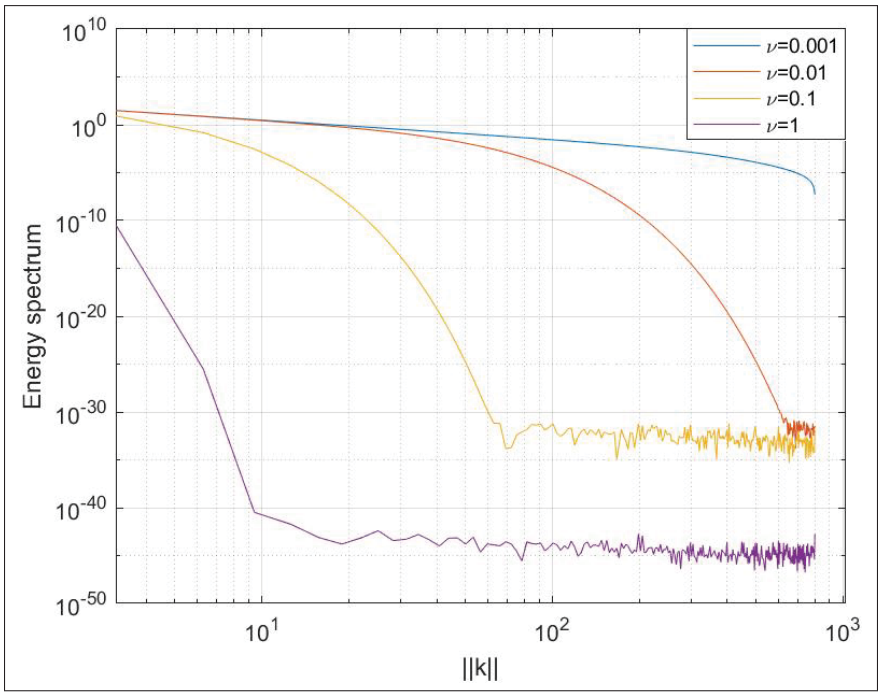

Figure 5.5 Energy spectrum $E(k)$ of the velocity field in Decaying Burgers equation across various viscosities $\nu = 0.001, 0.01, 0.1, 1$, demonstrating accelerated energy damping at higher viscosities prior to transfer to smaller scales which means the boundaries of dissipative and inertial subranges will change in wavenumber domain $N = 512$ and $\Delta t = 10^{-6}$

5.5 Decaying Burgers' Turbulence with a uniform random initial velocity field

In this stage of the present research work, our objective is to investigate the behavior of Decaying Burgers' Turbulence which is subjected to the uniform random initial velocity field.

The process to generate the uniform random initial velocity field was discussed in the Methodology chapter. Here we just provide the results of simulations and further discussions to analyze the behavior of the solutions. One significant observation in Figure 5.6 is what we experienced in earlier subsections, that intensifying the viscous effects enhances the effectiveness of the diffusion behavior in our simulations. The increased diffusion tends to dampen the high-frequency

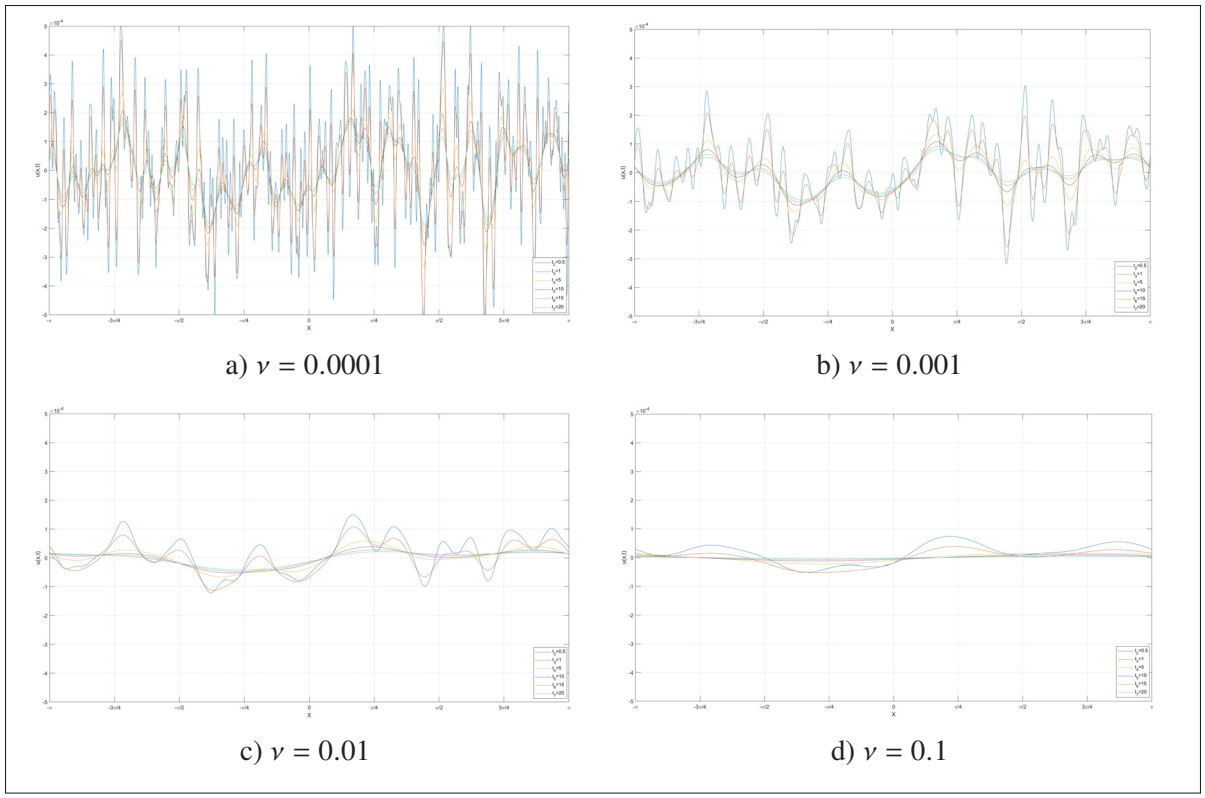

a) $\nu = 0.0001$ b) $\nu = 0.001$

c) $\nu = 0.01$ d) $\nu = 0.1$

Figure 5.6 Numerical approximations of the decaying Burgers' equation in different viscosities with uniform random initial velocity field using Fourier-Galerkin method in space and 3rd-order Runge-Kutta scheme in time ($N = 2048$)

fluctuations and dissipate energy at smaller scales. but unlike Navier-Stokes turbulence which this energy tends to the formation of small eddies, in Burgers' turbulence, the energy tends to concentrate at the shocks and dissipate rapidly due to the presence of the viscous term. This behavior leads to the formation of shock waves rather than an energy transfer to smaller scales. Thus, a higher diffusion behavior can lead to the formation of smaller structures including ramp-like structures and shock waves (She *et al.*, 1992).

5.5.1 Evolution of the energy spectrum affected by various viscosities

As mentioned in section 5.3, the diffusion term within the equation is known to dampen higher wavenumbers. Illustrated in figure 5.7, elevating the kinematic viscosity intensifies the effect

of viscous diffusion. This process effectively eliminates small-scale structures, redistributing energy to favor larger scales or smaller wavenumbers.

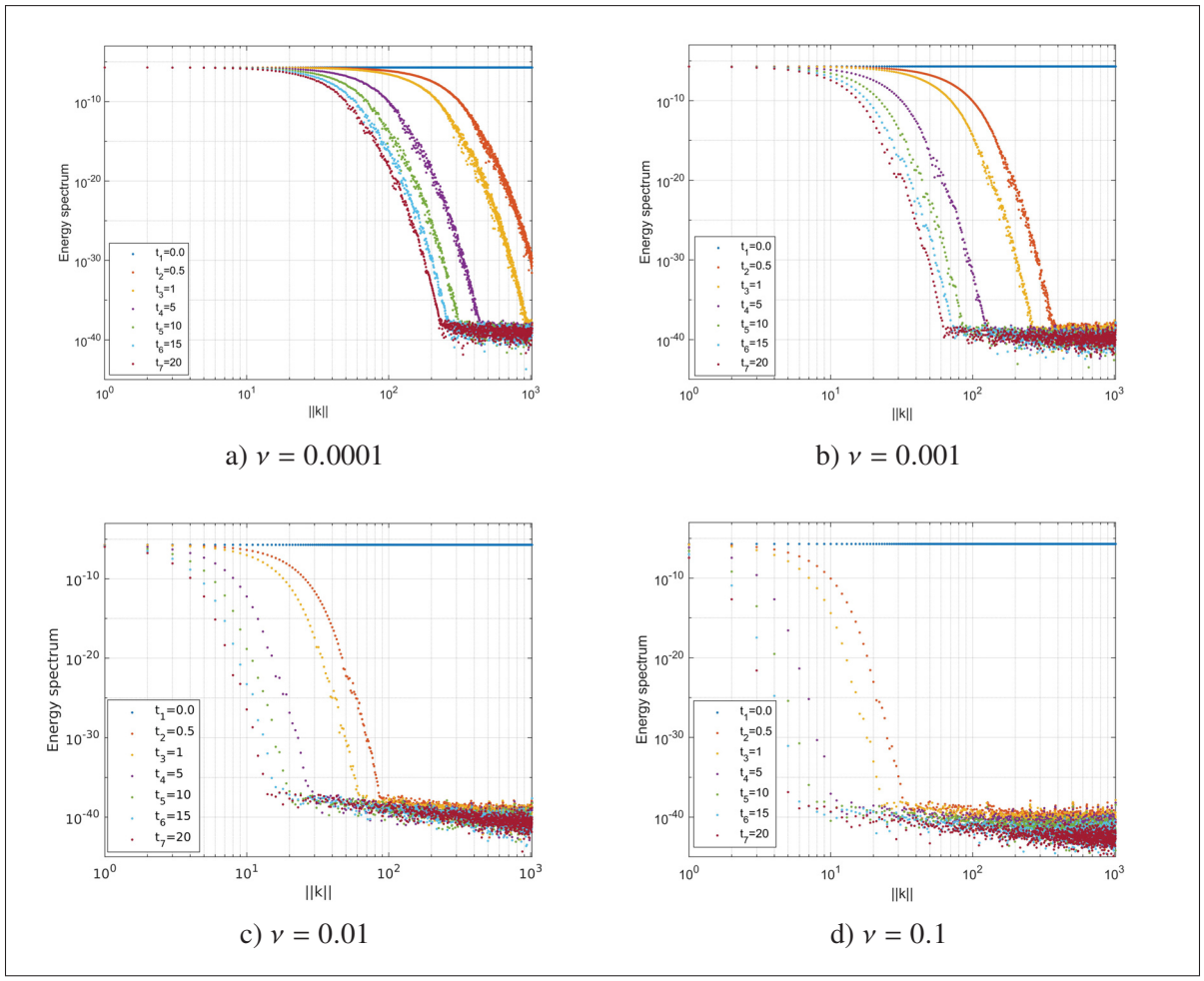

Figure 5.7 Evolution of the energy spectrum of the decaying Burgers' turbulence in different viscosities with uniform random initial velocity field shows increasing kinematic viscosity intensifies viscous diffusion effects and damp out smaller scale structures ($N = 2048$)

5.5.2 Inverse energy cascade

It is a well-established fact that three-dimensional Navier-Stokes (NS) turbulence does not allow for the inverse cascade of energy from smaller to larger scales. However, analyses by Kraichnan (1968) suggest that the Burgers equation might support such an inverse cascade.

Girimaji & Zhou (1995) numerical investigations have demonstrated this energy transfer. We now aim to confirm their results using a spectral method. We employed a decaying form of Burgers turbulence using the initial data which presented earlier in section 3.1.1, where $k_i = 190$ and $k_f = 260$ define the wavenumbers that describe the boundaries of the inertial sub-range. To determine the boundaries of this sub-range, we conducted a simulation of forced Burgers turbulence and allowed the system to evolve until it reached an equilibrium state. Subsequently, we identified the boundaries of the inertial subrange by analyzing the k^{-2} scaling behavior. Figure 5.8 illustrates the evolution of the energy spectrum associated with this decaying velocity field.

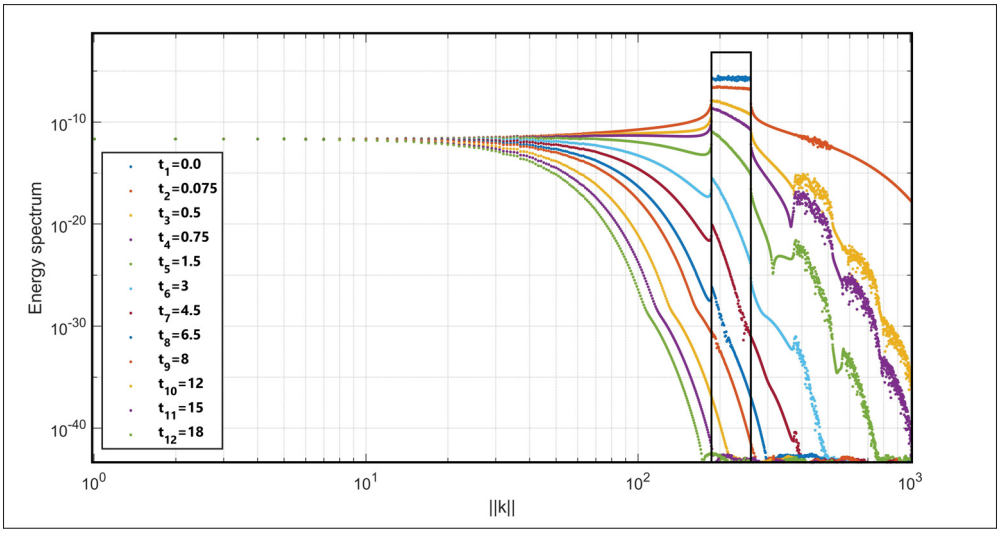

Figure 5.8 Inverse energy transfer in illustrated. Energy spectrum of the decaying Burgers with the initial velocity field bounded in $k = [190, 260]$ in the wavenumber space $\nu = 1e - 4$

As the initial velocity field undergoes evolution under the Burgers equation, kinetic energy is swiftly distributed among all wavenumber modes, including those smaller and larger than the initially energized ones. This process reveals a clear inverse transfer of energy from the initially active scales to the larger scales. Following this swift initial phase, the energy spectrum begins to decay, showing no further signs of inverse energy transfer. Over time, the higher wavenumbers tend to lose their energy more quickly compared to the lower ones. Indeed, in the later decay phases, $t \geq 16$, only large scale wavenumbers that are smaller than 190 remain significantly

energized. The prompt energization of the larger scales ($k < 190$) serves as a clear indicator of inverse energy transfer. Nonetheless, whether this transfer occurs through a cascading process remains uncertain.

One strategy to understand the details of this energy transfer is to investigate the triadic interactions among local wavenumbers (Girimaji & Zhou, 1995), an area reserved for subsequent research studies.

While it is true that the inverse cascade of energy is not permitted in 3D Navier-Stokes turbulence, it is important to note that the phenomenon observed in Burgers turbulence, namely the inverse transfer of energy (as opposed to an energy cascade), is also a common feature in 3D Navier-Stokes turbulence simulations. This is particularly evident in the interactions between local wavenumbers within the spectral space.

5.5.3 Evolution of the probability density function in dissipative Burgers turbulence

We obtained the PDF of the velocity field evolving in time, using the kernel smoothing density function, to analyze the evolution of small structures figure 5.9.

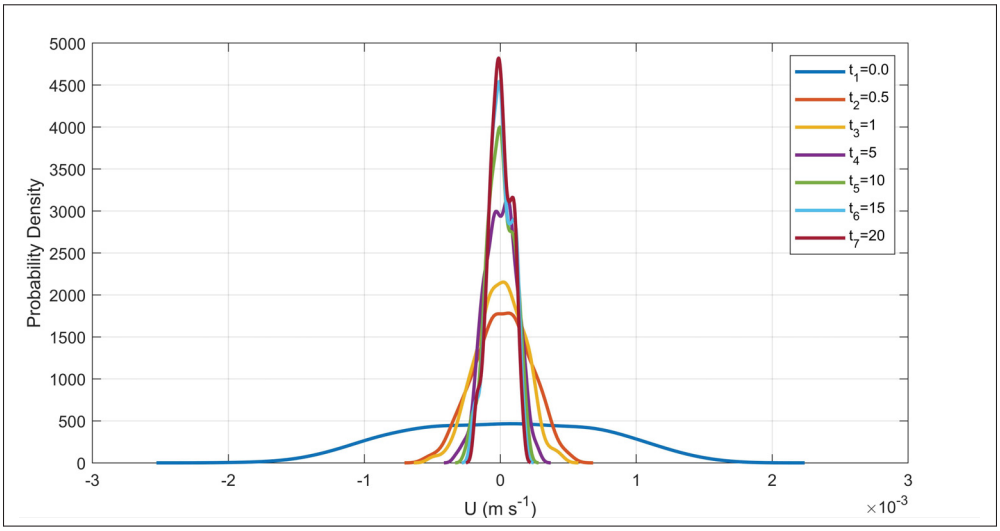

Figure 5.9 As the simulation evolves, emerge of the small-scale structures can lead to the existence of non-zero skewness in addition to more peaked PDF with fatter tails, which results in an increase in kurtosis $\nu = 0.001$

As can be seen, it changes to the interplay between the nonlinear advection term and the viscous diffusion term. The development of shocks and small-scale structures cause the PDF to develop a more complex structure, often characterized by long tails and sharper peak, power law behavior, which means an increase in kurtosis, in addition to losing its symmetry, and non-zero skewness. In the inviscid limit $\nu \rightarrow 0$, the PDF becomes singular, with most of the probability mass concentrated around the shock locations. It has a good agreement with the behavior explained by the literature (Bec & Khanin, 2007), (Tennekes & Lumley, 1978).

5.5.4 Evolution of the statistical central moments of distribution in dissipative Burgers' turbulence

Two essential statistical central moments that were previously discussed in section 3.3.5 are skewness and kurtosis. These central moments offer valuable insights into the characteristics and patterns of turbulent flows, shedding light on their behavior and structure. In this subsection, we discuss the evolution of these statistical concepts over time and explore the interplay of nonlinearity and viscosity in Burgers turbulence on the behavior of these central moments in Figures 5.10 and 5.11.

As depicted in the following Figures, in a decaying, one-dimensional viscous Burgers turbulence, the skewness and kurtosis evolve in a particular way due to the nonlinear nature of the Burgers equation and the presence of viscosity. In Figure 5.10 the skewness remains close to zero at very early times because of the initial uniform random data, which typically have a symmetric distribution. However, as time progresses and the nonlinearity of the Burgers equation comes into play, the skewness increases in magnitude. This increase is due to the formation of extreme events and sharp gradients or "shocks" in the solution, caused by the nonlinear advection term. This leads to an asymmetry in the distribution of velocity, which gets reflected as non-zero skewness. The negative sign of the skewness indicates a distribution with a long tail on the left side of the PDF plot Figure 5.9, meaning there are a significant number of regions with low velocity.

As viscosity increases in Figure 5.10, the dissipation effects due to the linear diffusion term will become more dominant over the nonlinear advection term which leads to the diffusion of extreme

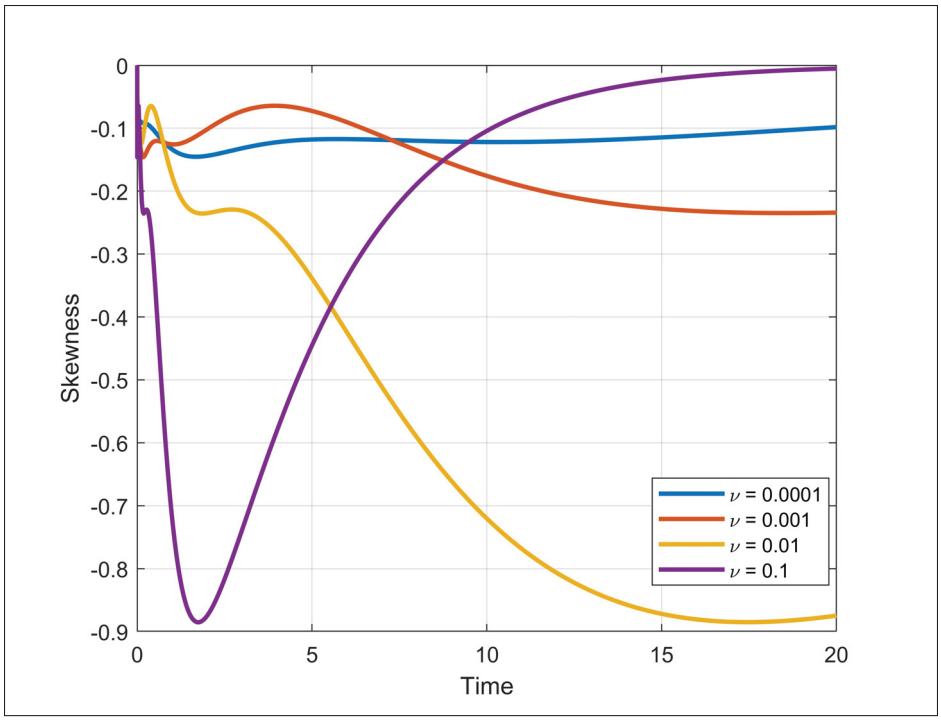

Figure 5.10 Evolution of skewness in time with different viscosities. The plot demonstrates the impacts of the interplay between linear advection and nonlinear diffusion terms on the behavior of the skewness curve. The increase in the magnitude of skewness indicates the formation of sharp gradients or shocks in the solution

events and shocks, and consequently, the flow field becomes more symmetric. This leads to a decrease in the magnitude of skewness, as skewness is a measure of the asymmetry of the distribution. Thus, when the viscosity is large enough $\nu = 0.1$, the flow can become essentially Gaussian with skewness tending toward zero. In Figure 5.10 this interplay between linear and nonlinear phenomena is interestingly presented when viscosity $\nu = 0.1$. In the beginning, the magnitude of a symmetric skewness increased from zero due to the impact of nonlinear advection caused to the formation of intermittent, extreme events. but shortly after, the viscous effects due to the linear diffusion term come into account as a regularizer and dissipates these small-scale outliers, making the solution smoother and more symmetric with a skewness moving toward zero.

The evolution of Kurtosis over time is also dependent on viscosity in Decaying Burgers'

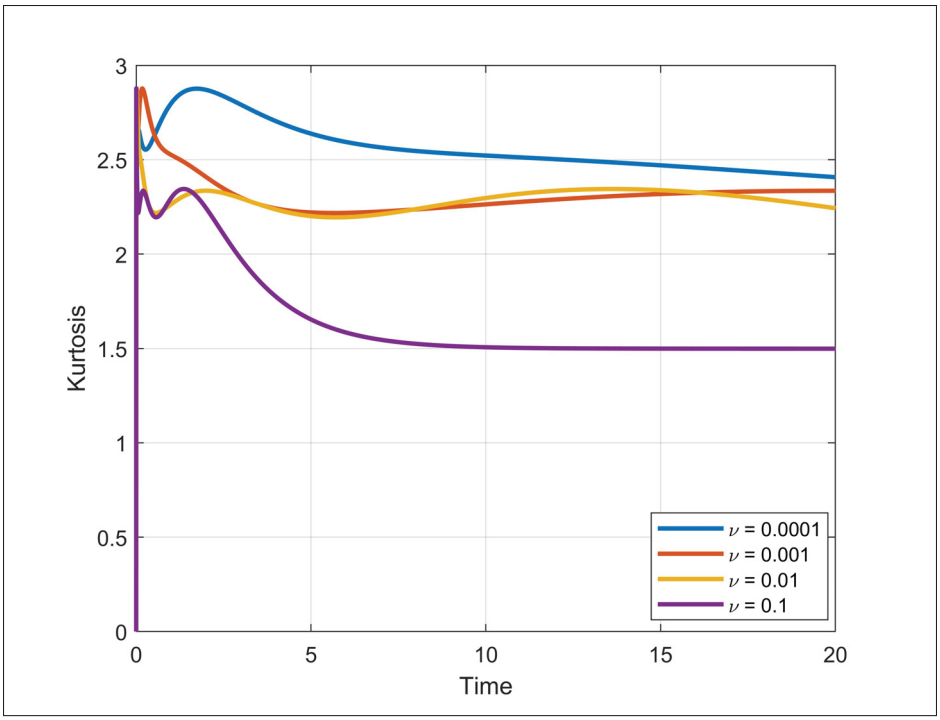

Figure 5.11 Evolution of Kurtosis in time with different viscosities. The plot demonstrates the impacts of the interplay between linear advection and nonlinear diffusion terms on the behavior of the Kurtusis curve. Positive Kurtosis indicates the development of sharp gradients or shocks in the solution

turbulence. As illustrated in Figure 5.11, similar to Skewness, the Kurtosis starts from a low value (close to zero for Uniform initial data) due to the lack of sharp gradients in the initial velocity field. As the solution evolves in the early stages of the simulation, the Kurtosis begins to increase initially going toward Normal distribution, Kurtosis close to 3. This increase is due to the development of sharp gradients or shocks in the solution caused by the nonlinear advection term. In Fig.5.11, it is observed that in $\nu = 0.001$ after the initial stages, as time progresses, the viscosity caused by linear viscous term starts to dominate, which smooths out the shocks and the PDF starts to form a flatter crown compared to the normal distribution, Fig.5.9. This indicates a decrease in the magnitude of Kurtosis, as shown in Fig.5.11, which as mentioned, can be attributed to viscous effects. However, it appears that these viscous effects, $\nu = 0.001$, were insufficient to fully dissipate energy, and in the third stage, the formation of extreme events

leads to an increase in Kurtosis once again after $t = 5$ for $\nu = 0.001$. These shocks appear as extremes in the velocity distribution, leading to heavier PDF tails. 5.9. This implies the presence of extreme events or outliers. In turbulence, this could indicate intense and intermittent events (Davidson, 2015).

In the last stage of evolution, after the system has evolved for a long enough time, the balance between the nonlinearity and the dissipation stabilizes, leading to a more or less constant Kurtosis.

With a sufficient increase in viscosity, $\nu = 0.1$, is observed that the viscous effects become more pronounced, significantly damping out extreme events. This results in the elimination of the third stage, previously associated with a second increase in kurtosis.

5.5.5 Self-similarity of the stochastic velocity field in the decaying Burgers turbulence

Building on the research by (Sefik & Christov, 1992), this section presents the normalized spectrum of the time evolution for both second-order and fourth-order multi-point correlation functions of the velocity field. The aim is to qualitatively examine the stochastic self-similarity in the behavior of these correlation functions within dispersive Burgers turbulence, starting with initial uniform random data. Building on the formulas outlined in Section 2.2, we calculated the correlation functions and integrated the data using the trapezoidal rule. We then derived the correlation curves at various times by employing a normalization technique, as explained in the same section. From our observations, both the second-order, Fig. 5.12, and fourth-order, Fig. 5.13, correlation functions associated with the velocity field exhibited substantial shape consistency. This serves as evidence of the self-similarity observed up to the forth-order correlation function in our findings, allowing us to extract a unique and specific insight from each turbulence simulation. This implies that for considerably large times, there is no need to obtain results for different times, potentially reducing computational resources in future simulations. Our findings show a qualitative alignment with the results presented by Sefik & Christov in their 1991 study, thereby facilitating a clearer understanding of Burgers turbulence.

Another observation worth mentioning from the correlation figures 5.12 and 5.13, is the vanishing

of correlation functions as the separation distance increases, indicating a strong manifestation of the mixing property within the turbulent flow under examination.

This phenomenon suggests that, over large distances, the fluid elements become statistically independent of each other, a hallmark of effective mixing. As the flow evolves, the initial conditions or localized variations in the fluid properties (such as velocity, temperature, or concentration of a substance) dissipate across the entire domain, leading to a state where these properties are uniformly distributed. The diminishing correlation at large separations implies that any two points in the fluid, when far enough apart, no longer influence each other's state in a statistically significant manner. This is a direct consequence of the turbulence's capacity to homogenize the fluid's characteristics, breaking down initial inhomogeneities and distributing energy, momentum, and scalar quantities evenly throughout the flow. Such observations are critical for understanding the dynamics of turbulent mixing and validate the theoretical models predicting the decay of correlations as a signature of effective turbulent mixing.

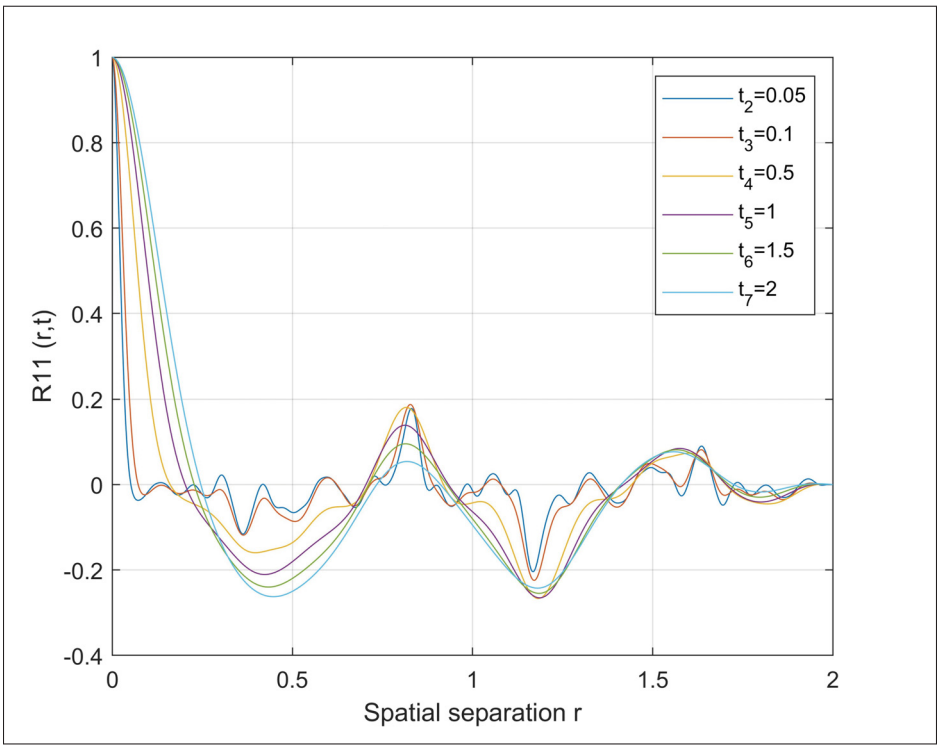

Figure 5.12 Evolution of normalized two-point second-order correlation functions over time. The curves exhibit significant shape consistency, suggesting evidence of self-similarity

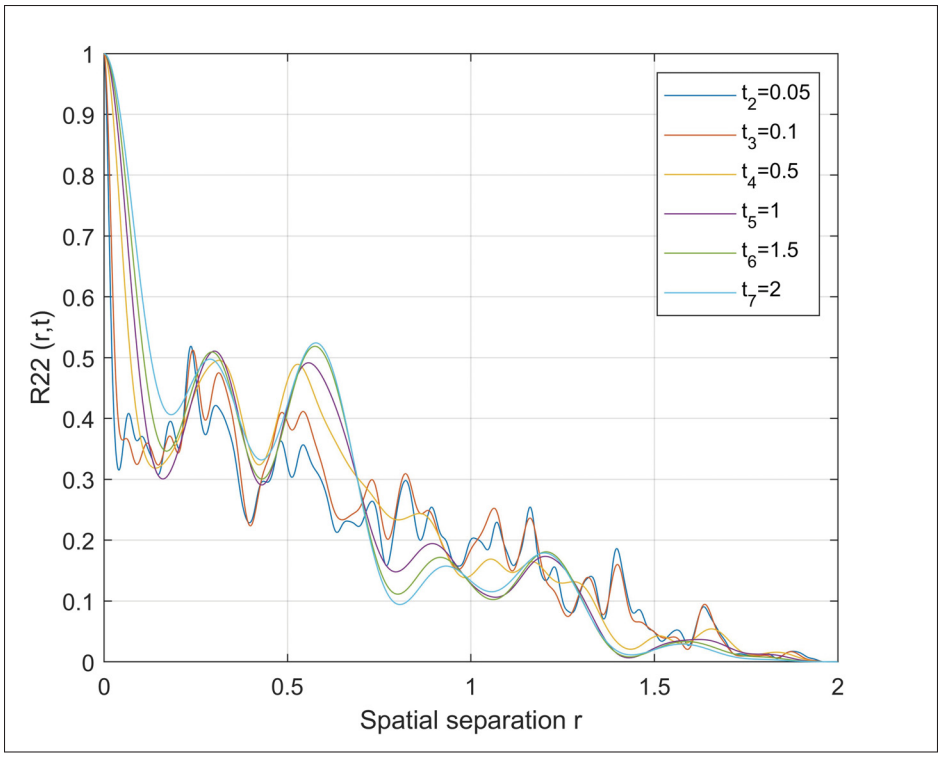

Figure 5.13 Evolution of normalized two-point fourth-order correlation functions over time. The curves exhibit significant shape consistency, suggesting evidence of self-similarity

5.6 Forced Burgers turbulence simulations

As mentioned previously in section 1.1.4, the forced Burgers equation is a versatile model for various physical problems. This section starts with a discussion on the results of forced Burgers turbulence using a sinusoidal forcing function 2.9, revisiting the work of Jeng & Meecham (1972).

$$F = -Asin\left(kx - \omega t\right), \quad A > 0 \tag{5.1}$$

In line with the simulations by Jeng & Meecham (1972), the calculations were carried out in equilibrium states introducing the forcing term to the smallest wavenumber, largest scale at $k = 2\pi$ with $A = 10$ and c equal to unity. This was done using various Reynolds numbers: $Re = 100, 250, 500$. These were determined with a reference length scale of 1 and a reference

velocity scale of 1, making the Reynolds number the inverse of the numerical value of viscosity. The domain length is designated as $L_x = 1$ in the range $0 \leq x \leq 1$ and the number of spatial collocation points $N = 2^{10}$.

Figure 5.14 illustrates the evolution of TKE over time in different Reynolds numbers in our simulations, showcasing a strong concordance in the shape of the curves obtained by Jeng & Meecham, but not the magnitude. The similarity between the curves of TKE at different Reynolds numbers underscores the observation that the development of TKE remains nearly independent of Reynolds number, particularly at sufficiently large Reynolds numbers.

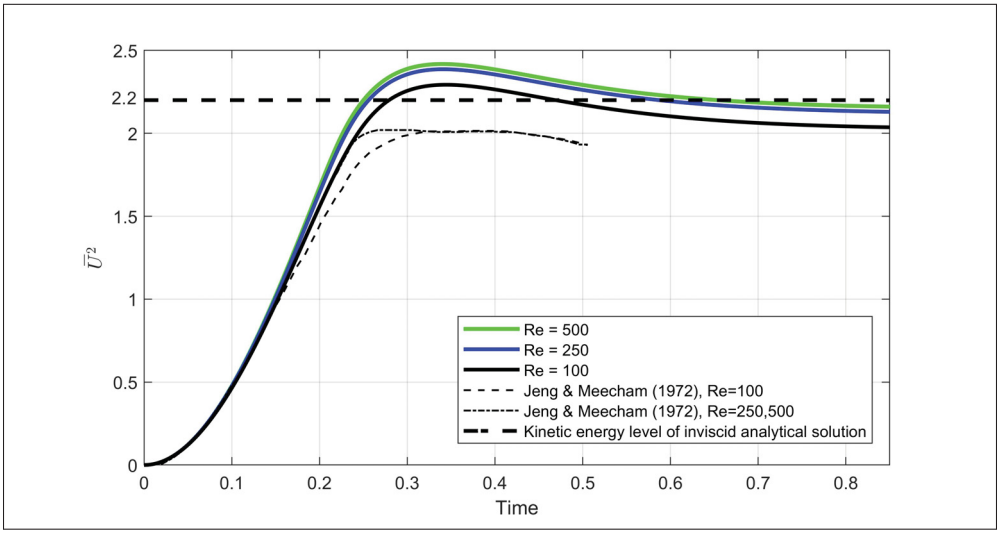

Figure 5.14 The Total Kinetic Energy (TKE) remains consistent despite changes in viscosities. The discrepancy in the TKE levels between our findings and those of Jeng et al. is attributed to energy losses observed in their simulations. The TKE level in our simulations when reaching equilibrium state are almost identical to TKE of inviscid analytical solution

However, the difference in the magnitude of TKE between our results and those of Jeng & Meecham warrants further attention and we confirm that the values of analytical TKE closely align with the energy content of our model and are in stark contrast to their findings.

Another interesting observation is that when we decrease the viscosity, the kinetic energy content of the system in the equilibrium state tends to approach the analytical kinetic energy content of the inviscid solution, which endorsed the accuracy of our simulations.

In Figure 5.15 we can observe the velocity fields acquired by us and by Jeng & Meecham, compared to the analytical solution, which describes the similarity between velocity fields with different viscosities except in the dissipation region. By comparing the results with the analytical solution, we find that the shift in shock positions is observed in the Jeng & Meecham; but not in our simulations.

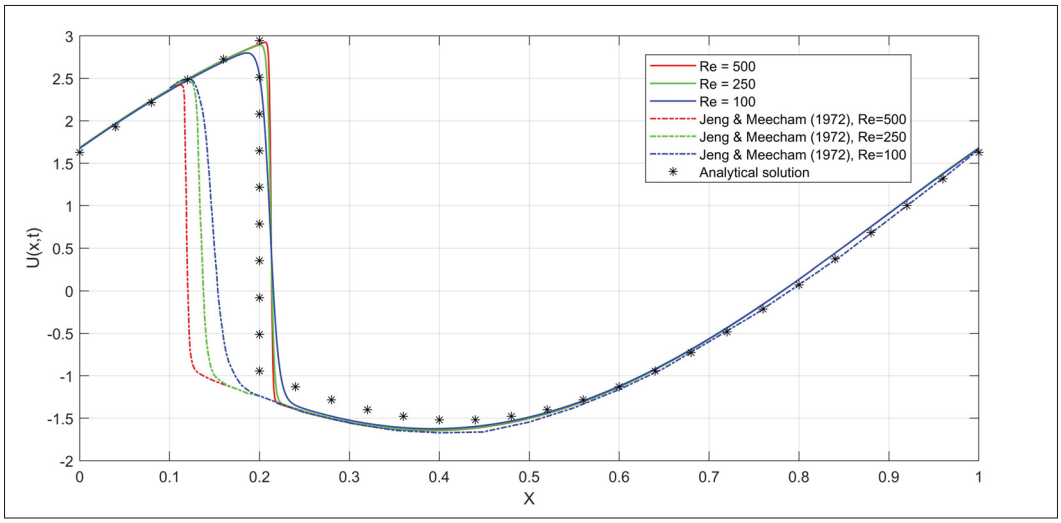

Figure 5.15 The velocity profiles of forced Burgers turbulence in various Reynolds numbers stay nearly identical, except within the dissipation region. In contrast to our results, a shift in shock positions is observed in the Jeng et al. simulations, which is attributed to energy losses

It appears their model lost a portion of energy, potentially due to the inherent errors in the finite difference scheme. This discrepancy is observed in three distinct ways: firstly, weaker maximum velocity values are observed at the shock position; secondly, a notable shift in shock positions is apparent in their results, details of which are more evident in Figure 5.16, yet are not detected in our results. Lastly, and importantly, their model reached equilibrium earlier than expected ($t \geq 0.25$) compared to almost ($t \geq 0.8$) in our simulations.

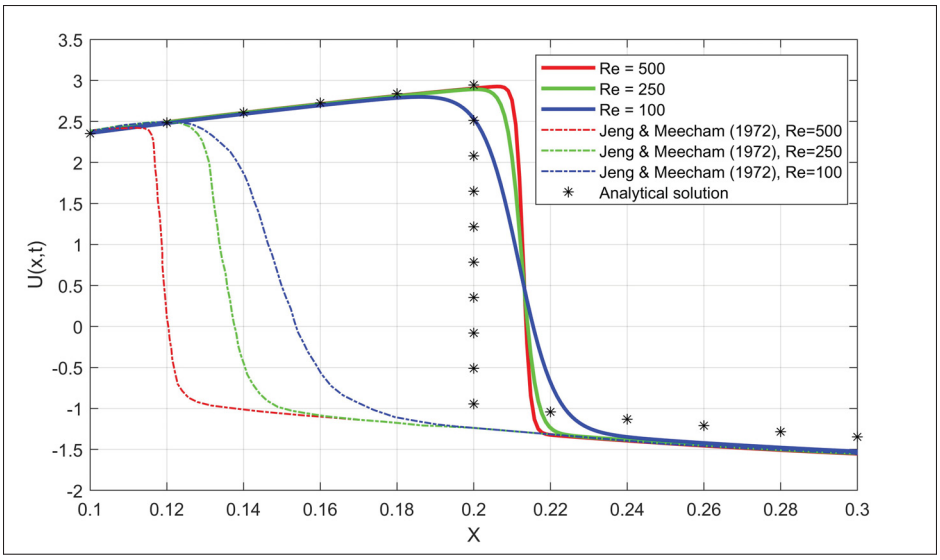

Figure 5.16 The details of shock structure in different Reynolds numbers. The difference in shock position of our simulations and Jeng et al. results are obvious

5.6.1 Evolution of the energy spectrum in the forced Burgers turbulence

The energy spectrum of forced Burgers turbulence with a sinusoidal forcing function can be found in Figure 5.17. As evident, changing the viscosity does not significantly affect the energy distribution across different wavenumbers in forced Burgers turbulence. This stability is attributed to the forcing term, which compensates for the energy dissipated due to viscosity by injecting energy into the system, thereby maintaining the shape of the energy spectrum in smaller wave numbers. Different energy spectra at various wavenumber, fig 5.18, while maintaining nearly the same total kinetic energy (TKE) fig 5.14, reveal that notable variations in energy distribution occur predominantly at larger wavenumbers, though these variations have little effect on the total energy held within the system. This behavior is evident in fig 5.18, where deviations in the energy spectrum occur at higher wavenumbers, rather than at lower wavenumbers that are affected by the large-scale forcing term.

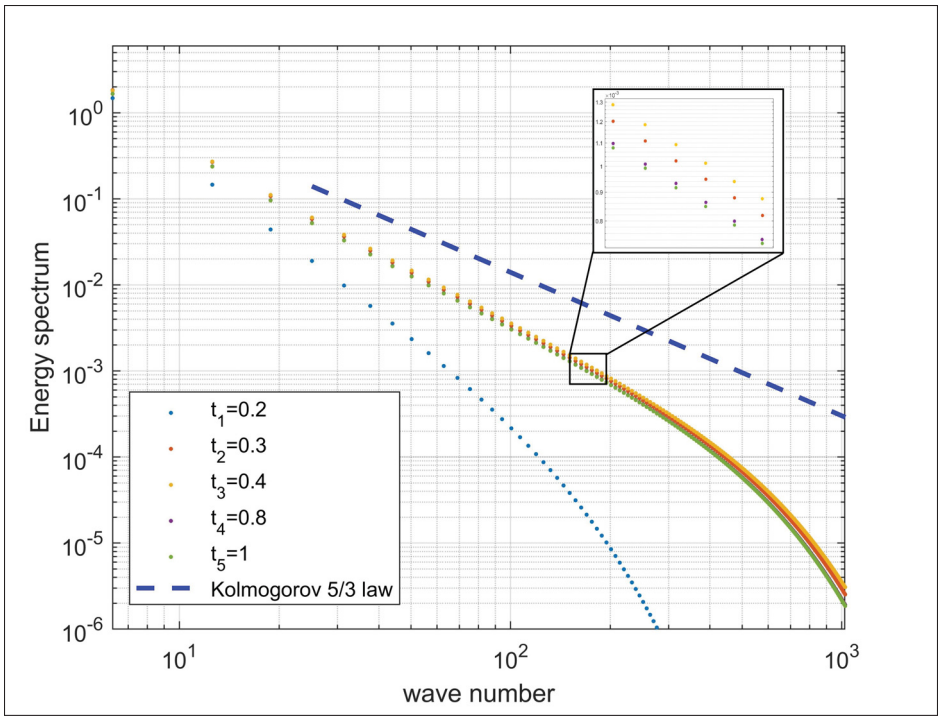

Figure 5.17 The details of energy spectrum with a sinusoidal forcing term in $Re = 500$

5.6.2 Evolution of the Probability Density Function in forced Burgers' turbulence

We can have access to valuable insights by investigating the behaviour of PDF. In Fig.5.19 we observe a bulk shift to the right with a significant concentration of data points on the right side of the mean. The forcing term continuously pumps energy into the system. At the same time, energy dissipates through dissipation mechanisms. Ideally, a balance between this energy input and dissipation will result in a stationary, invariant in time, probability distribution for the solution (Iturriaga & Khanin, 2003). The mentioned observation is explored in greater detail in the following subsection. Note that altering the Reynolds number does not impact the behavior of the PDF. Moreover, the PDF function retains its shape upon reaching the equilibrium state ($t \geq 0.8$).

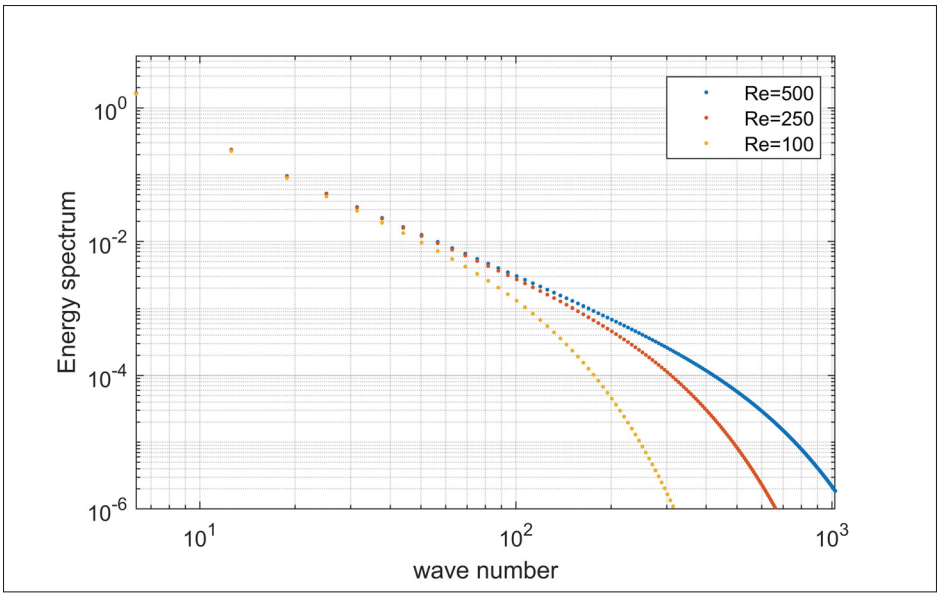

Figure 5.18 The energy spectrum across various wavenumbers, despite similar total kinetic energy (TKE), illustrates that significant differences in energy distribution are just confined to higher wavenumbers, yet these discrepancies minimally impact the system's overall energy content

5.6.3 Evolution of the statistical central moments of distribution in forced Burgers' turbulence

The skewness of a probability density function (PDF) is a measure of its asymmetry, particularly in terms of the direction and extent of the tail.

If a PDF has a long tail on the left side (negative side), figure.5.19, it is typically considered negatively skewed. However, in our simulations, the bulk of the distribution is shifted towards positive values. This shift effectively outweighs the effect of the negative left tail on skewness, resulting in a net positive skewness, figure 5.20.

This can be interpreted that while a small number of sharp gradients or shocks occur with strong negative magnitudes, the majority of events have smaller magnitudes with positive values, which explains the presence of shock waves and rarefaction waves.

Concerning the behavior of kurtosis, figure 5.21, it initially starts at a value of zero, indicative of a zero initial velocity field. This quickly changes after the first timestep, rising to 1.5, a value that is still below the standard kurtosis of a normal distribution, Kurtosis equal to 3. This

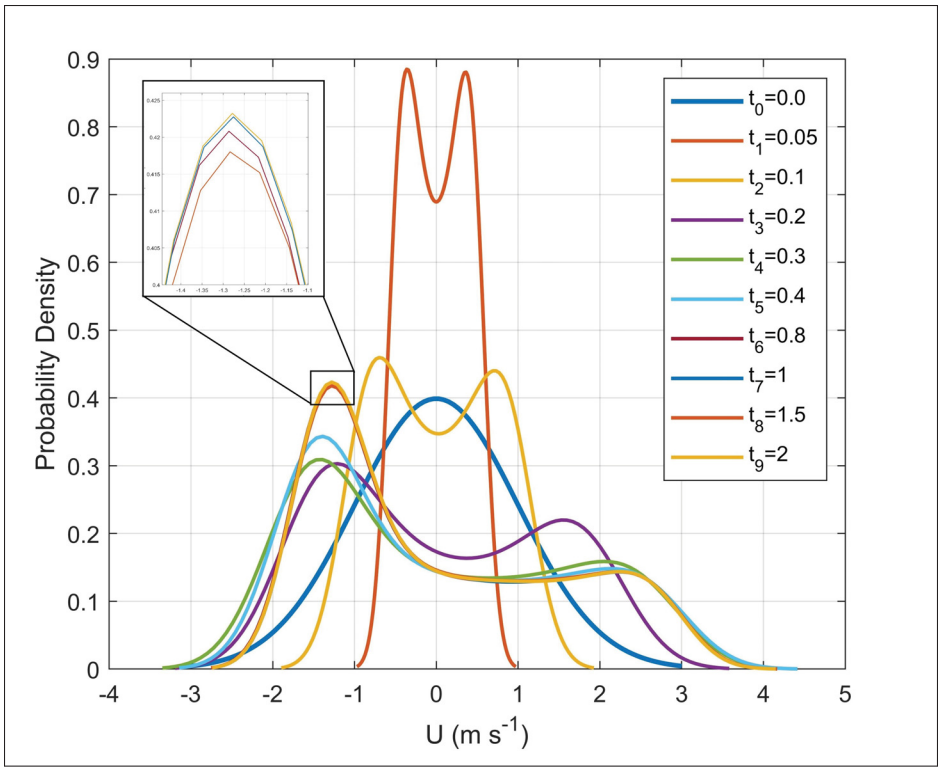

Figure 5.19 The evolution of PDF in time. A bulk shift to the right with a tailed concentration in the left. PDF becomes stationary once the system reaches a steady state

initial phase signifies a platykurtic distribution, where the tails are lighter than those of a normal distribution, suggesting a lower likelihood of extreme values or outliers. As the simulation progresses, there is a slight decrease in kurtosis, dropping to 1.45 around $t = 0.2$. This mild change indicates a stable phase in terms of tail heaviness and the probability of outliers. As the simulation continues towards $t = 0.8$, the kurtosis gradually increases to 1.9, indicating a shift towards a more normal-tailed distribution. This phase shows a subtle increase in the likelihood of outliers and shocks, reflecting a gradual intensification of extreme events within the turbulence. Notably, as the forced Burgers turbulent system approaches an equilibrium state, the kurtosis stabilizes at 1.9. This stabilization suggests that the final equilibrium state of the system is characterized by a distribution with tails that are less heavy than a normal distribution, indicating a moderately low probability of extreme values, but heavier than at the initial stages of the simulation. The overall behavior of kurtosis throughout the simulation highlights the

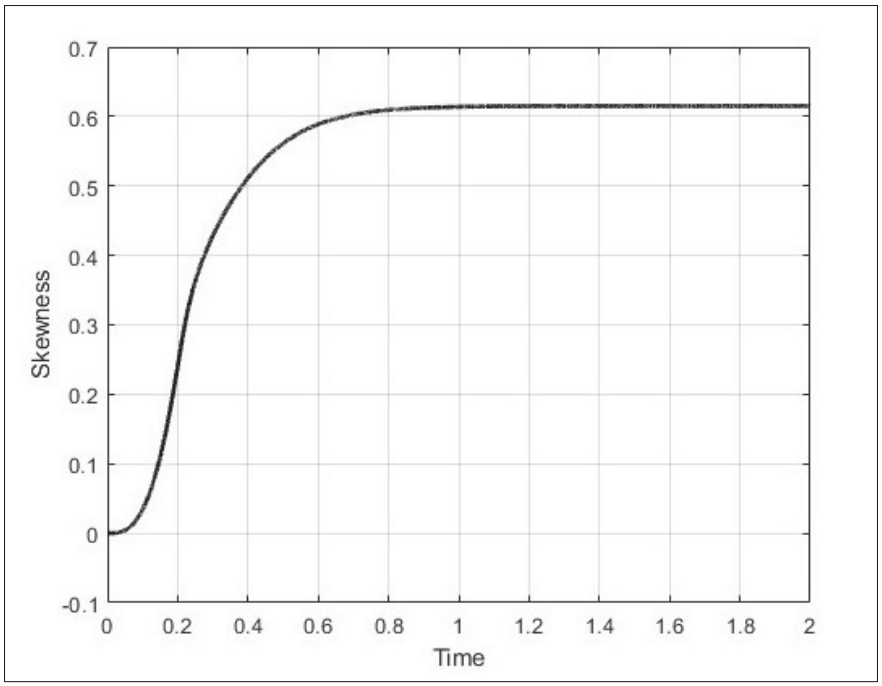

Figure 5.20 The evolution of skewness in the velocity field dataset shows that the positive skewness stabilizes at a constant value once the system reaches an equilibrium state

dynamic and complex nature of forced Burgers turbulence, especially in how extreme events and tail probabilities evolve from the initial stages to the equilibrium state. This behavior, in conjunction with the observed positive skewness and fat left tail of the PDF, illustrates the asymmetrical and intricate characteristics of the distribution in our turbulence simulations.

In forced Burgers turbulence, changing the Reynolds number does not affect the statistical central moments of the distribution.

5.6.4 Gaussianity and Quasinormal assumption

Building upon the findings of Jeng (1969), which highlighted the insensitivity to initial data in Burgers turbulence, we replicated their study to confirm these observations. To this aim we implemented Forced Burgers turbulence with the initial Gaussian velocity field subjected to Gaussian random force, the details of simulations were discussed earlier in chapters 2 and 3.

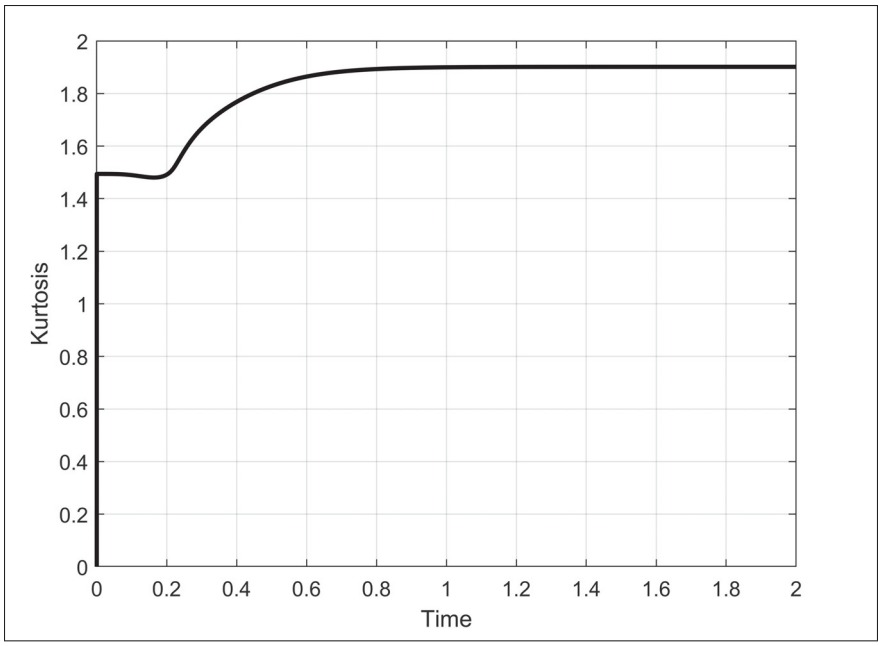

Figure 5.21 The evolution of Kurtosis in time. Kurtosis demonstrates the evolving complexity of turbulence, particularly in how extreme events change from start to equilibrium

To evaluate the system's Gaussianity, and see whether it keeps this distribution form, we use the Quasinormal approximation, which links the fourth-order correlation to the second-order correlation. The formula is expressed as:

$$\langle u^2(x+r)u^2(x)\rangle = \langle u(x)^2\rangle^2 + 2\langle u(x+r) + u(x)\rangle^2 \tag{5.2}$$

Under this approximation, a purely Gaussian velocity field would conform to the Quasinormal condition.

Assessing how much the velocity field deviates from the quasinormal assumption can be used as a method to evaluate its Gaussian characteristics. In figure 5.22 Quasinormal assumption compared with the fourth-order correlation for the velocity field at $t_f \geq 1$ is depicted.

As evident from Figure 5.22, there is a notable congruence with the quasi-normal assumption. This leads us to conclude that the velocity field closely approximates a Gaussian distribution, suggesting that our system maintains its Gaussianity over time. This observation is consistent

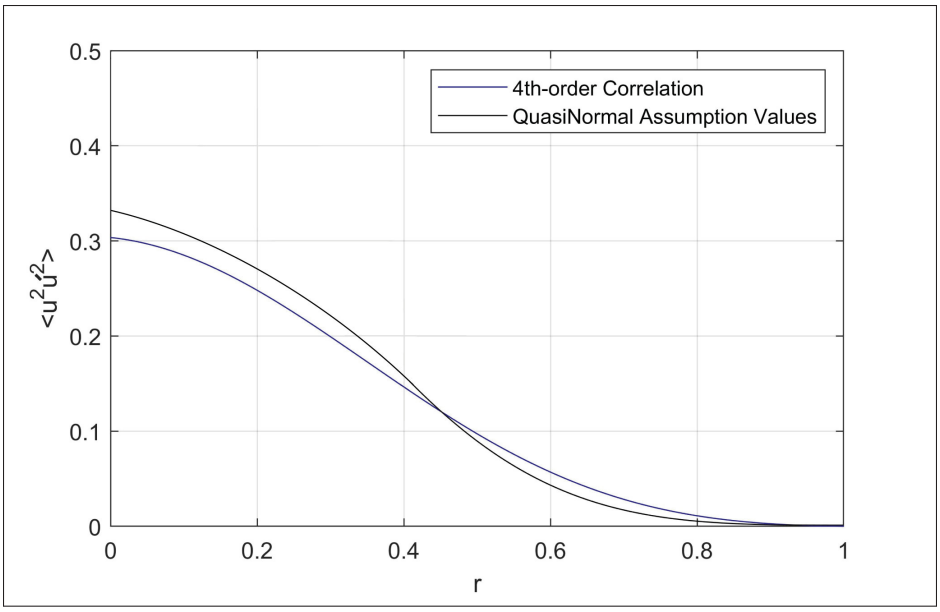

Figure 5.22 The comparison of the fourth-order correlation function of the velocity field with the quasi-normal assumption reveals an acceptable alignment, serving as evidence that the system has preserved its Gaussianity

with various experiments on actual turbulence (UBEROI, 1956), as well as the numerical simulations conducted by (Jeng, 1969).

5.6.5 Dynamic adaptation of the Burgers turbulence to the external inputs utilizing multi-point statistical correlations of the velocity field

Building on the discussion from the previous section, we delve deeper into the analysis. Up to this point, we have shown that the system retains its Gaussianity when initialized with Gaussian data and subjected to the forcing from the same distribution. In this section, we aim to show that the system's behavior is not about preserving Gaussianity; rather, it just closely reflects the dynamics of the forcing term over time.

To this aim we evaluate second-order and fourth-order two-point correlations based on the formula discussed in section 2.2.

In figures 5.23 to 5.26, the correlation functions are presented, for both the velocity field and the forcing term. The aim is to showcase the resemblance between the central correlation functions

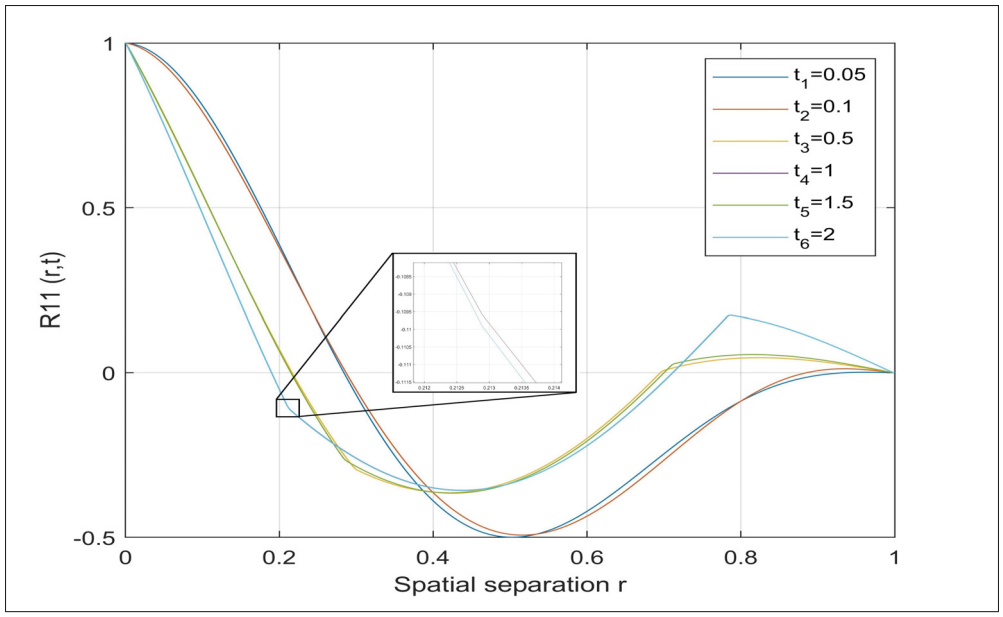

Figure 5.23 Evolution of normalized two-point second-order correlation functions of the velocity field over time. The curves are increasingly aligned with the phase of the random driving force

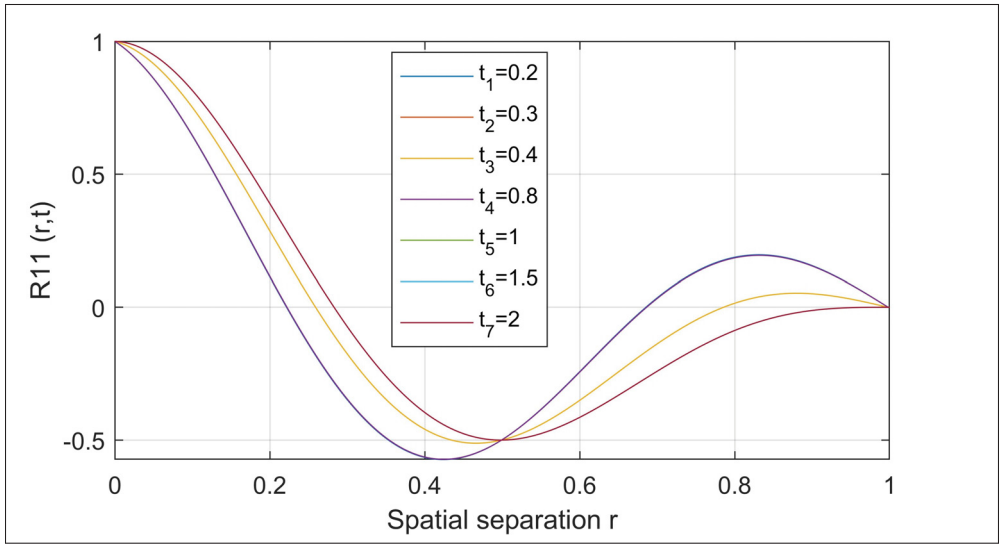

Figure 5.24 Evolution of the second-order correlation functions of the forcing term over time. The curves exhibit alignment with their counterpart correlation functions of the velocity field

of the velocity field at various time stages and the correlation functions of the forcing term as they evolve over time.

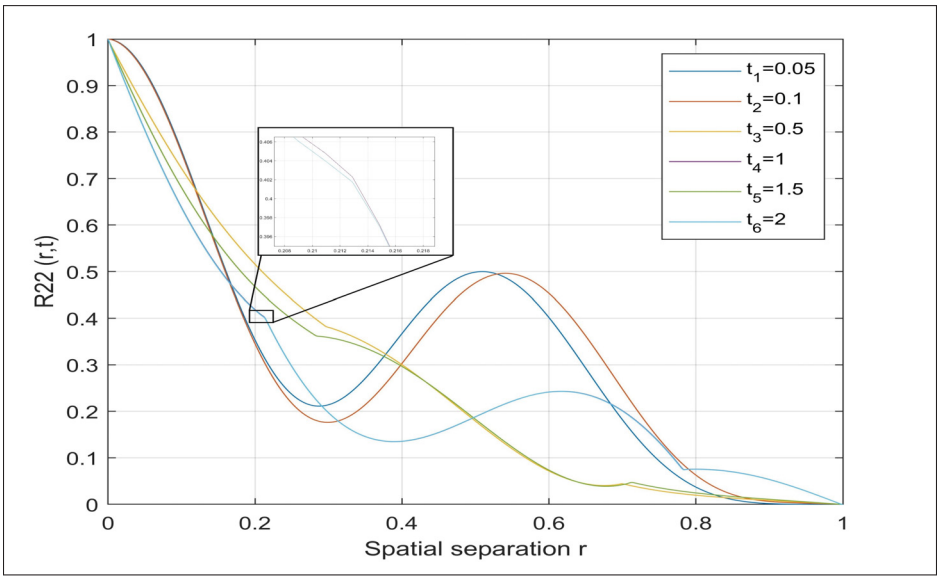

Figure 5.25 Evolution of normalized two-point fourth-order correlation functions of the velocity field over time. The curves are increasingly aligned with the phase of the random driving force

This resemblance underscores a significant distinction between the dynamics of decaying Burgers turbulence and those of forced Burgers turbulence. In the case of decaying Burgers turbulence, there is a noted similarity between the characteristics of the initial velocity field and those observed at later stages of evolution. This similarity suggests a certain degree of preservation of initial conditions over time.

However, the scenario markedly changes in the context of forced Burgers turbulence. Here, the velocity field does not merely retain its initial characteristics; instead, it increasingly aligns itself with the phase and dynamics of the external driving force as the system evolves. This progressive correlation between the velocity field and the forcing term underscores a dynamic adaptation of the system to the external inputs, rather than a simple preservation of its initial state.

This phenomenon, where the velocity field in forced Burgers turbulence becomes more intricately linked with the characteristics of the driving force over time, was also observed and noted by

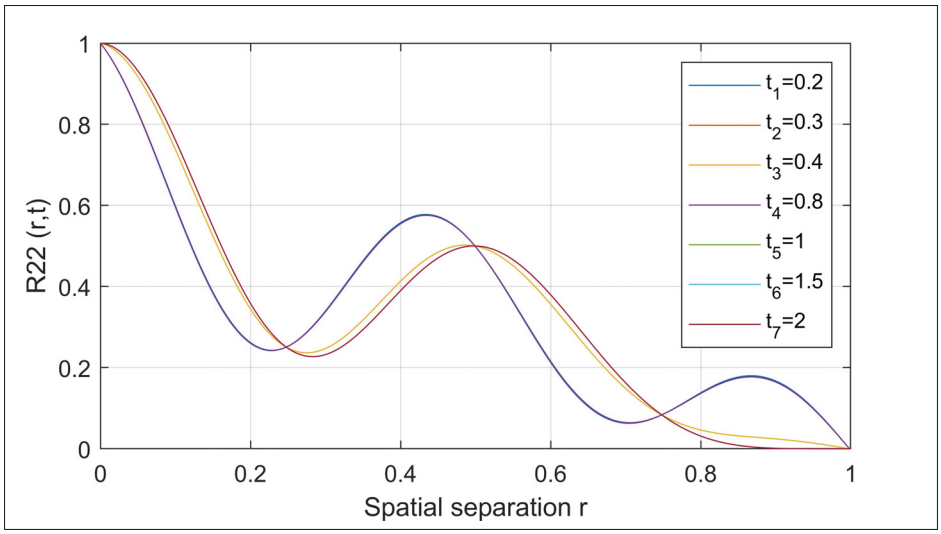

Figure 5.26 Evolution of the fourth-order correlation function of the forcing term over time. The curves exhibit alignment with their counterpart correlation functions of the velocity field

Dah-Tang Jeng in 1969. Jeng's observations highlight the adaptability and responsiveness of the velocity field within forced Burgers turbulence to external influences, marking a clear departure from the behavior seen in decaying turbulence. This evolving correlation provides a deeper insight into the mechanisms governing forced Burgers turbulence and emphasizes the significant role of the forcing term in shaping the system's dynamics.

5.6.6 Intermittency

In our exploration of forced Burgers turbulence, the observation of intermittency within the dissipation range of the correlation function of the energy dissipation rate in the presence of hyper-dissipation provides a significant insight into the complex dynamics of turbulence. We can observe intermittent behavior in figure 5.27.

This intermittency, characterized by irregular, intense bursts of energy dissipation amidst less active phases, underscores the non-linear and scale-dependent nature of turbulence.
Based on the study by Polyakov (1993), viscosity in turbulent flows acts analogously to ultraviolet (UV) regularization in quantum field theory by setting a cutoff at high energies or

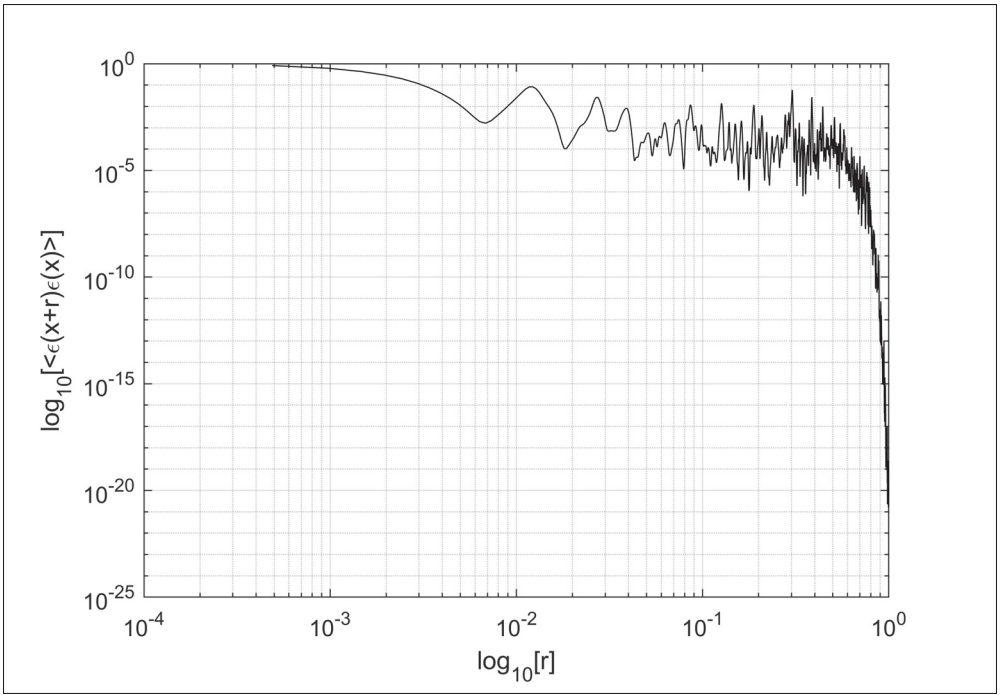

Figure 5.27 The energy dissipation correlation function exhibits intermittent behavior at small scales in forced Burgers turbulence with random Wiener initial velocity field and the forcing term

small scales, thereby preventing non-physical infinities and facilitating energy dissipation at large wavenumbers. Contrarily, infrared (IR) divergence, which primarily affects large scales, leads to the formation of large-scale condensate states. These states, made of collections of strong shocks moving at very low velocities, do not simply transfer small-scale fluctuations by large-scale structures. Instead, they embody coherent condensate structures that significantly impact the turbulence dynamics, highlighting a complex interplay between small-scale dissipative processes and large-scale flow structures Chekhlov & Yakhot (1995b). This interaction results in a disruption of Galilean invariance, ultimately leading to intermittent effects within the dissipative range.

This mechanism affects the energy cascade across scales, contributing to the observed intermittency caused by disruption of Galilean invariance (Polyakov, 1995).

It's important to note that, on a superficial level, Burgers turbulence displays behavior in line with Kolmogorov's $5/3$ law (Chekhlov & Yakhot, 1995b), a phenomenon that can also be tied to

the underlying mechanisms involved. This highlights the intricate balance between small-scale dynamics, managed through UV regularization, and large-scale behaviors, influenced by IR divergence, in shaping turbulence's intermittent nature. Identifying research gaps, future studies could focus on quantitatively linking these theoretical concepts to empirical observations of intermittency, providing a deeper understanding of turbulence's fundamental mechanisms.

CONCLUSION AND RECOMMENDATIONS

This thesis has made substantial contributions to the understanding of Burgers Turbulence, illuminating various dynamical aspects through a combination of theoretical analysis and computational simulations. Our comprehensive investigation began with an exploration of the effects of viscosity on linear and non-linear Burgers equations. By extending foundational research and employing advanced simulation techniques, we have deepened the understanding of forced Burgers turbulence and its sensitivity to initial conditions and forcing terms.

Key findings from our study include

- Analyzing the critical impact of viscosity on the solution of the Burgers class of equations, assessing the intricate interplay between Advection and Diffusion phenomena in various scales.
- Confirmation of self-similarity in the velocity field's correlation functions of the decaying Burgers turbulence, which suggests a methodological improvement for future turbulence simulations, reducing computational efforts without compromising the accuracy of results.
- Observation of a sudden inverse transfer of energy from the inertial range to the large-scale range in the non-forced Burgers turbulence. This phenomenon is attributed to local triadic interactions within the spectral space.
- Demonstration that the development of Turbulent Kinetic Energy (TKE) in forced Burgers turbulence is remarkably robust to changes in the Reynolds number, highlighting the system's inherent stability under varied fluid dynamic conditions.
- Identification of consistent velocity profiles across different Reynolds numbers after reaching equilibrium, with dissipation being the primary area of variation, which underscores the nuanced effects of viscosity in turbulent flow dynamics.

- Evidence supporting the Gaussian nature of turbulence when initiated with a random Gaussian velocity field and subjected to a random Gaussian forcing term, emphasizing the Burgers equation's reduced sensitivity to initial conditions compared to Navier-Stokes turbulence.
- Adaptability and responsiveness of the dynamics of the Burgers turbulence to the external influences
- The study examines intermittent behavior within the dissipative range, focusing on the interactions between large-scale infrared (IR) divergence and the viscous ultraviolet (UV) regularization. This approach highlights the complex dynamics where large-scale coherent structures influenced by IR divergence interact with small-scale dissipation processes, akin to UV regularization in quantum fields, to shape turbulence characteristics.

Comments

The insights gained from this research not only bridge several gaps in the existing literature but also pose new questions for future exploration. The observed self-similarity and the robustness of TKE development across varying Reynolds numbers offer promising avenues for optimizing turbulence simulations, potentially leading to more efficient computational models. Furthermore, the distinct behavior of Burgers turbulence, especially its reduced sensitivity to initial conditions and specific forcing terms, invites further investigation into its potential applications in modeling and controlling turbulent flows in various engineering and environmental contexts.

Our research underscores the importance of a detailed examination of turbulence dynamics, extending beyond traditional analyses. The findings encourage a reevaluation of existing assumptions in turbulence modeling, particularly concerning the scalability and universality of turbulent behavior. As we advance our understanding of Burgers Turbulence, it becomes evident that the complexities of turbulent flow are both a challenge and an opportunity for researchers and practitioners alike.

Future Directions

Building upon the findings of this thesis, future research should explore the application of these insights to more complex fluid dynamics problems, including three-dimensional turbulence and the interaction between turbulence and complex boundaries. Additionally, the development of new computational methods to further reduce the computational load of simulations while maintaining accuracy could revolutionize the field. Moreover, experimental validation of the theoretical predictions made in this study would be invaluable in solidifying the understanding of Burgers Turbulence and its applications in real-world scenarios. Finally, future research could aim at establishing a quantitative connection between the theoretical frameworks and empirical evidence of intermittency, advancing towards a comprehensive understanding of Kolmogorov turbulence through the lens of the one-dimensional Burgers equation.

APPENDIX I

NUMERICAL INTEGRATION SCHEMES

The following simple one-step method is called the first-order Euler Explicit scheme,

$$u^{n+1} = u^n - \Delta t f^n \tag{A I-1}$$

To describe the time discretization, we denote the time step by Δt and the n-th time level by $t_n = n\Delta t$, the approximated solution at time n by u^n and the operator f contains the spatial part of our PDE. This scheme has truncation error (T.E.) with the order of accuracy $O(\Delta t, \Delta x)$ (Canuto, 2006). We know this as a first-order accurate scheme based on the lowest-order term in the T.E.; and Explicit since only one unknown is present in the equation. However, this scheme is unconditionally unstable (**?**).

The next time integration method we used was the second-order Adams-Bashforth method for time discretization,

$$u^{n+1} = u^n + \frac{1}{2}\Delta t \left[3f^t - f^{n-1}\right] \tag{A I-2}$$

Adam-Bashforth is a class of explicit multistep method which is written based on the explicit Euler model. This scheme is weakly unstable, to be more precise, for a periodic hyperbolic problem the acceptable Δt decreases when the time interval of interest T increases (Canuto, 2006). Finally, the last scheme was the following simple scheme which is called third-order Compact Runge-Kutta (RK3) method,

$$u^{n+1} = u^n - \frac{1}{9}\Delta t \left[2k_1 + 3k_2 + 4k_3\right] \tag{A I-3}$$

In which,

$$
\begin{aligned}
k_1 &= f\left(u^n, t_n\right) \\
k_2 &= f\left(u^n + \frac{1}{2}\Delta t k_1, t_n + \frac{1}{2}\Delta t\right) \\
k_3 &= f\left(u^n + \frac{3}{4}\Delta t k_2, t_n + \frac{3}{4}\Delta t\right)
\end{aligned}
\qquad \text{(A I-4)}
$$

The Runge-Kutta scheme is a single-step but multistage time discretization method which uses several intermediate stages in each time step (**?**).

APPENDIX II

ASSESSMENT OF THE TEMPORAL DISCRETIZATION SCHEMES

In the initial step, we explore a range of simulations that employ three distinct time discretization methods. These include the 1st-order Explicit Euler, the 2nd-order Adam-Bashforth, and the 3rd-order compact Runge-Kutta. These methods are applied to the Advection-Diffusion and Decaying Burgers equations. Our objective is to identify the most suitable time discretization scheme for our simulation. To this aim, We begin with the Advection-diffusion, equation 2.4.

1. Accuracy of time discretization schemes

One of the most common and informative plots for comparing numerical schemes is the Error vs. Step size plot on a log-log scale, figure II-1.

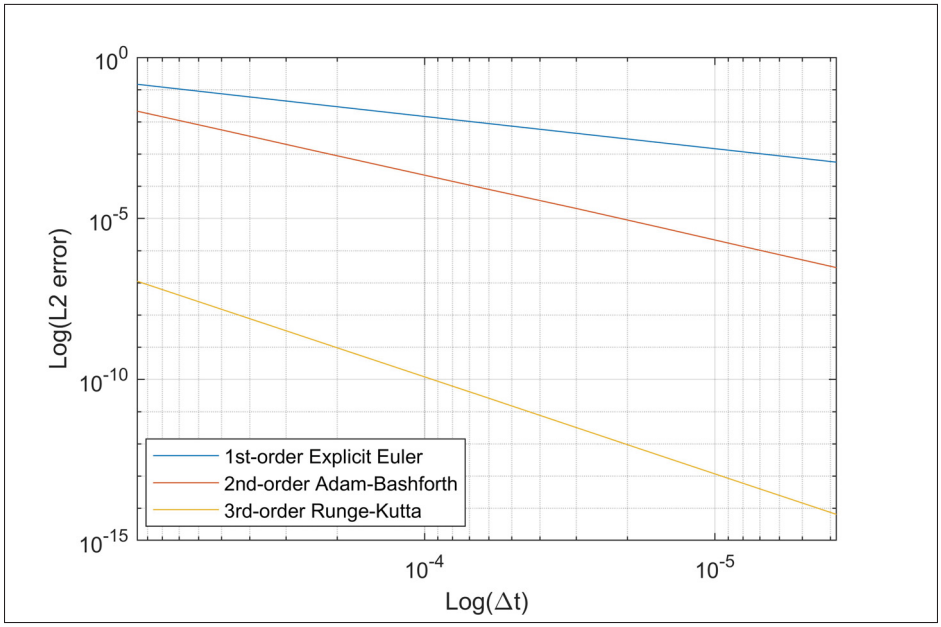

Figure-A II-1 Comparison between L2 Error of various time discretization schemes for the decaying Burgers' equation in $\nu = 0.001$

In the mentioned plot, the error (typically calculated as the L2 norm of the difference between numerical and analytical solutions) will be on the y-axis. The rate at which the error decreases

as the step size is halved (the slope of the line in the log-log plot) corresponds to the order of the accuracy of the method.

As demonstrated in Figure II-1, if halving the step size $\Delta t = 2^{P-19}$ for $1 \leq P \leq 9$ (which corresponds to moving one unit to the right on the log scale) results in the L2-error being reduced by a factor of one in 1st-order Explicit Euler, by a factor of two in 2nd-order Adam-Bashforth and by a factor of 3 in 3rd-order Runge-Kutta scheme. So, as we expected and demonstrated in the following plots, the Runge-Kutta scheme shows a steeper decrease (higher order of convergence) or a lower error for the same step size compared to the two other schemes so we will get a more accurate solution with fewer grid points which means less computational effort.

One characteristic that can be observed in our simulations, figure 5.3, by evaluating the behavior of the spectral approximation compared to the analytical solution, is the dissipation error, which emerges and increases by moving in time, specifically in higher wavenumbers as more energy dissipates; however, refining the mesh size, will make it smaller.

2. Stability considerations (Advection-Diffusion)

In this section, we try to investigate the stability considerations of the schemes discussed earlier. On this wise, we are going to use the Von Neumann stability analysis, which is a procedure to evaluate the stability of linear partial differential equations based on the Fourier decomposition of numerical error. In order to clarify the concept of stability, we know that in each stage of our numerical solution, we will obtain some errors. Our solution is called stable if this error will decrease from stage n to stage $n + 1$. So, our solution is considered stable if the error decreases when the simulation advances through each time level. So we define an amplification factor G which is as follow (Li & Wang, 2021b),

$$G = \frac{u^{n+1}}{u^n} \tag{A II-1}$$

The amplification factor G could also be defined as the Taylor expansion of $e^{\lambda_k \Delta t}$ in which n is the order of the Runge-Kutta scheme (Moin, 2010) (de Moura & Kubrusly, 2012).

$$|G| = \left| 1 + \lambda_k \Delta t + \frac{(\lambda_k \Delta t)^2}{2!} + \frac{(\lambda_k \Delta t)^3}{3!} + \ldots + \frac{(\lambda_k \Delta t)^n}{n!} \right| \qquad \text{(A II-2)}$$

To better understand the stability analysis, we plot the region in which the scheme is absolutely stable inside its boundaries which is called the absolute stability region, figure II-2.

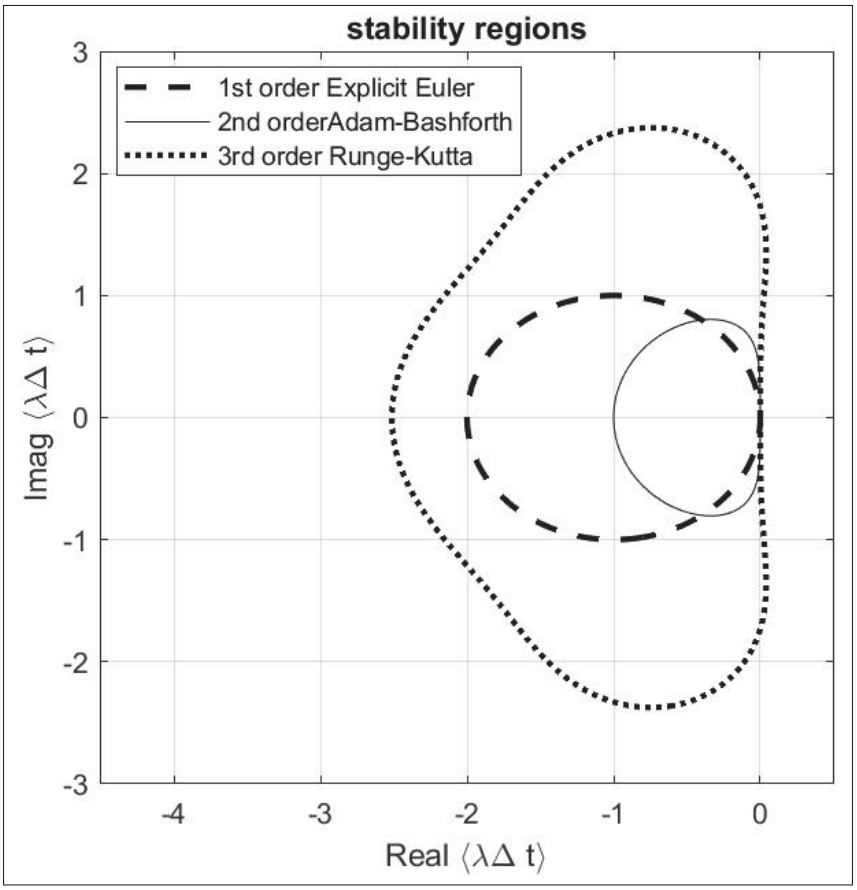

Figure-A II-2 Comparing absolute stability region of Convection-Diffusion equation for three different numerical schemes

As we know, The Runge-Kutta methods are the simplest family of Multi-stage schemes, and the Adam-Bashforth methods are the simplest family of Explicit Multi-step schemes. The stability contours illustrated below are the locus of the complex $\lambda_k \Delta t$, in which $|G| = 1$, for multi-stage

numerical schemes like the 3rd-order Runge-Kutta method and are the region of characteristic polynomial for the multi-step methods like the 2nd-order Adam-Bashforth scheme (Lomax, Pulliam & Zingg, 2001).

Keep in mind that the stability regions of multi-stage methods become larger by increasing the order of accuracy; however, the stability region of multi-step methods will shrink by increasing the order of accuracy (de Moura & Kubrusly, 2012). So, to maintain our schemes' stability, we kept their complex contours inside the locus of the stability region by choosing the approximation parameters based on the stability diagram. stability and the viscosity Note that according to figure II-2, the size of the stability region in the 3rd Order Runge-Kutta is larger than the 1st Order Explicit Euler, and for the Explicit Euler, it is larger than the 2nd Order Adam-Bashforth scheme. Moreover, it's the RK3 scheme only that remains inside the stable domain even if it crosses the imaginary axis. In other words, as the imaginary values are responsible for the convection effects so this scheme will remain stable in purely convective problems in the case that the amplitude of the imaginary part remains less than 1.73. Another thing that could be observed in figure II-2 is that the absolutely stable regions end when the real part of the complex $\lambda_k \Delta t$ reaches -1 for AB2, -2 for Explicit Euler, and -2.5 for RK3, which could be helpful in studying the behavior of such schemes.

3. Stability considerations (Decaying Burgers equation)

As we know, the Von-Neumann stability analysis, which was discussed earlier, is designed for linear problems, while the main feature of the Burgers equation is Non-linearity. One approach to circumvent this barrier is linearizing our problem and performing the evaluations locally. To make it more straightforward, as we decided to do the time marching discretization in physical space thus, we evaluate the stability of the obtained linear ODE in physical space at every point of the domain through each time level.

As we know, the CFL condition essentially states that the fluid should not travel more than one computational cell per time step. In this case, the speed of information propagation is not constant and can depend on the local flow conditions, including the velocity. So, the CFL

condition is typically applied in a conservative way, using the maximum possible speed of information propagation to calculate the time step size. Thus, for the non-linear equations, we can reform the CFL condition to define the time step as,

$$\Delta t = C_{cfl}\ \frac{\Delta x}{S^n_{max}} \tag{A II-3}$$

Where Δx is grid space size, S^n_{max} is the maximum wave speed at the time step n and C_{cfl} is the CFL coefficient with $C_{cfl} \in (0, 1]$ (Toro, 1997). To choose a proper value for S^n_{max} we should use the following formula carefully,

$$S^n_{max} = max \left|u^n_i\right| \tag{A II-4}$$

In which i is the number of grid points through the domain, so, in non-linear cases, we evaluate the Modified CFL condition locally in each time step through the whole spatial domain. It is worth mentioning here that underestimating S^n_{max} can cause to choose extra-large Δt, which can lead to developing instability in our solution. A conservative approach to deal with such cases is to choose a safety factor for the CFL coefficient, for instance, 0.9 C_{cfl} instead of 1.0 C_{cfl} (Toro, 1997).

From our simulations, it is evident that only the Runge-Kutta scheme remained stable at low viscosities.

4. Viscosity and Stability

During our simulations we observed an intriguing behavior regarding how viscosity impacts the stability of the numerical schemes. Although higher viscosity is theoretically associated with enhanced stability through solution smoothing by the diffusion term, practical stability in numerical simulations also hinges on the appropriate selection of time and spatial discretizations. The relationship between viscosity and the eigenvalue λ_k of the amplification factor G defined as $\lambda_k = -iak - \nu k^2$, Indicates that increased viscosity can lead to instability. This occurs when higher viscosity shifts the stability complex contours outside the locus of the A-stability region,

as depicted in Figure II-2. Therefore, to ensure stability at higher viscosities, it is necessary to reduce the size of the time step. Additionally, adhering to the CFL condition requires an increase in the number of spatial collocation points. Furthermore, for similar reasons to those previously mentioned, higher frequencies can also alter the stability complex contours, moving them outside the locus of the A-stability region. According to $\lambda_k = -iak - \nu k^2$, this may heighten instability in the nonlinear advection term. Conversely, the viscous term becomes more effective at higher wavenumbers, contributing to the regularization of our equation.

BIBLIOGRAPHY

Thesis_20February_2024. Retrieved on 2024-03-04 from: https://www.overleaf.com/project/65d50da3114006f03558a910.

Anguelov, R., Djoko, J. & Lubuma, J.-S. (2007). Energy Properties Preserving Schemes for Burgers' Equation. *Numerical Methods for Partial Differential Equations*, 24(1), 41–59. doi: 10.1002/num.20227.

Atangana, A. (2018). Chapter 2 - Principle of Groundwater Flow. In Atangana, A. (Ed.), *Fractional Operators with Constant and Variable Order with Application to Geo-Hydrology* (pp. 15–47). Academic Press. doi: 10.1016/B978-0-12-809670-3.00002-3.

Bakhtin, Y. (2013). The Burgers Equation with Poisson Random Forcing. *The Annals of Probability*, 41(4). doi: 10.1214/12-AOP747.

Basdevant, C., Deville, M., Haldenwang, P., Lacroix, J. M., Ouazzani, J., Peyret, R., Orlandi, P. & Patera, A. T. (1986). Spectral and Finite Difference Solutions of the Burgers Equation. *Computers & Fluids*, 14(1), 23–41. doi: 10.1016/0045-7930(86)90036-8.

Bateman, H. (1915). SOME RECENT RESEARCHES ON THE MOTION OF FLUIDS. *Monthly Weather Review*, 43(4), 163–170. doi: 10.1175/1520-0493(1915)43<163:SRROTM>2.0.CO;2.

Beardsell, G. (2016). *Spectral Simulations of the Reconnection Process of Two Vortices*. (Ph.D. thesis).

Bec, J. & Frisch, U. (2000). Probability Distribution Functions of Derivatives and Increments for Decaying Burgers Turbulence. *Physical Review E*, 61, 1395–1402. doi: 10.1103/PhysRevE.61.1395.

Bec, J. & Khanin, K. (2007). Burgers Turbulence. *Physics Reports*, 447(1-2), 1–66. doi: 10.1016/j.physrep.2007.04.002.

Bec, J. & Khanin, K. (2003). Forced Burgers Equation in an Unbounded Domain. *Journal of Statistical Physics*, 113(5), 741–759. doi: 10.1023/A:1027356518273.

Benton, E. R. & Platzman, G. W. (1972). A Table of Solutions of the One-Dimensional Burgers Equation. *Quarterly of Applied Mathematics*, 30(2), 195–212. doi: 10.1090/qam/306736.

Bowman, J. C. & Roberts, M. (2011). Efficient Dealiased Convolutions without Padding. *SIAM Journal on Scientific Computing*, 33(1), 386–406. doi: 10.1137/100787933.

Boyd, J. P. (2001). *Chebyshev and Fourier Spectral Methods: Second Revised Edition* (ed. Second Edition, Revised). Mineola, N.Y: Dover Publications.

Burgers, J. M. (1939). Mathematical Examples Illustrating Relations Occurring in the Theory of Turbulent Fluid Motion. In Nieuwstadt, F. T. M. & Steketee, J. A. (Eds.), *Selected Papers of J. M. Burgers* (pp. 281–334). Dordrecht: Springer Netherlands. doi: 10.1007/978-94-011-0195-0_10.

Canuto, C. (Ed.). (2006). *Spectral Methods: Fundamentals in Single Domains*. Berlin ; New York: Springer-Verlag.

Canuto, C., Hussaini, M. Y., Quarteroni, A. & Zang, T. A. (1988). *Spectral Methods in Fluid Dynamics*. Berlin, Heidelberg: Springer. doi: 10.1007/978-3-642-84108-8.

Capasso, V. & Bakstein, D. (2005). *An Introduction to Continuous-Time Stochastic Processes: Theory, Models, and Applications to Finance, Biology, and Medicine*. Boston: Birkhäuser.

Chekhlov, A. & Yakhot, V. (1995a). Kolmogorov Turbulence in a Random-Force-Driven Burgers Equation: Anomalous Scaling and Probability Density Functions. *Physical Review E*, 52(5), 5681–5684. doi: 10.1103/PhysRevE.52.5681.

Chekhlov, A. & Yakhot, V. (1995b). Kolmogorov Turbulence in a Random-Force-Driven Burgers Equation. *Physical Review E*, 51(4), R2739-R2742. doi: 10.1103/PhysRevE.51.R2739.

Christov, C. I. (1980). On a Canonical Representation for Some Stochastic Processes with Application to Turbulence. *Bulg. Acad. Sei., Theor. Appl. Mech*, 59–66.

Christov, C. I. (1990). Flows with Coherent Structures: Application of Random Point Functions and Stochastic Functional Series. *Continuum models and discrete systems*, 1, 232–252.

Cole, J. D. (1951). On a Quasi-Linear Parabolic Equation Occurring in Aerodynamics. *Quarterly of Applied Mathematics*, 9(3), 225–236. doi: 10.1090/qam/42889.

Davidson, P. (2015). *Turbulence: An Introduction for Scientists and Engineers*. Oxford University Press. doi: 10.1093/acprof:oso/9780198722588.001.0001.

De, S., Mitra, D. & Pandit, R. (2023). Dynamic Multiscaling in Stochastically Forced Burgers Turbulence. *Scientific Reports*, 13(1), 7151. doi: 10.1038/s41598-023-29056-3.

de Moura, C. A. & Kubrusly, C. S. (Eds.). (2012). *The Courant–Friedrichs–Lewy (CFL) Condition: 80 Years After Its Discovery* (ed. 2013th edition). New York: Birkhäuser.

Fujisawa, N. & Gotoh, F. (1992). Visualization Study of the Flow in and around a Savonius Rotor. *Experiments in Fluids*, 12(6), 407–412. doi: 10.1007/BF00193888.

Giorgini, A. & Fluid Mechanics and Diffusion Laboratory, C. o. E. (1967). A Numerical Experiment on a Turbulence Model: Technical Report.

Girimaji, S. S. & Zhou, Y. (1995). Spectrum and Energy Transfer in Steady Burgers Turbulence. *Physics Letters A*, 202(4), 279–287.

Gotoh, T. & Kraichnan, R. H. (1993). Statistics of Decaying Burgers Turbulence. *Physics of Fluids A: Fluid Dynamics*, 5(2), 445–457. doi: 10.1063/1.858868.

Gottlieb, D. & Orszag, S. A. (1977). Numerical Analysis of Spectral Methods: Theory and Applications. doi: 10.1137/1.9781611970425.

Higham., D. J. (2001). An Algorithmic Introduction to Numerical Simulation of Stochastic Differential Equations. *SIAM Review*, 43(3), 525–546. doi: 10.1137/S0036144500378302.

Hopf, E. (1950). The Partial Differential Equation $u_t + Uu_x = \mu_{xx}$. *Communications on Pure and Applied Mathematics*, 3(3), 201–230. doi: 10.1002/cpa.3160030302.

Iturriaga, R. & Khanin, K. (2003). Burgers Turbulence and Random Lagrangian Systems. *Communications in Mathematical Physics*, 232(3), 377–428. doi: 10.1007/s00220-002-0748-6.

Jaiswal, S., Chopra, M. & Das, S. (2019). Numerical Solution of Non-Linear Partial Differential Equation for Porous Media Using Operational Matrices. *Mathematics and Computers in Simulation*, 160, 138–154. doi: 10.1016/j.matcom.2018.12.007.

Jeng, D. T. & Meecham, W. C. (1972). Solution of Forced Burgers Equation. *The Physics of Fluids*, 15(3), 504–506. doi: 10.1063/1.1693936.

Jeng, D. T., Foerster, R., Haaland, S. & Meecham, W. C. (1966). Statistical Initial-Value Problem for Burgers' Model Equation of Turbulence. *The Physics of Fluids*, 9(11), 2114–2120. doi: 10.1063/1.1761581.

Jeng, D.-T. (1969). Forced Model Equation for Turbulence. *The Physics of Fluids*, 12(10), 2006–2010. doi: 10.1063/1.1692305.

Kida, S. & Murakami, Y. (1988). Numerical Study of the Energy Decay Law of Turbulence. *Journal of the Physical Society of Japan*, 57(11), 3657–3660. doi: 10.1143/JPSJ.57.3657.

Kraichnan, R. H. (1968). Small-Scale Structure of a Scalar Field Convected by Turbulence. *The Physics of Fluids*, 11(5), 945–953. doi: 10.1063/1.1692063.

Kuo, H.-H. (1996). *White Noise Distribution Theory*. CRC Press.

Lawler, G. F. (2006). *Introduction to Stochastic Processes* (ed. 2nd edition). Boca Raton: Chapman and Hall/CRC.

Li, Y. & Wang, Y. (2021a). Numerical Solution and Stability Analysis for a Class of Nonlinear Differential Equations. *International Journal of Theoretical Physics*, 60. doi: 10.1007/s10773-020-04679-8.

Li, Y. & Wang, Y. (2021b). Numerical Solution and Stability Analysis for a Class of Nonlinear Differential Equations. *International Journal of Theoretical Physics*, 60. doi: 10.1007/s10773-020-04679-8.

Logan, J. & Zlotnik, V. (1995). The Convection-Diffusion Equation with Periodic Boundary Conditions. *Applied Mathematics Letters*, 8(3), 55–61. doi: 10.1016/0893-9659(95)00030-T.

Lomax, H., Pulliam, T. H. & Zingg, D. W. (2001). *Fundamentals of Computational Fluid Dynamics* (ed. 1st ed. 2001 Corr. 2nd printing 2003 edition). Berlin ; New York: Springer/Sci-Tech/Trade.

Lord, G. J., Powell, C. E. & Shardlow, T. (2014). *An Introduction to Computational Stochastic PDEs*. Cambridge: Cambridge University Press. doi: 10.1017/CBO9781139017329.

Matsumoto, M. & Nishimura, T. (1998). Mersenne Twister: A 623-Dimensionally Equidistributed Uniform Pseudo-Random Number Generator. *ACM Transactions on Modeling and Computer Simulation*, 8(1), 3–30. doi: 10.1145/272991.272995.

Meecham, W. C. & Siegel, A. (1964). Wiener-Hermite Expansion in Model Turbulence at Large Reynolds Numbers. *The Physics of Fluids*, 7(8), 1178–1190. doi: 10.1063/1.1711359.

Moin, P. (2010). Fundamentals of Engineering Numerical Analysis. *Canadian Journal of Civil Engineering - CAN J CIVIL ENG*, 29, 344–345. doi: 10.1139/l02-006.

Mojtabi, A. & Deville, M. O. (2015). One-Dimensional Linear Advection–Diffusion Equation: Analytical and Finite Element Solutions. *Computers & Fluids*, 107, 189–195. doi: 10.1016/j.compfluid.2014.11.006.

Montgomery, D. C. & Runger, G. C. (2011). *Applied Statistics and Probability for Engineers* (ed. 5th ed). Hoboken, NJ: Wiley.

Moura, R., Sherwin, S. & Peiró, J. (2016). Eigensolution Analysis of Spectral/Hp Continuous Galerkin Approximations to Advection–Diffusion Problems: Insights into Spectral Vanishing Viscosity. *Journal of Computational Physics*, 307, 401–422. doi: 10.1016/j.jcp.2015.12.009.

Okamura, M. & Kawahara, T. (1983). Steady Solutions of Forced Burgers Equation. *Journal of The Physical Society of Japan - J PHYS SOC JPN*, 52, 3800–3806. doi: 10.1143/JPSJ.52.3800.

Orszag, S. A. (1971). On the Elimination of Aliasing in Finite-Difference Schemes by Filtering High-Wavenumber Components. *Journal of the Atmospheric Sciences*, 28(6), 1074–1074. doi: 10.1175/1520-0469(1971)028<1074:OTEOAI>2.0.CO;2.

Patterson, G. & Orszag, S. (1971). Spectral Calculations of Isotropic Turbulence: Efficient Removal of Aliasing Interactions. *Physics of Fluids - PHYS FLUIDS*, 14, 2538–2541. doi: 10.1063/1.1693365.

Polyakov, A. M. (1993). The Theory of Turbulence in Two Dimensions. *Nuclear Physics B*, 396(2), 367–385. doi: 10.1016/0550-3213(93)90656-A.

Polyakov, A. M. (1995). Turbulence without Pressure. *Physical Review E*, 52(6), 6183–6188. doi: 10.1103/PhysRevE.52.6183.

Pope, S. B. (2000). Turbulent Flows. Cambridge University Press. Retrieved on 2024-02-07 from: https://www.cambridge.org/highereducation/books/turbulent-flows/C58EFF59AF9B81AE6CFAC9ED16486B3A.

Rabinovich, M. I. & Sushchik, M. M. (1983). Coherent Structures in Turbulent Flows. *Nonlinear Waves: Self-organization*, 56–85.

Saffman, P. G. (1968). Lectures on Homogeneous Turbulence. *Topics in Nonlinear Physics*, pp. 485–614. doi: 10.1007/978-3-642-88504-4_6.

Sahnkar,Dale Anderson, J. C. T. R. H. P. R. M. V. D. A. J. C. T. R. H. P. R. M. V. S. (2020). *Computational Fluid Mechanics and Heat Transfer* (ed. 4). Boca Raton: CRC Press. doi: 10.1201/9781351124027.

Sefik, B. & Christov, C. (1992). Numerical Simulation of Burgers' Turbulence Revisited. *Probabilistic Engineering Mechanics*, 7(2), 75–89. doi: 10.1016/0266-8920(92)90011-6.

She, Z.-S., Aurell, E. & Frisch, U. (1992). The Inviscid Burgers Equation with Initial Data of Brownian Type. *Communications in Mathematical Physics*, 148(3), 623–641. doi: 10.1007/BF02096551.

Sinai, Ya. G. (1992). Statistics of Shocks in Solutions of Inviscid Burgers Equation. *Communications in Mathematical Physics*, 148(3), 601–621. doi: 10.1007/BF02096550.

Singh, A. & Das, S. (2019). STUDY AND ANALYSIS OF SPATIAL-TIME NONLINEAR FRACTIONAL-ORDER REACTION-ADVECTION-DIFFUSION EQUATION. *Journal of Porous Media*, 22(7). doi: 10.1615/JPorMedia.2019025907.

Sreenivasan, K. R. (1995). On the Universality of the Kolmogorov Constant. *Physics of Fluids*, 7(11), 2778–2784. doi: 10.1063/1.868656.

Taigbenu, A. E. (1999a). Burgers Equation. In Taigbenu, A. E. (Ed.), *The Green Element Method* (pp. 195–216). Boston, MA: Springer US. doi: 10.1007/978-1-4757-6738-4_7.

Taigbenu, A. E. (1999b). Further Considerations. In Taigbenu, A. E. (Ed.), *The Green Element Method* (pp. 315–331). Boston, MA: Springer US. doi: 10.1007/978-1-4757-6738-4_12.

Tennekes, H. & Lumley, J. (1978). *A FIRST COURSE IN TURBULENCE*. MIT PRESS.

Tokunaga, H. (1976). The Statistical Theory of One-Dimensional Turbulence in a Compressible Field. *Journal of the Physical Society of Japan*, 41(1), 328–337. doi: 10.1143/JPSJ.41.328.

Toro, E. F. (1997). *Riemann Solvers and Numerical Methods for Fluid Dynamics*. Berlin, Heidelberg: Springer. doi: 10.1007/978-3-662-03490-3.

UBEROI, M. S. (1956). Effect of Wind-Tunnel Contraction on Free-Stream Turbulence. *Journal of the Aeronautical Sciences*, 23(8), 754–764. doi: 10.2514/8.3651.

Węglarczyk, S. (2018). Kernel Density Estimation and Its Application. *ITM Web of Conferences*, 23, 00037. doi: 10.1051/itmconf/20182300037.

Yakhot, V. & She, Z.-S. (1988). Long-Time, Large-Scale Properties of the Random-Force–Driven Burgers Equation. *Physical Review Letters*, 60(18), 1840–1843. doi: 10.1103/PhysRevLett.60.1840.

Zel'dovich, Ya. B. (1970). Gravitational Instability: An Approximate Theory for Large Density Perturbations. *Astronomy and Astrophysics*, 5, 84–89.